CELLULAR ZINC TRAFFICKING: THE ZINC PROTEOME AND ITS REACTIONS WITH CADMIUM

by

Mohammad Ali Namdarghanbari

A Dissertation Submitted in

Partial Fulfillment of the

Requirements for the Degree of

Doctor of Philosophy

in Chemistry

at

The University of Wisconsin-Milwaukee

December 2014

ABSTRACT

CELLULAR ZINC TRAFFICKING: THE ZINC PROTEOME AND ITS REACTIONS WITH CADMIUM

by

Mohammad Ali Namdarghanbari

The University of Wisconsin-Milwaukee, 2014
Under the Supervision of Professor David H. Petering

Metals play a crucial role in living systems. Iron, zinc, copper, molybdenum, and manganese are involved in many essential biological activities. Among transition metals, zinc after iron is the most abundant transition metal in the human body and the most abundant in the brain. It exists in more than 3000 proteins, which comprise about 10% of the human proteome. Zn^{2+} dyshomeostasis is associated with chronic diseases such as metabolic syndrome, diabetes and related complications, bone loss, growth retardation in young children, and neurological and behavioral problems. Despite a good knowledge obtained for metabolism of some metal ions such as copper, our understanding about Zn^{2+} trafficking still remains immature. External or internal metal ions, which are chemically similar to Zn^{2+} may disrupt or interfere with the process of Zn^{2+} trafficking and make complications. Metallothionein (MT) and the proteome, two major players of cell Zn^{2+} trafficking, and their metal binding and metal exchange reactions with different ligands were studied in this research.

Metallothionein, a small protein molecule rich in cysteine, binds to seven Zn^{2+} ions with a stability constant of about 10^{11}. A previous study, on the other

hand, has reported that one of the seven Zn^{2+} ions binds to MT with a relatively weak binding constant of 10^8. Purified Zn_7-MT extracted from rabbit liver under neutral conditions (pH 7) was reacted with different competing ligands and did not exhibit such a weak binding affinity to Zn^{2+} ion. Reaction of Zn_7-MT with strong acid resulted in the formation of MT* species, which was converted into Zn_7-MT* upon neutralization and reaction with 7 Zn^{2+} ions. Zn_7-MT* exhibited a reactivity of 1 Zn^{2+} per MT molecule with chelating agents of modest affinity for Zn^{2+} ion. Titration of Zn_7-MT with acid to pH 2 or below produced Zn_7-MT*, which exhibited a biphasic titration curve upon base titration demonstrating the binding of 1 Zn^{2+} ion per MT molecule weakly between pH 5 and 7. Because MT generally undergoes acidification during preparation, care must be taken to document which form of the protein is present in subsequent experiments at pH 7.

Zn-proteome as another significant player in Zn^{2+} trafficking was studied. It has been hypothesized that Zn-proteome has a measurable capacity to bind to metal ions such as Zn^{2+} or Cd^{2+} through metal ion exchange chemistry. To test this hypothesis the Zn-proteome of pig kidney LLC-PK_1 cells was reacted with competing ligands such as Zinquin acid (ZQ_{ACID}), TSQ, EDTA, and apo-MT, exhibiting negligible metal exchange reactivity. Reaction of Cd^{2+} or Zn^{2+} with the Zn-proteome shows that Cd^{2+} or Zn^{2+} associates with the proteome and almost stoichiometric amounts of Zn^{2+} become available to react with these chelating agents. The results strongly support the hypothesis that Cd^{2+} displaces Zn^{2+} from native proteomic binding sites resulting in the formation of Cd-proteome•Zn

species. Mobilized Zn^{2+} adventitiously binds to the proteome and becomes available to react with the metal binding ligands. Cd-proteome and Zn-metallothionein exchange metal ions that increase the possibility that this reaction may recover the functionality to the Cd-protein.

Proteome and supernatant from LLC-PK_1 cells were titrated with Zn^{2+} in the presence of zincon (ZI), a relatively weak competing ligand, to study the role of Zn-bound proteome in Zn^{2+} trafficking . Titration curves confirmed that a significant amount of unoccupied sites exist within the proteome to bind to metal ions. The smaller slope in the second part of the curve compared with the one obtained in the titration of ZI with Zn^{2+} along with the red-shifted absorbance spectrum indicate that the formed species are different form Zn-ZI species. We hypothesize that these species are ternary adduct complexes, proteome-Zn-ZI. Model proteins such as CA, BSA, and trypsin and the fluorescent ligand, TSQ, were employed to further investigate this hypothesis. BSA reacted with Zn-ZI and the resulted absorbance spectra exhibited a shift in λ_{max} from 620 nm to 640 nm. Furthermore, no Zn^{2+} was released from the product upon size exclusion chromatography, indicative of adduct complex formation. In contrast, two other proteins, carbonic anhydrase and trypsin did not show any reaction with Zn-ZI indicated by lack of change in λ_{max} in their absorbance spectra. The former is a Zn-protein without unoccupied Zn^{2+} binding sites and the latter has neither Zn^{2+} nor documented Zn^{2+} binding sites. Reaction of TSQ with Zn-ZI also resulted in an emission spectrum with a λ_{max} at 470 nm, characteristic of adduct complex formation.

TABLE OF CONTENTS

LIST OF FIGURES

LIST OF TABLES

LIST OF ABBREVIATIONS

AAS	Atomic Absorption Spectroscopy
ADH	Alcohol Dehydrogenase
ATPase	Adenosine tri-phosphatase
BSA	Bovine serum albumin
CAT	Catalase
DEAE	Diethylaminoethanol
DMSO	Dimethyl sulfoxide
DNA	Deoxyribonucelic acid
DTNB	5,5'-Dithiobis(2-nitrobenzoic acid)
EDTA	Ethylenediaminetetraacetic acid
EGTA	Ethylene glycol tetraacetic acid
FCS	Fetal calf serum
FluoZin-3	2-[2-[2-[2-[bis(2-oxido-2-oxoethyl)amino]-5-methoxyphenoxy]ethoxy]-4-(2,7-difluoro-3-oxido-6-oxo-4a,9a-dihydroxanthen-9-yl)anilino]acetate
GLUT	Sodium-independent cotransporter protein
GSH	Glutathione
GSH-Px	Glutathione peroxidase
HEPA	High-efficiency particulate absorption
HPLC	High-performance liquid chromatography
H_2KTS	3-ethoxy-2-oxobutyraldehyde bis(thiosemicarbazone)

ICP-MS	Inductively Coupled Plasma Mass Spectroscopy
kDa	kilodalton
LA-ICPMS	Laser ablation ICPMS
LD_{50}	Median lethal dose
LMW	Low Molecular Weight
mRNA	Messenger RNA
MT	Metallothionein
MTF-1	Metal transcription factor-1
NMR	Nuclear magnetic resonance
NSDS-PAGE	Native SDS-PAGE
NTA	Nitrilotriacetic acid
PAGE	Polyacrylamide gel electrophoresis
PBS ,DPBS	Dulbecco's Phosphate buffered Saline
PYR	pyrithione or 1-hydroxypyridine-2-thione
RNA	Ribonucleic acid
ROS	Reactive oxygen species
SDS	Sodium dodecyl sulfate
SGLT	Sodium-dependent glucose cotransporter protein
SOD	Superoxide dismutase
TCEP	Tris(2-carboxyethyl)phosphine
TNB	5-thio(2-nitrobenzoic acid)

TPEN	Tetrakis-(2-Pyridylmethyl)ethylenediamine
TSQ	6-Methoxy-(8-p-toluenesulfonamido)-quinoline
USP	U.S. Pharmacopeial convention
UV	Ultraviolet
ZFL	Zebrafish liver
ZI	Zincon
ZQ_{ACID}	6-Methoxy-(8-*p*-toluenesulfonamido) quinolinoxy acetate

ACKNOWLEDGEMENTS

First and foremost, I would like to express my deep gratitude to my supervisor, Dr. Petering, and appreciate his support during the years of my graduate study working under his supervision. Not only I learned from him specifically about biochemistry but also learned in general how to approach scientific problems. He has been always encouraging and supportive throughout these years and the time that I was writing this thesis.

I would also like to greatly thank Susan Krezoski, who was very helpful and gave effective suggestions whenever I had a question about the lab techniques needed to conduct my experiments. She has done very much for our laboratory during her more than 30 years of work and still after those dedicated years, she stops by sometimes to troubleshoot any lab problem that could not be fixed.

I would like to thank my thesis committee, Dr. Indig, Dr. Pacheco, Dr. Woehl, and Dr. Arnold very much for listening to my thesis proposal and giving very helpful suggestions. I also appreciate their careful reading of my thesis and their helpful comments on it. I very much appreciate their time being available and prompt via e-mail to set up the time of my defense.

Several people in our lab, former and current members, provided me with a pleasant environment for doing research and discussing different things from biochemistry and physics to philosophy and religion. I like to especially thank Jeffery Meeusen and Ujala Rana for being very good friends and being very helpful in the lab. I would like to thank WonRong who shared a lab with me during the first

year of my research. I also like to thank Reza, Kaniz, Drew, Brian, and Erick for being good friends throughout all these years.

Finally, my very special thanks are extended to my family especially my parents and my brother Reza that have been very supportive and caring in every day of my life

1. Introduction

1.1. Zinc, its importance, and regulation in living organisms

Metals play a crucial role in living systems. About 33% of all proteins have metals in their structure and 40% of enzyme-catalyzed reactions engage metals such as Fe, Zn, Mg, Mn, Ca, Cu, Co, Ni, Mo, W, Na, K, and V [1]. Iron, copper, molybdenum, and manganese are involved in many essential biological redox processes such as respiration, photosynthesis, and nitrogen fixation [2]. Like prokaryotes, Eukaryote cells rely on metals for many biochemical functions. For example, they are highly dependent on Zn containing proteins [3]. Among transition metals, Zn after iron is the most abundant transition metal in the human body and the most abundant metal in the brain [4]. It exists in more than 3000 proteins, which comprise about 10% of the human proteome [5]. These proteins include 397 hydrolases, 302 lygases, 167 transferases, 43 oxidoreductases, 24 lyases/isomeases, 957 transcription factors, 221 signaling proteins, 141 transport/storage proteins, 19 proteins with DNA-repair, replication and translation functions, and about 1000 Zn-finger and other Zn proteins with unknown functions. [6,7]. As such Zn is involved in a wide range of protein function; it participates in more than 300 cellular processes such as DNA transcription, protein synthesis, assisting in enzyme structural and catalytic activity, neurotransmission, intracellular signaling, and antibiotic activities [8,9]. Disruption of transition metal homeostasis in human is involved with pathological conditions in brain, liver and kidney. Fe, Cu, and Zn dysregulation has been hypothesized to be associated with

Alzheimer disease. [10-12]. Zn deficiency and dyshomeostasis are associated with chronic diseases such as metabolic syndrome, diabetes and related complications, bone loss, growth retardation in young children, and neurological and behavioral problems [13-16].

Zn^{2+} binds to proteins with a predominant tetrahedral coordination that can be in the form of mononuclear complexes or clusters. Examples of mononuclear complexes and Zn clusters are seen in enzymes such as alcohol dehydrogenase (ADH) and metallothionein, respectively [17]. Zn^{2+} exhibits both catalytic and structural roles in Zn proteins. Diverse ligand-Zn interactions in the catalytic or structural sites of proteins play significant roles in Zn enzyme function or Zn protein structure and function. Ligands interact with the metal ion in two coordination shells. In the first shell S from cysteine, N from histidine, O from aspartate, glutamate or water directly interacts with the metal ion. In the second shell, hydrogen bonding of Zn-bound ligands with the surrounding amino acids plays a crucial role for the stability of the Zn^{2+} ligand complex. **Figure 1.1.** shows different modes of interaction between Zn^{2+} and ligands in the first coordination shell [2, 18]. All of these interactions may include formation of Zn bridges between two ligating groups. In case of cysteine ligand 1, 2, 3 zinc bridges might form; metallothionein clusters (Zn_3S_9 and Zn_4S_{11}) are examples involving formation of 2 and 3 Zn bridges. Metallothionein and its clusters will be further discussed in chapter 3. **Figure 1.2.** illustrates how the second coordination shell with the help of hydrogen bonding makes a stable complex of Zn^{2+} in human carbonic anhydrase II. In the first shell Zn^{2+} binds in a tetrahedral coordination to N of 3 imidazole groups from

His (94, 96, and 119) and O from a water molecule. In the outer shell 3 His and O-H make hydrogen bonds to the surrounding amino acids and the protein backbone [2].

In Zn enzymes the necessity for flexibility of the the catalytic site toward substrate leads to the more dynamic coordination of Zn by ligands from side chains of the protein. Therefore, for mononuclear Zn enzymes one or two small molecules (e.g. H_2O from the surrounding solution) ligate Zn^{2+}. The rest of tetrahedral coordination is formed by amino acid side chains (Cys, His, Glu, Asp) ligands. Furthermore, such coordination environments might contribute to the reactivity of these sites with other metals and therefore metal exchange [2]. On the other hand, in structural Zn^{2+} binding sites there is a full tetrahedral coordination of Zn^{2+} by protein side chains that produces more rigidity and stability in the protein structure. These coordination sites commonly involve S_4 (4 cysteine sulfhydryl groups), S_3N (of 3 cysteines and 1 histidine), and S_2N_2 (of 2 cysteines and 2 histidines) around Zn^{2+}. None of these general patterns negates the existence of fully coordinated Zn^{2+} with catalytic activity or partially coordinated Zn^{2+} with structural properties. Examples of these exceptions are tetrathiolate coordinated Zn^{2+} in Ecoli ada protein and structural Zn^{2+} in hexamer insulin. The former has one loose thiolate that contribute to DNA repair (catalytic) [19] and the latter is coordinated with 3 histidine side chains [20].

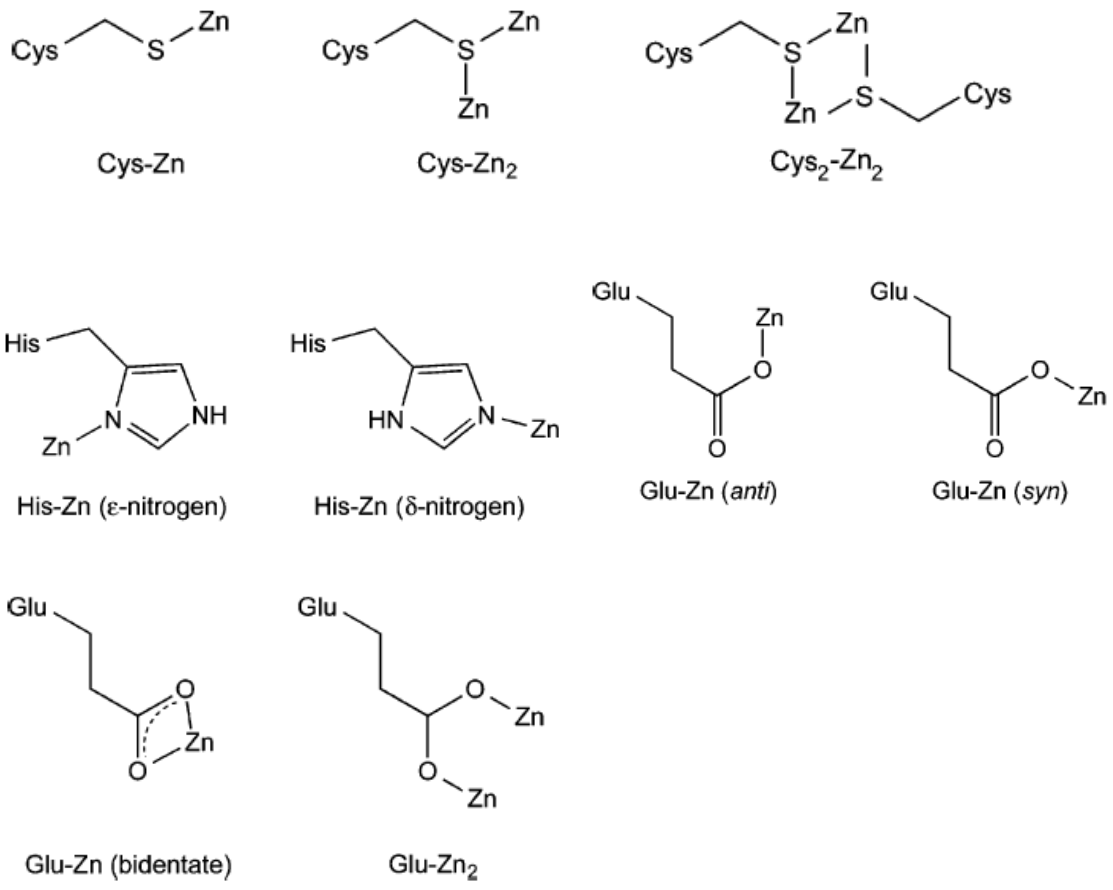

Figure 1.1. Interaction of Zn with ligands. The first row shows the interaction of S from cysteine as the electron donor to Zn^{2+}. In the second and third rows the modes of interaction of N from imidazole of histidine and O of glutamate or aspartate (not shown) with Zn^{2+} are displayed (lone pair electrons are not shown) [2, 18].

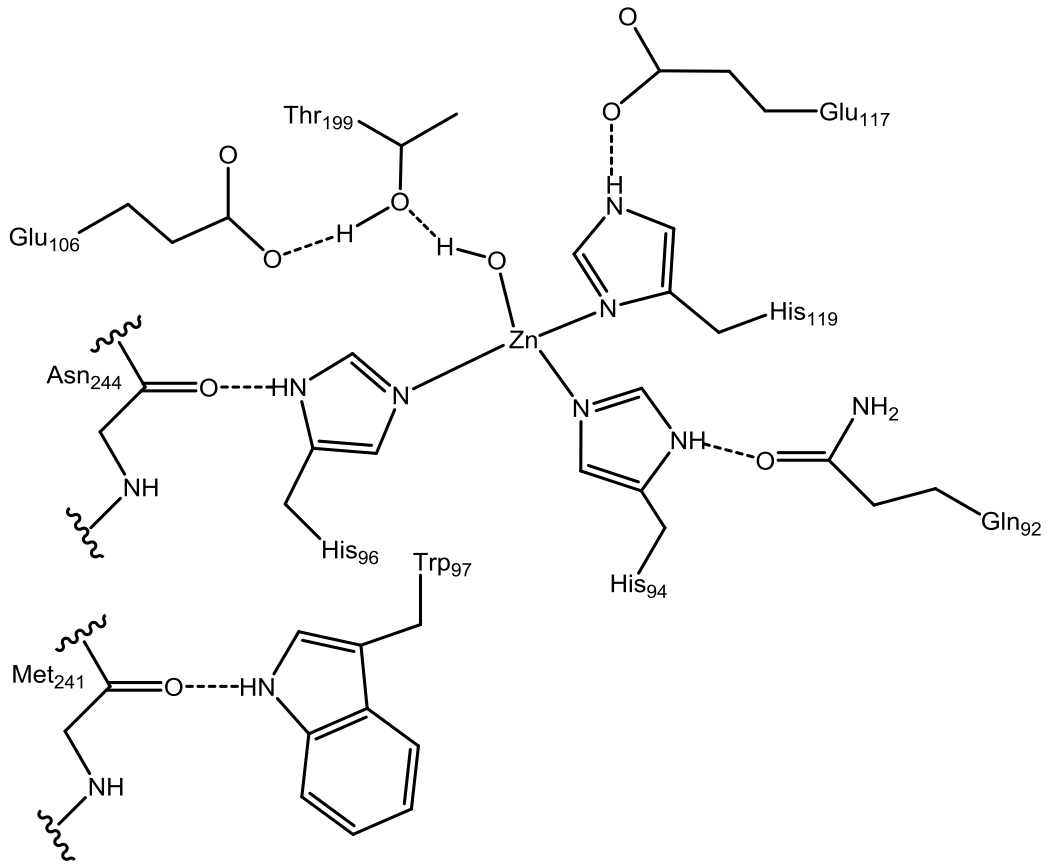

Figure 1.2. Interaction of Zn^{2+} and chelating ligands in human carbonic anhydrase II. First and second coordination shells are shown [2].

1.2. Metal ion trafficking in cells

The combination of chemical reactions in living organism that leads to cellular influx, distribution, and efflux of metal ions is defined as metal ion metabolism or trafficking. Binding of metals by ligands, which are electron donors and compete with each other for binding, facilitates metal ion trafficking. There are several types of reactions involved in metal ion trafficking that can be listed as metal-ligand binding, ligand substitution, metal exchange, and adduct formation. Ligands are usually chemical groups on proteins and nucleic acids bearing negative charges (phosphate on DNA backbone) or electron lone pairs on donor atoms N, O, and S (amine, imidazole, carboxyl, and thiol groups of proteins or N and O elements of DNA bases). Influx of the metal ions to the cell occurs through different mechanisms such as facilitated diffusion (as the concentration of metal outside the cell may be greater than that in the cytosol [17]) involving various metal transporters [21-23].

Metal ions can exist in cytosol in three major forms: tightly or adventitiously bound to ligands on proteins or other macromolecules, bound to small molecules (e.g. glutathione), and ligated only by water molecules (known as free metal ion). Metal ions bound in kinetically labile forms play a significant role in metal trafficking within the cytosol. Once the metal reaches the cytosol, it binds to ligands in the above mentioned forms. During the last two decades, attempts have made to determine the concentration of labile metals in cells by either measuring them directly or calculating their concentration using their binding constants to

biomolecules [17]. **Table 1.1** summarizes the labile concentration of metals in eukaryotic cells.

Table 1.1. Estimated concentration of labile metal ions in eukaryotic cells [17].

Metal ion	Labile ion conentration	Organism/Cell type
Potassium	10^{-1} M	
Sodium	10^{-2} M	
Magnesium	10^{-3} M	
Iron	5×10^{-6} M	Rat hepatocyte (cytosol)
	11.8×10^{-6} M	Rat hepatocyte (nucleus)
	9.8×10^{-6} M	Rat hepatocyte (mitochondria)
Manganese	10^{-7} M	
Calcium	$1\text{-}5 \times 10^{-8}$ M	Eukaryote (cytosol)
Zinc	10^{-11} M	
	10^{-12} M	Eukaryotic cells
	$< 10^{-9}$ M (none)	E. coli (bacteria)
Copper	10^{-15} M	
	$< 10^{-18}$ M	Yeast

Metal trafficking not only contributes to the regulation and distribution of vital metals in living cells but also to the toxicity of heavy metal ions such as Cd^{2+}, Pb^{2+}, and Hg^{2+}. The therapeutic effect of the complex cis-diamminedichloro-Pt (II) also stems from the metal ion trafficking principle.

Metal ion trafficking in living systems is initiated by metal ions binding to ligands as shown in reaction (1).

$$M + L \rightleftharpoons M\text{-}L, \qquad K, k_1, k_{-1} \qquad (1)$$

In this equation *K* is the chemical equilibrium representing the thermodynamic stability of the product complex M-L; k_1 and k_{-1} are rate constants for the formation and decay of the product complex, respectively. L is the ligand, which binds to the metal ion (M). Another phenomenon that is involved in metal ion trafficking is the ligand substitution of the complex M-L that takes place according to the following chemical equation.

$$M\text{-}L + L' \rightleftharpoons ML' + L \qquad (2)$$

The sequence of metal-ligand binding and ligand substitution in cellular metal ion trafficking can be summarized as binding of metal ion to protein transporters in cell membrane, substitution of protein transporter with components of the cytoplasmic or nuclear proteome or complement of small molecules, and finally ligand substitution involving the cytoplasmic proteome and metal-transporter proteins responsible for metal efflux.

$$M + Transporter_o \rightleftharpoons M{\bullet}Transporter_o \rightleftharpoons M\text{-}Transporter_i \qquad (3)$$

$$\text{M-Transporter}_i + L_1 \rightleftharpoons ML_1 + \text{Transporter}_i$$

$$ML_1 + L_2 \rightleftharpoons ML_2$$

.
.
.

$$ML_n + \text{protein (binding site)} \rightleftharpoons \text{M-protein}$$

With large binding constants for seven Zn^{2+} ions and kinetic lability of its two thiolate clusters, metallothionein plays a major role in Zn^{2+} trafficking. Metallothionein is also a major protein to traffic Zn^{2+} between cytoplasm and the nucleus [21]. Studies on hepatocytes of Zn^{2+} injected rats has shown a high Zn^{2+} uptake by their nuclei [24]. Because of low localization of Zn^{2+} transporters to the nuclear membrane and small concentration of free Zn^{2+} in the cytoplasm, neither Zn^{2+} transporters nor diffusion could be candidates for that observation. Further study by other groups has shown that MT is actually responsible for the high zinc uptake by the nuclei [25-28].

Metal-ligand binding and ligand substitution comprise the major chemical reactions in normal metal ion trafficking. In addition, metal ion exchange and adduct formation can play major roles in special conditions such as exposure of cells to toxic metals and ligands. In metal exchange reactions, metals compete to bind to the ligand via two groups of reactions shown as following.

$$M_1\text{-}L + M_2 \rightleftharpoons M_2\text{-}L + M_1 \quad K, k_1, k_{-1}$$

$$M_1L_1 + M_2L_2 \rightleftharpoons M_2L_1 + M_1L_2 \qquad (4)$$

The affinity of a ligand toward a specific metal (*K*) determines formation of that metal complex assuming the kinetics of reaction are favorable. Under normal

conditions, the specificity of the ligand, which is determined by the kinetics, energetics, and mechanism of the reaction, insures that metal ions and ligands avoid reactions unrelated to metal trafficking. On the other hand, in case of toxicity; ligands might prefer some toxic over essential metals leading to cell injury.

Another form of ligand-metal binding involves adduct formation. In this type of interaction a ternary complex forms among metal and two ligands. The following chemical equation represents adduct formation among a metal M, ligand L, and ligand L':

$$M\text{-}L + L' \rightleftharpoons L'\text{-}M\text{-}L \qquad (5)$$

One ligand could be the metalloprotein and the other ligand, which should be at least bidentate, may be an internal small molecule such as glutathione (GSH) or any externally administered ligand.

1.3. Cadmium trafficking and toxicity

Cadmium (Cd) is a heavy metal and one of the major pollutants on earth. Cd is widely distributed within the earth crust, but its natural concentration in water, soil and atmosphere that mainly originate from weathering of earth minerals, forest fires, and volcanoes is too low to be a threat to living systems [29]. During the last century due to the human industrial and agricultural activities, the concentration of toxic metals in the environment has been increasing. Cigarette smoke, food, compounds used in electronics, pigments, alloys, and rechargeable Ni-Cd batteries are the major sources of exposure to Cd for humans [30]. In particular, Cd can be accumulated in some certain foods such as rice [31], fish [32], and leafy

vegetables [29, 33, 34]. Cd is poorly taken up by the digestive tract; however, its absorption is efficient in lungs with 50% uptake of inhaled Cd. Therefore, most of human exposure to Cd is either through smoking or in the workplace [35, 36].

After uptake, Cd^{2+} is transported and accumulated in the liver, kidney, and some other organs, where it causes adverse effects [37-40]. The biological half-life of Cd^{2+} in human body is about 20 years [41]. Cd^{2+} induces reactive oxygen species (ROS eg. O_2^-, H_2O_2, OH) that result in oxidative stress on normal physiological functions in the body [42, 43]. Cd^{2+}-induced ROS damages DNA, proteins and lipid structure and function, which leads to cell apoptosis [44-47]. It also decreases the concentration of glutathione (a small tripeptide with a SH group) resulting in the increase of radical species and carcinogenesis [48]. Cd^{2+} accumulated in the liver and kidney is mostly bound to metallothionein [49-54]. The half-life of MT is variable - 18-20 hours for Zn-MT and 3 days for Cd-MT in rodents but also depends on the organism, organ, and age [55-59].

MT protein synthesis is induced in animals with low doses of Cd^{2+} [60, 61], Zn^{2+} [62, 63], and other metal ions as well as a variety of organic compounds including ethanol [64, 65], and diethylmalate [66, 67]. The transcription factor MTF1 is responsible for the induction of MT mRNA upon increase of intracellular concentration of heavy metal ions such as Zn^{+2}, Cd^{2+}, and Cu^{1+}[68-70].

The well-known and probably the major role of MT is to protect cells against toxic metal ions especially Cd^{2+}. Studies with mouse kidney epithelial culture cells have shown that there is a strong correlation between MT levels and resistance to Cd^{2+} [71]. MT induction also protects against lethal and hepatotoxic levels of Cd^{2+}

[72]. High level of MT in the livers of newborn animals is also correlated with their resistance to Cd^{2+}-induced hepatotoxicity [73, 74] The recombinant sheep gene MTII inserted into E. Coli protects against elevated levels of toxic metals including Cd^{2+} [75]. MTI/II null mice display high susceptibility to Cd^{2+} toxicity such as hepatotoxicity, hematotoxity, immunotoxicity and bone toxicity [76]. Median lethal dose (LD_{50}) of Cd^{2+} in MT-null mice decreased seven times in comparison to that in wild-type mice [77].

The mechanism of Cd^{2+} toxicity has been studied for many years. Petering et al. investigated the mechanism of Cd^{2+} nephrotoxicity using mouse and pig kidney cell models and have proposed the only cause-effect mechanism linking Cd^{2+}-binding sites to toxicity [78-80]. Upon exposure of kidney cells to micromolar concentrations of Cd^{2+}, they observed down regulation of sodium-dependent glucose cotransporter protein (SGLT) and sodium-independent cotransporter protein (GLUT) and their corresponding mRNAs [81-83]. After removal of Cd^{2+} from cell culture media, they observed that transcriptional depression was retained for at least 48h. In other studies, it was demonstrated that Zn_3-Sp1, a common Zn-finger transcription factor, is involved in down regulation of SGLT1 and 2 upon binding to Cd^{2+} [80, 84]. It was also found that Cd^{2+} binds to the Zn-finger motif of Zn_3-Sp1 with a binding constant of 1 order of magnitude higher than that for Zn^{2+} [80].

In previous studies, Wong and Petering observed the similarity in Cd- and Zn-finger stability constants in transcription factor IIIA (TFIIIA) and one of its fingers [85]. Krepkiy and Petering compared the NMR spectrum of a Cd- and Zn-finger

[86]. While generally similar, Cd^{2+} binding perturbed the conformation of the ligating groups around Cd^{2+}. This shift, in turn, changes the orientation and position of the amino acids in the recognition helix with regard to the complementary DNA base-pair edges and reduces the binding affinity of Cd^{2+}-finger to its cognate DNA. Applying their results to Cd_n-Sp1 reduction in the binding of the transcription factor to DNA leads to the decrease in mRNA biosynthesis and down regulation of transporters SGLT and GLUT, hence nephrotoxicity. In their chemical mechanism, Cd^{2+} displaces Zn^{2+} from a protein binding site to cause toxicity as in reaction 7.

Wang et al have reported that rPT cells exposed to Cd^{2+} display elevation of ROS and free calcium and reduction of mitochondrial membrane potential, intracellular GSH concentration, and enzymatic activities of Na+, K^+-ATPase, Ca^{2+}-ATPase, glutathione peroxidase (GSH-Px), catalase (CAT), and superoxide dismutase (SOD) [87]. Cd^{2+} renal toxicity, pancreatic toxicity and hepatotoxicity at the cellular and molecular levels have been attributed recently to production of ROS species and mitochondrial dysfunction [30, 88, 89].

In recent years a phenomenological mechanism that has been proposed and studied is the interference of Cd^{2+} with Zn^{2+} uptake [90-92] and the Zn proteome [93, 94]. From studies of the levels of intracellular ROS, antioxidants, enzyme activities, and gene expression in a Zebrafish liver cell line (ZFL), Zhu et al. have concluded that toxicity of Cd^{2+} is at first due to its binding to the proteome and interference to many biological activities rather than induction of ROS. Indeed, ROS induction might be one of the secondary phenomena within the cascade of reactions resulting from Cd^{2+} binding to the proteome. Their proteomic analysis of

Cd^{2+}-exposed ZFL cells showed that 34% of differentially expressed proteins were metal binding proteins and 12% were enzymes, which were not involved in redox reactions. Twenty percent of analyzed proteins, which exhibited metal ion binding properties, were transcription factors, 11% were transporters, and 9% were involved in signaling pathways. The carcinogenic effect of Cd has also been attributed to the substitution of Cd^{2+} for Zn^{2+} in Zn-binding proteins that are responsible for nucleotide excision repair, base excision repair, and mismatch repair [95]. Does Cd^{2+} react with enzymes involved in redox reactions, proteins in the mitochondria membrane, or other Zn-binding proteins? The questions remain; where are those binding sites in the proteome, which react with Cd^{2+} and what are the roles of Zn^{2+} in those reactions.

From cellular and molecular perspectives we and others hypothesize that Cd^{2+} first binds to the proteome of the cytosol and other compartments then after inducing the biosynthesis of metallothionein, it becomes bound to it [95-97]. Hypothetical Cd^{2+} trafficking can be summarized in the following reactions:

$$Cd^{+2}_{(out)} \rightleftharpoons Cd^{+2}_{(in)} \quad (6)$$

$$Cd^{+2}_{(in)} + (Zn\bullet)\text{proteome} \rightleftharpoons Cd\bullet\text{proteome} + (Zn^{2+}) \quad (7)$$

$$Cd\bullet\text{proteome} + (\text{apo-or Zn-})MT \rightleftharpoons \text{Cd-MT} + \text{proteome} + (Zn^{2+}) \quad (8)$$

$$\text{Cd-MT} + \text{Zn-MT} \rightleftharpoons \text{Cd, Zn-MT} \quad (9)$$

After transport into the cytoplasm (reaction 6), Cd^{2+} binds to the proteome either tightly through reaction with native metal (Zn) binding sites or adventitiously to other proteins (reaction 7). Transcription factors and regulatory proteins may react

with cadmium leading to the induction of MT mRNA transcription and apo-MT translation [69, 70, 98]. Upon increase in the concentration of apo-MT, reactions (7)-(9) are shifted to the right with a higher production of Cd-MT and Cd,Zn-MT. As more Cd^{2+} binds to MT, enough apo-MT is biosynthesized to exceed the amount necessary for Cd^{2+} binding. As a result Cd_n, Zn_{7-n}-MT results through exchange of Zn^{2+} and Cd^{2+} between Zn_7-MT and Cd_7-MT.

$$(7\text{-}n)Zn_7\text{-MT} + nCd_7\text{-MT} \rightleftharpoons 7Cd_n, Zn_{7-n}\text{-MT} \qquad 1 \leq n \leq 7 \qquad (10)$$

1.4. Zn fluorophores and their application in studying Zn-proteome

Detection and studying metals especially heavy metals, both free or in metalloproteins, requires sensitive (as metals exist in trace concentrations) and specific analytical methods. Zn^{2+}, which has a filled set of d orbitals, cannot be detected and measured using usual spectroscopic methods such as absorption spectrophotometry, nuclear magnetic resonance spectroscopy or electron spin resonance spectroscopy. Fluorescence methods, on the other hand, are commonly highly sensitive and may be specific, making them suitable for metal detection and metalloprotein imaging in vitro and in vivo [99, 100]. Zn fluorophores have been widely synthesized and used to study Zn^{2+} and its physiological properties in living cells and tissues [99, 101-104].

Emily L. Que et al have recently reviewed Zn sensors. **Figure 1.3** shows some of the most commonly used Zn fluorophores. Fluorescence properties of these Zn flurorophores are summarized in **Table 1.2** [99]. Reagan McRae et al have also recently reviewed in situ imaging of metals in cells and tissues [105].

The first fluorophores used to selectively detect Zn^{2+} were quinoline-based fluorophores [105]. Mahannad and Houck used 8-hydroxy–quinoline to detect Zn^{2+} in blood plasma and urine [106]. The problem with 8-hydroxy-quinoline was that although it exhibited high fluorescence with Zn^{2+}, it showed only moderate Zn^{2+} specificity and also emitted elevated fluorescence in presence of Mn^{2+} and Ca^{2+} [107]. Different sulfonamide derivatives of 8-amino-quinoline that affected more specific detection of Zn^{2+} were studied by russian biochemists Toroptsev and Eschenko [108-111].

Among those compounds, 6-methoxy-(8-*p*-toluenesulfonamido)-quinoline (TSQ) gained popularity after Frederickson CJ et al. introduced a histochemical method to visualize Zn^{2+} in the brain. They compared four quinoline-based fluorophores in their study and found TSQ to be the most suitable one [112, 113]. TSQ was also the first fluorophore to specifically detect Zn^{2+} in presence of Mn^{2+} and Ca^{2+}. It demonstrated 100 fold increase of fluorescence upon reacting with Zn^{2+}. Since then TSQ has been actively used for imaging Zn^{2+} in cells and tissues [114-117].

Despite all mentioned advantage of TSQ, it has some disadvantages such as low water solubility and low cell membrane permeability. To improve water solubility and cell membrane permeability of TSQ, methyl and carboxylate groups were added to it and the newly synthesized fluorophores: [2-methyl-8-*p*-toluenesulfonamido-6-quinolyloxy]aceticacid and ethyl[2-methyl-8-*p*-toluenesulfonamido-6-quinolyloxy]acetate were designated as Zinquin Acid

(ZQ_{ACID}) and Zinquin Ester (ZQ_{Ester}). ZQ_{ACID} has more water solubility while ZQ_{Ester} exhibits more cell membare permeability.

ZQ has high Zn^{2+} specificity and low toxicity, which makes it a suitable fluorophore to study intracellular chemistry of labile Zn^{2+}. ZQ was actually the first Zn flurophore that was used for imaging Zn^{2+} in living cells [118]. ZQ_{ACID} and ZQ_{Ester} has been intensively used to visualize and detect Zn^{2+} and Zn-proteins both in vivo and in vitro [112, 119-122]. ZQ has been used to study Zn^{2+} distribution among different compartments in cortical neurons [123], to detect Zn^{2+} in glutameric vesicles of the brain [124], in apoptosis studies [122, 125], in pancreatic carcinogenic studies [126], and in vitro studies on Zn^{2+} in normal human prostate cells [127]. Petering et al. have used ZQ_{Acid} and ZQ_{Ester} in different invivo and invitro studies to study mechanism of Zn^{2+} imaging in cells and tissues [128, 129].

TSQ and ZQ are bidentate ligands and bind to Zn^{2+} through quinoline and sulfonamide nitrogens [114, 130]. Therefore, the stoichiometry of ligand to metal binding is 2:1.

$$L + Zn^{2+} \rightleftharpoons ZnL_2 \qquad (L= TSQ \text{ or } ZQ) \qquad (11)$$

$Zn(TSQ)_2$ or $Zn(ZQ)_2$ emits visible fluorescence light with a λ_{max} at 490 nm upon excitation by UV light with the wavelength 365 nm. Traditionally the fluorescent image obtained from cell or tissue upon their reaction with Zn fluorophores was assumed to originate only from free Zn^{2+}, but recently Petering and Nowakowski. have demonstrated that fluorescence emission, depending on the properties of the sensor, can come from chelatable and adductable Zn^{2+} [131]. It has been though that there is a possibility that the fluorophore sequesters metals from

metalloproteins and therefore interferes with physiological reactions under in vivo studies [114]. Upon reaction of the bidentate fluorophore with metalloprotein two possible reactions may occur:

$$\text{Zn-protein} + 2L_{\text{Bidentate}} \rightleftharpoons \text{apo-protein} + ZnL_2 \quad (12)$$

$$\text{Zn-protein} + 2L_{\text{Bidentate}} \rightleftharpoons \text{L-Zn-protein (adduct)} \quad (13)$$

In the first reaction metal ion is sequestered by the ligand and the free complex ZnL_2 is formed that gives a fluorescence spectrum with a λ_{max} at 490 nm. In the second reaction an adduct (ternary) complex forms between metalloprotein and the bidentate ligand, which gives a fluorescence spectrum with a λ_{max} blushifted to 470 nm. A spectrum with a λ_{max} at 470 nm and a shoulder at λ_{max} 480 nm indicates occurrence of a mixture of both above-mentioned reactions. Fluorophores ZQ_{ACID} and TSQ have been used in this project to study the effect of Cd^{2+} on the distribution of chelatable and adductable Zn^{2+} in the proteome.

Table 1.2. Fluorescence properties of some common Zn fluorophores [132, 133].

Probe	Kd for Zn^{2+}	$\lambda_{exitation}$, nm, free(Zn^{2+})	$\lambda_{emission}$, nm, free(Zn^{2+})	Cellular/membrane partition
FluoZin-1	7.8 μM	491	520	Impermeable, permeable ester
FluoZin-2	2.1 μM	492	521	Impermeable, permeable ester
FluoZin-3	15 nM	492	517	Impermeable, permeable ester
RhodZin-1	23 μM	548	589	Impermeable, permeable ester
RhodZin-3	65 nM	545	575	Impermeable, permeable ester
FuraZin	3.4 μM	378 (330)	550 (550)	Impermeable, permeable ester
TFLZn		360	498	permeable
	0.55 pM	330	553 (528)	permeable
		345	448	permeable
	0.5 μM	343	450	
TSQ	10 nM[b]	365	485	permeable
ZQ_{ACID}	85 ± 15 nM[a]	368	490	Impermeable, permeable ester
NG-DCF	1 μM[b]	505	530	Impermeable, permeable ester
NG-PDX	30-40 μM	491	520	Impermeable, permeable ester

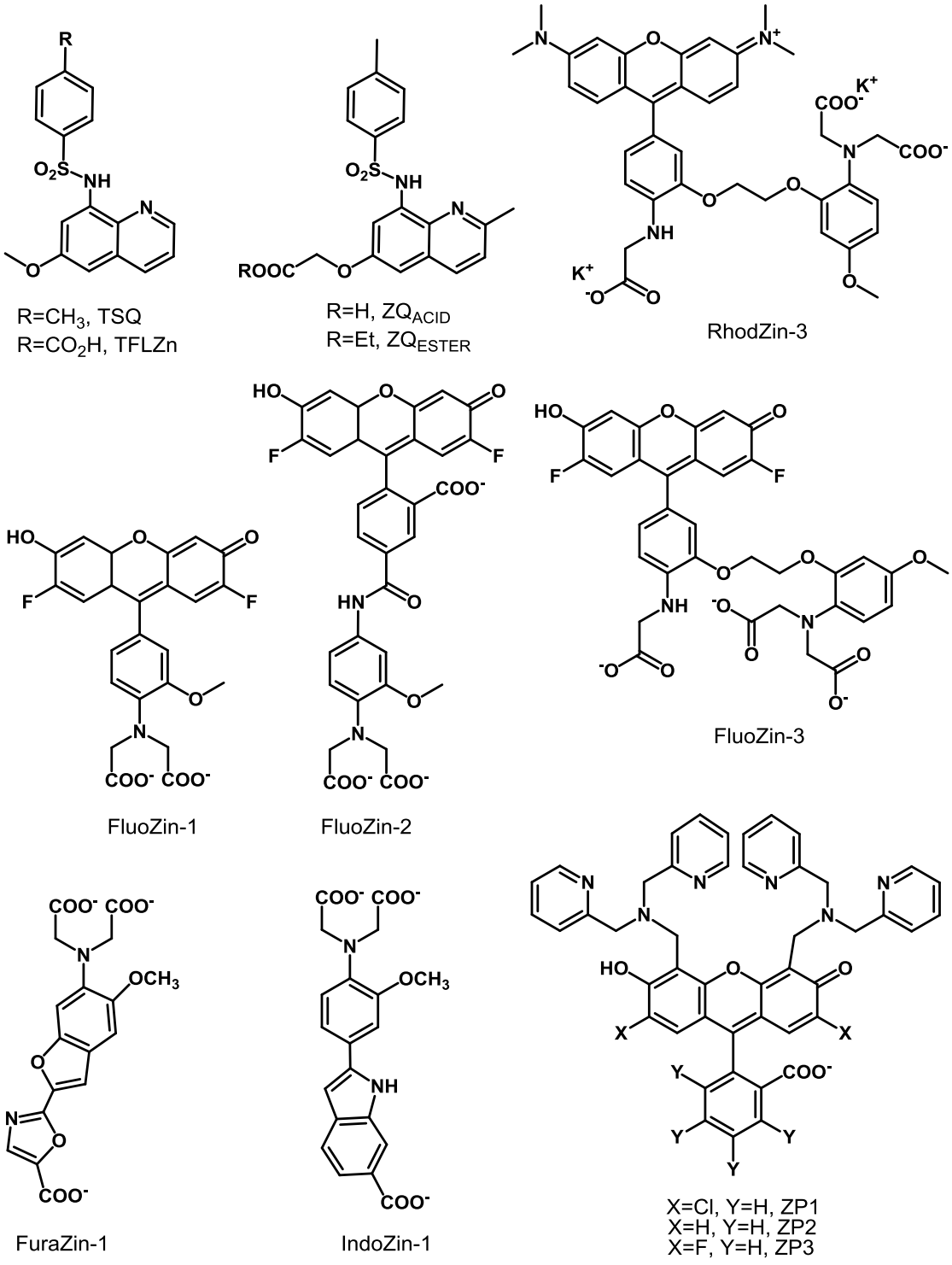

Figure 1.3. Structures of Some Common Zn Fluorophores [99].

2. Methods

2.1. Isolation, purification, and characterization of rabbit liver metallothionein

2.1.1. Preparation of Rabbit Liver

Female New Zealand white rabbits (2.2-2.7 kg) purchased from New Franken Research Rabbit Inc. were injected with 2 mL 0.15 M sterile $ZnSO_4$ in saline (pH 6.0) every 24 hours for 8 consecutive days. The rabbits were anaesthetized in the necropsy room, at least 6 hours after the last Zn-injection by an injection of Xylazine (95mg/kg) and ketamine (35mg/kg) followed by a lethal dose of sodium pentobarbital (120 mg/kg) into the heart. The livers were removed immediately from the rabbits and washed with cold saline to remove excess blood, divided into about 20 g samples and stored at -80℃ until further use.

2.1.2. Isolation of Zn_7-MT from liver

About 20 g of frozen rabbit liver were thawed and minced into small pieces. Then, 200 ml homogenizing buffer was prepared in 5 mM Tris-Cl buffer solution at pH 8.0 containing 0.25 M sucrose, 0.01 M 2-mercaptoethanol and 200 µl of phenyl-methyl-sulphonyl fluoride (PMSF)) saturated solution. Tissue was divided into two portions and each portion was mixed with 15 ml cold and degassed homogenizing buffer. PMSF-serine protease inhibitor- saturated solution was prepared by dissolving excess PMSF powder in 2 ml USP grade (200 proof) ethanol. 2-Mercaptoethanol and PMSF were added to the homogenizing solution just before mixing the minced liver in it. The mixture was homogenized using a Potter

Helvansen homogenizer, 50 ml size, for 10 cycles per liver portion. The homogenate was centrifuged in the Sorvall highspeed centrifuge in the SS34 rotor at 20,000 rpm (48000 g) and the Beckman L-70 ultracentrifuge in the 70TI rotor at 31,000 rpm (75000g) for 20 and 60 minutes, respectively. The final supernatant was divided in half and loaded onto two 2.7×85 cm Sephadex G-75 columns equilibrated with degassed and cold 20 mM Tris-Cl, pH 7.4, and 5 mM 2-mercaptoethanol and eluted with a flow rate of 0.5-0.7 ml/min. at 4℃. Eluted fractions in the high molecular weight band coming before hemoglobin were collected, referred to as rabbit liver proteome, and stored at –80 ºC. Fractions (4 ml) of MT were collected after almost the red-color band of hemoglobin was eluted. The MT fractions were located by measuring the Zn^{2+} profile of the eluate. Altogether about 1-1.5 liters of MT solution were pooled.

2.1.3. Separation of MT1 and MT2

The two isoforms, MT1 and MT2, were separated by anion exchange HPLC using a Protein-Pak^{TM} DEAE 5PW 7.5×75 mm column purchased from Waters. The pooled MT solutions were loaded onto the column with a flow rate between 1-1.5 ml/min. Eluted fractions were analyzed to check for the minimum release of Zn or MT at this stage. MT was eluted with a gradient of 5-300 mM Tris-Cl at pH 7.4 in 1ml fractions. MT-containing fractions were determined by measuring the concentrations of Zn^{2+} and thiol as described below and then stored at -20°C for future use.

2.1.4. Preparation of modified metallothionein (MT^*)

The reaction of Zn_7-MT with H^+ was studied. Concentrated HCl (12 N) was added to 1–2 mL of Zn_7-MT to a final concentration of 1.2 M HCl, reducing the pH to −0.4. The solution was left at low pH for 20 min and then neutralized to pH 7.5 by titration with 10 N KOH. In other experiments a range of hydrogen ion concentrations was used to test the pH dependence of the reaction.

2.1.5. Acid-base titration of metallothionein

Metallothionein in 5 mM Tris buffer solution, pH 7.6, KCl 0.1 M, was titrated with HCl solutions of different concentrations down to pH about 2 and then back titrated with NaOH solutions with similar concentrations to those of HCl solutions. Different concentrations of HCl or NaOH were used to minimize the volume change and to optimize the pH change of solution with regard to UV absorption of MT at 215 nm upon each acid addition. Absorbance at 215 nm was measured in 1cm-wide quartz cuvette for each pH point. Titration curves for the forward and backward titrations were obtained by plotting absorbance versus pH.

2.1.6. Preparation of apo metallothionein

Apo metallothionein was prepared by acidifying Zn_7-MT at pH 2 or 3 depending on the future reaction it would be used for. After acidification, the sample was chromatographed over a 0.5 cm x 25 cm sephadex G-15 column equilibrated with degassed 0.01 M HCl and the absorbance of 2-ml fractions was measured in the spectrophotometer at the wavelength of 220 nm to locate apoMT

fractions. 2 to 3 fractions with the highest apoMT concentration were pooled and immediately stored in an anaerobic chamber. Apo MT was characterized by its absorbance at 220 nm and SH and Zn analysis.

The anaerobic chamber was evacuated and purged with nitrogen gas in an anaerobic train consisting of vacuum and Nitrogen-purging lines. An Oxygen scrubbing catalyst from BASF was used (at 200°C) to remove any oxygen impurities from N_2. The BASF catalyst removed oxygen by reaction of Cu at the surface of its beads at high temperatures about 200-240°C. BASF catalyst was occasionally regenerated using H_2 and N_2 at high temperatures.

2.1.7. Characterization of Zn_7-MT

Isolated MT was characterized by measuring the metal and sulfhydryl contents in the sample. The metal concentration was obtained by atomic absorption spectrophotometry and the sulfhydryl concentration was determined using the 5,5-dithiobis-2-nitrobenzoic acid (DTNB) assay [134]. The concentration of MT was also determined spectrophotometrically at 220 nm (ε_{220}=1.59 x 10^5 $M^{-1}cm^{-1}$) [135]. The ratio of sulfhydryl to Zn in the purified samples was typically 2.9±0.1, compared to the theoretical ratio of 20 SH/7 Zn (2.86).

2.1.8. Characterization of Zn_7-MT and Zn_7-MT* using various competing ligands

H_2KTS, ZI, NTA, and FluoZin-3 were used to study the Zn^{2+} binding properties of metallothionein. All of these ligands form one-to-one complexes with Zn^{2+} [136]. Zn-KTS has a pH dependent log stability constant of 5.9 at pH 7.4 and

a maximum absorbance at 417 nm with extinction coefficient of 11,300±100 M^{-1} cm^{-1}, as determined by titration of the ligand with a standard solution of $ZnCl_2$ [137]. Nitrilotriacetic acid (NTA) has an intermediate Zn(II) binding affinity. The log apparent stability constant of Zn-NTA at 25º C, pH 7.4, and in 0.1 M KCl has been reported as 8.32 [138]. Zn-ZI complex displays a maximum absorbance at 620 nm with an extinction coefficient of 23,200 M^{-1} cm^{-1}. Its log apparent stability constant is 4.9 [139]. FluoZin-3 is a Zn^{2+} responsive fluorophore with a related log stability of 7.8 [140].

2.1.8.1. FluoZin-3

Native and non-native, modified metallothionein (1.6 µM protein), and $ZnCl_2$ (1.54 µM) were reacted with FluoZin-3 (5 µM) in 50 mM Hepes buffer, 50 mM KNO_3, pH 7.4 anaerobically. Fluorescence intensity was measured at 517 nm with excitation at 492 nm. In later confirmatory reactions, TCEP, a non-thiol reducing agent, substituted for anaerobiosis.

2.1.8.2. H_2KTS

H_2KTS dissolves in Tris-buffer very slowly; so it was first dissolved in ether in a 10- ml Pyrex test tube and vigorously shaken until it was slowly extracted into the buffer phase; the ether vapor was removed during shaking. The rendered ether was then evaporated with heating between 30-40°C. The concentration of H_2KTS was determined spectrophotometrically by titrating an aliquot of its solution with a Zn standard solution. H_2KTS was reacted with MT and MT^* anearobically to detect

the modestly bound Zn in the modified protein. Reaction products for each reaction were monitored in the spectrophotometer at 620 nm.

2.1.8.3. NTA

Modified and normal metallothinein were also reacted with the NTA ligand anaerobically or in presence of TCEP and the product solution was loaded on a G-75 column. G-75 column was previously run under degassed 20 mM Tris-HCl buffer, pH 7.4 for at least 2 times of its bed volume. Fractions were analyzed for Zn, SH and protein concentrations.

2.2. Size exclusion chromatography (gel chromatography)

G-75, G-25, and G-15 size exclusion chromatography beads were purchased from GE Healthcare Bio-Sciences AB. Beads were soaked in 20 mM Tris buffer pH 7.4 or Millipore water at room temperature for 24 hours. Columns for G-75 were prepared cutting borosilicate glass to 90 cm lengths and fitting with a plastic stopcock at one end. A small piece of soaked glass wool leaded by a long glass rod, was fit to the bottom of the column as a stopper. Gel slurry was aspirated for typically 40-50 minutes and loaded onto columns slowly using a large transfer pipet about 5 ml at a time. Pouring columns was continuous, especially for the second half of the columns, in order to achieve homogenously packed columns with the optimum separation efficiency. Air bubbles were avoided during pouring. Upon completion, buffer reservoirs were connected to the top of the column using a length of tygon® flexible plastic tubing. In order to get the complete and fine packing, columns were equilibrated with 5 times their bed volume of the degassed

buffer, pH 7.4 right after being poured. Samples of 0.5-1.5 ml were typically loaded onto the column for separation of high molecular weight proteins (more than 10 KDa) from metallothionein (6 KDa) and/or low molecular weight species (less than 1 KDa). Fractions of 1 or 2 ml were collected using a Cygent^{TM} fraction collector based on optical drop counts.

2.3. Quantification of sulfhydryl group of proteins (DTNB Assay)

Concentration of thiol groups of proteins was measured by applying 5,5-dithiobis (2-nitrobenzoic acid) (DTNB or Ellman's reagent) assay[134]. Stock solution of 10 mM DTNB in Millipore water was prepared and its pH adjusted to 6.2-6.4 using Tris powder. Tris increases the pH and solubility of DTNB in water because it is only slightly soluble at low pH. The solution was then filtered using Whatman #2 filter paper to remove any slight amount of non-dissolved solid DTNB. DTNB stock solution was kept in dark for later use up to one month from preparation.

Sulphhydryl concentration of samples was determined by reacting proteins in 1 ml aliquots with 1mM DTNB, vortexing the mixture, and waiting about 50-60 minutes prior to reading their absorption at 412 nm. Concentrations were obtained using the Beer-Lambert law and TNB extinction coefficient of 13,600 $M^{-1}cm^{-1}$. The following scheme shows DTNB reaction with SH, which causes TNB release that is detected due to its absorbance at 412 nm.

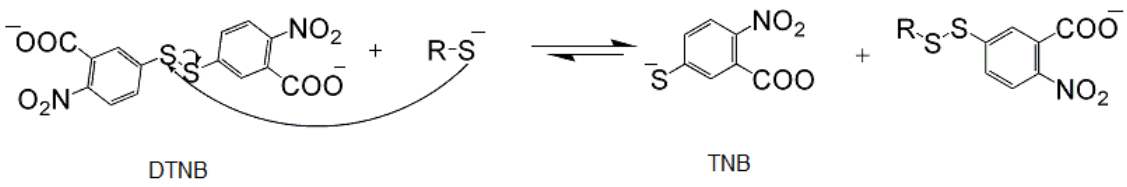

2.4. SDS-PAGE gel electrophoresis

SDS-PAGE was carried out on the normal and modified metallothionein in order to verify the quality of modified protein versus its normal counterpart. Fifteen percent Bis-Tris gel was used for electrophoresis. The wells were rinsed well with NuPAGE® MOPS SDS (1X) running Buffer. The gel cassette was then positioned in the Invitrogen Xcell Surelock™ Mini-Cell tank and upper and lower chambers were filled with the running buffer. The gel was pre-run for 5 minutes and then samples were loaded into the wells on top of the gel. Samples were heated at 50 ˚C for 15 minutes prior to loading on the gel. Electrophoresis was performed for 45-60 minutes at the voltage of 200 V until the bromophenol blue reached almost at the end of the gel. Gels were fixed and stained using Bio-Rad BioSafe Coomassie blue.

2.5. Culture of LL-CPK1 cells

The LL-CPK1 cell line is commercially available. (transformed renal epithelial cells from porcine kidney). This cell line was purchased from the American Tissue Culture Company (ATCC CL101) for use in our laboratory including this project. Cells, kept at -80 ˚C, were thawed and transferred to Media culture containing 10% fetal calf serum (FCS) and 50 mg/L of each of penicillin and streptomycin antibiotics. Media culture for LL-CPK1 cell, M199- modified by

Hepes buffer, Catalogue M2520, was purchased from Sigma. Media was prepared in 1 L Milli-Q (18MΩ resistant) purified water and the pH was adjusted to 7.2 using 2.2 g of sodium bicarbonate and 10 M NaOH. The media was also supplied with 50 mg of each penicillin and streptomycin antibiotics. Media was then sterilized using sterile 0.45 µm Corning© Bottle-top vacuum filters. Media containing cells was incubated in sterile culture flasks in an incubator with 5% CO_2, 100% humidity at 37°C. After 48-72 h media was replaced with new media and 4% fetal calf serum (FCS). After 6-8 days of supplying cells with this new media every other day, confluent cells were harvested either by scraping method or using 1ml of Sigma Trypsin-EDTA (10X) in saline to release them from culture plates. Harvested cells were divided to grow in experimental cell plates and/or culture flasks. All cells were handled under sterile conditions using laminar-flow hood equipped with HEPA particle filter, sterile lab wares, and sterile solutions.

2.5.1. Preparation of cell supernatant

Cells collected from 2 flasks through the above mentioned procedure were transferred to 200 ml media containing 10% FCS and divided into 20 plastic cell plates. Cells were incubated and grown to confluence while supplemented by 10ml media and 0.4 ml FCS every 48h. Then, cell plates were removed from the incubator; after decanting the media cells were rinsed three times with a lab-made saline solution. Saline solution was prepared one gallon at a time by dissolving 32.3 g NaCl, 25.3 g choline chloride, 4.7 g Na_2HPO_4, and 1.0 g NaH_2PO_4 in Milli-pore (18MΩ resistant) purified water. Cleansed cells were scraped very gently from cell plates and transferred to cold Sigma-Dulbecco's phosphate buffered saline in

45 ml plastic centrifuge tubes. After rinsing the plates and draining saline, one plate per batch was used for cell count. The cells of that plate were treated with 1ml trypsin and incubated 10 minutes. Suspended cells were diluted in 10 ml saline solution and counted using hemocytometer.

Cells were centrifuged at 680 g for 4 minutes and saline solution was decanted. The pellet was re-suspended in small amount of fresh cold saline and transferred to small tubes for further centrifugation at 1200 g for another 3 minutes. Saline solution was decanted and removed as much as possible and 1ml cold Milli-pore water added to the tube and vortexed. Vortexed cells were sonicated immediately with a flat cold tip for 60 pulses. The homogenate was centrifuged in a sorvall high-speed centrifuge in the SS34 rotor at 48,000 g for 20 minutes. The supernatant referred to as cell supernatant was loaded on a 80 cm G-75 column.

2.5.2. Cadmium pyrithione treatment of cell culture

Stock solutions of pyrithione and Cd^{2+} in mM concentrations were prepared and filtered using sterile filters (0.45 µm pore diameter) under the laminar hood. Certain volumes of stock solutions of pyrithione and Cd were added to M-199 Hepes modified media (with 10% FCS) in order to reach 3 µM pyrithione and 30 µM Cd^{2+}. Plates of non-confluent LLC-PK1 cells were treated with the above solution for 30 minutes and then the media was removed and cells were rinsed three times with DPBS. Cells were supplied with fresh media containing 4% FCS and kept in incubator for 4h and 24h (2 or 5 plates for each set). The same number of cell plates was taken as control. Sample and control cells were harvested by the scraping method and the cytoplasm was collected using the method previously

explained with the difference that ammonium acetate was used as the running buffer over the G-75 column. Chromatography was carried out under a lamiar flow hood. Pellets were also collected for analysis for each set of sample or control cells. Pellets were digested in concentrated nitric acid overnight and then diluted and filtrated for metal analysis. Metal analysis for the collected fractions and the pellet was done using ICP-MS on diluted solutions of samples in 2% HNO_3.

2.5.3. Metal quantification using Inductively Coupled Mass Spectrometer (ICP-MS)

Metal analysis of low concentration for samples (ppb level) was performed using a Waters Micromass Platform ICP-MS. Samples for ICP-MS analysis were diluted to 4 ml total volume in 2% HNO_3 in 8 ml Sarstedt plastic tubes, which were previously washed thoroughly with 10% HNO_3 to avoid any cross contamination. Each run was calibrated using a set of 0, 10, 50, and 100 ppb of Zn or Cd standard solutions in 2% HNO_3. Sample injection was carried out using auto sampler. Nebulizer and Torch gas flows were 0.7-1.2 L/min Ar, and 14-17 L/min Ar, respectively. ICP-MS run time for each sample took 1.65 min and the acquisition time was 1 min/sample. Susan Krezoski did all ICP-MS metal analyses.

2.5.4. Bio-Rad DC protein assay

The Bio-Rad DC protein assay, a test similar to the Lowry Assay, was used to measure protein concentrations. This assay is a colorimetric assay based on the reaction between copper and protein. Color development happens after copper treated tyrosine, tryptophan, and to lesser extent cystine, cysteine and histidine reduces Folin's reagent (sodium 1, 2-naphthoquinone-4-sulfonate). Reduction of

Folin's reagent produces species with maximum absorption at 750 nm. The advantage of using this assay over the Lowry method is that the reaction reaches 90% completion within 15 minutes in this test and the developed color remains stable up to 1 hour. In the assay, 50 µl of either standard or sample solutions were mixed with 125 µl of reagent A (alkaline copper solution) and 1 ml of reagent B (Folin's reagent) consecutively followed by 15 minutes incubation before reading the absorbance quantities at 750 nm.

A standard curve was obtained out of measured absorbances at 750 nm for bovine serum albumin (BSA) standard solutions with four different concentrations ranging between 1.4 and 0.14 mg/ml. Concentrations of proteins were calculated using the standard curve and the corresponding absorbance at 750 nm for their diluted solutions.

2.5.5. Treatment of cell supernatant and proteome with Zn^{2+} and Cd^{2+}

$CdCl_2$ or $ZnCl_2$ in different concentrations was reacted with cell supernatant and proteome. The reaction mixtures were loaded onto a G-75 column and HMW and low molecular weight fractions were located using AAS analysis. Fractions corresponding to high molecular weight proteins were collected and concentrated using an Amicon filtration device with 30,000 D cut off membrane. Concentrated Zn- or Cd-loaded proteome was either reacted immediately with competing ligands or stored in -80°C for later use.

2.5.6. Reaction of Cd-, Zn-loaded, and native proteome and cell supernatant with competing ligands

Cd- and Zn-proteome were reacted with apo- and Zn_7-MT to compare the metal lability of Cd-treated proteome with that of the native proteome. Zn and Cd loaded proteomes were also reacted with different competing ligands such as EDTA, NTA and Zincon (ZI) as well as fluorophores TSQ and ZQ_{ACID}. Sample solutions were loaded on sephadex G-75 column after 30 minutes for gel filtration chromatography and 1 ml fractions were collected. The proteome region and LMW fractions were located by Zn^{2+} or Cd^{2+} analysis and fluorescence measurement when TSQ or ZQ was employed.

2.6. Spectroscopy

2.6.1. Fluorescence spectroscopy

Fluorescence measurement of the fluorophores FluoZin-3, TSQ, and ZQ_{ACID} were carried out with a Hitachi F-4500 fluorimeter. The excitation wavelengths for FluoZin-3, TSQ, and ZQ_{ACID} were 492 nm, 370 nm, and 365 nm, respectively, and emission spectra were obtained over the 400 to 600 nm spectral range. Voltage of photomultiplier tube was set at 1200 mV and slits of aperture for emission and excitation at 5 nm. Excitation and emission spectra were recorded at a speed of 240 nm/min; the instrumental response was set at 0.8 seconds. For kinetic measurements of FluoZin-3 fluorescence, intensities were recorded at 517 nm with a response time 0.8 s, 1 reading/second, and lapse time of 0.2 seconds for each reading.

2.6.2 Ultraviolet-Visible spectroscopy

A Beckman Coulter, DU® 640 spectrophotometer was used to measure the absorption spectra of chromophores in samples or absorbances at their λ_{max}. Measurement of absorbances over time was used for kinetic studies. One-cm quartz or plastic cuivettes were used for UV (200-400nm) and Visible (400-600nm) measurements, respectively. The Beer-Lambert Law was applied to determine concentration of species based on their measured absorbances.

$$A=\varepsilon bc \quad (14)$$

Where,
A=Absorbance, ε =Extinction Coefficient ($M^{-1}Cm^{-1}$) and c= Concentration (M)

2.6.3. Atomic absorption spectroscopy

Metal quantification at the ppm levels for samples was done on a GBC 904AA flame atomic absorption spectrometer equipped with a computer for data acquisition and processing. Cd^{2+} and Zn^{2+} analysis were the most frequent measurements using AAS. Measurements were obtained using a Hollow-cathode lamp and a deuterium background lamp. Hollow-cathode lamp current was set at 8.0 mA and 3.0 mA and slit width at 1.0nm and 0.5 nm for Zn^{2+} and Cd^{2+}, respectively. Zn^{2+} and Cd^{2+} absorption intensities were detected at 213.9 nm and 228.8 nm, respectively. Calibration curves were obtained using 3 concentrations 0.5, 1, and 2 ppm of standard solutions, which were analytically prepared out of 1000 ppm standard solutions of Zn^{2+} and Cd^{2+} purchased from Fisher Scientific.

3. Results

3.1. **Reaction of Fluo-Zin3 with normal and modified Zn_7-metallothionein**

3.1.1 Introduction

Metallothioneins are a group of small size proteins (about 6 kDa), which are structurally unique and functionally complicated. It was Malyuga's discovery of high amount of cadmium accumulation in human kidney in 1941 that attracted scientists to investigate Cd^{2+} in kidney [141]. However, the main reason behind Cd^{2+} accumulation was not revealed until 1957[141], when Margoshes and Vallee isolated metallothionein from horse kidney. Since then, metallothioneins have been under intensive investigation and research both in vitro and in vivo. There is still much ambiguity related to their attributed functions such as cadmium detoxification, Zn^{2+} and copper regulation and metabolism, stress response and so on. Studying metal binding properties of metallothionein can provide crucial knowledge about its roles in heavy metal detoxification and Zn^{2+} or copper regulation.

Mammalian metallothioneins, which belong to class (I) out of three classes of metallothioneins, have 61 amino acids, among which 20 amino acids are cysteines (**Figure 3.1**). These cysteine residues are highly conserved in mammalian metallothioneins [142] and bind to seven Cd or Zn ions in two distinctive clusters. Detailed structure of these two clusters was first reported by Otvos and Armitage using ^{113}Cd NMR studies [143]. Thiolate groups of cysteine residues bind to the divalent metals as terminal and bridging ligands and form a three member (chair-shape M_3S_9) and a four member (extended chair-shape

M_4S_{11}) in the N-terminal β-domain and C-terminal α-domain of the protein, respectively [144] (**Figure 3.2**)

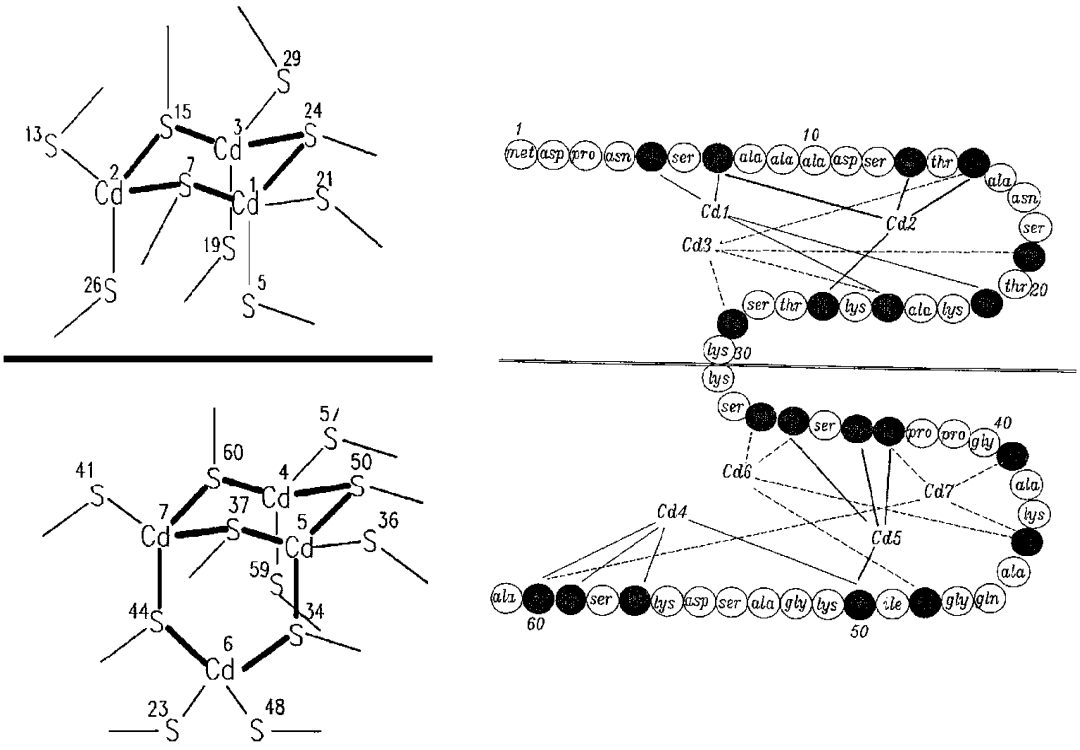

Figure 3.1. Sequence for Cd_7-MT from rabbit liver. Cd-S connectivity and position of two clusters within the protein are shown [142].

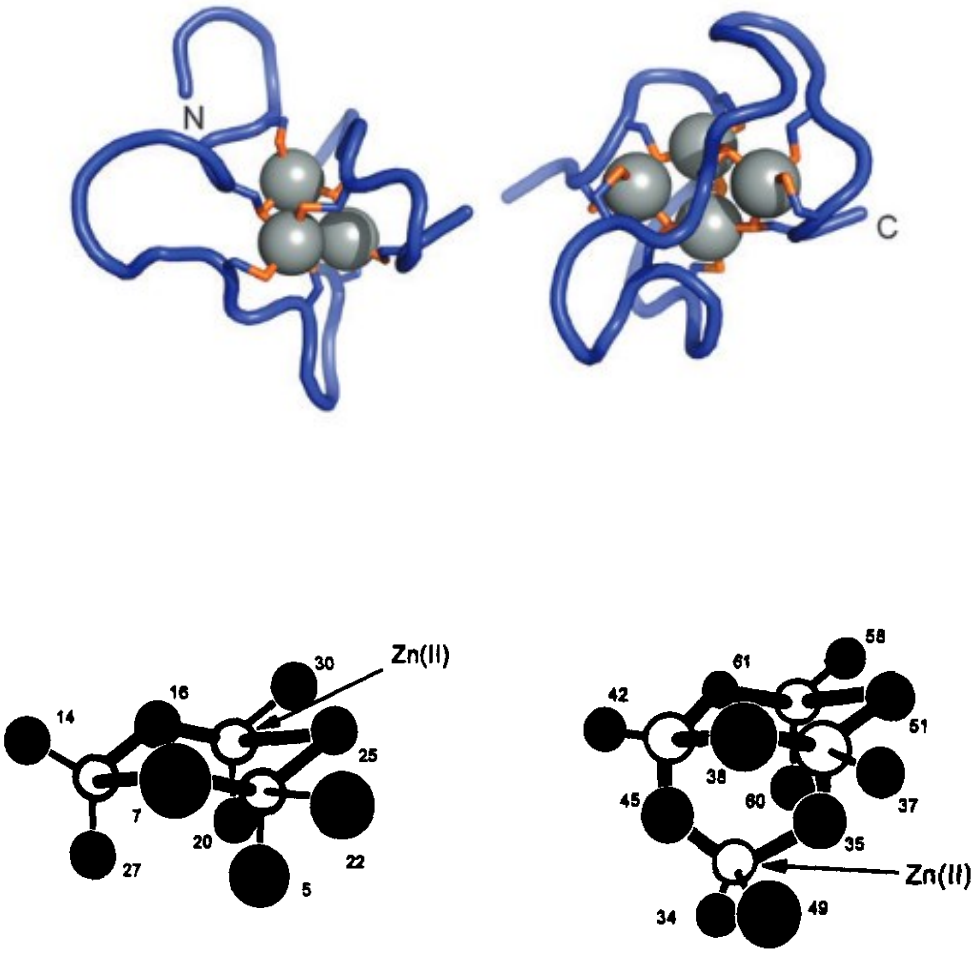

Figure 3.2. Structure of Zn_7-MT and its three-member, Zn_3S_9, and four-member, Zn_4S_{11} clusters [145]. Numbers refer to the position of the residue in the amino acid sequence.

Mammalian metallothionein such as rabbit-liver MT, which was isolated, purified and used in this project, has two major isoforms; MT1 and MT2. Because MT2 has one more negative charge compared to MT1 [146], it was possible to separate them using anion exchange chromatography.

3.1.2. Metallothioneine as a Zn- trafficking protein

Over-expression of mRNA for MT biosynthesis happens upon exposure of living cells to excess Zn^{2+} that results in an increasing concentration of apo-metallothionein [147]. These observations led to hypotheses about the role of MT in Zn trafficking. In one perspective metallothionein might be considered as a transient pool that buffers living cells from large changes of free or loosely bound Zn^{2+}.

$$\text{Apo-MT} + 7Zn^{2+} \rightleftharpoons Zn_7\text{-MT} \qquad (15)$$

On the other hand, it might provide Zn^{2+} for the biosynthesis of Zn-proteins.

$$1/7\ Zn_7\text{-MT} + \text{Apo-protein} \rightleftharpoons 1/7\ \text{Apo-MT} + \text{Zn-protein} \qquad (16)$$

Here, Apo-protein is assumed to have a higher stability constant, which thermodynamically favors reaction 16 [148].

3.1.3. Zn_7-MT stability constants and the proposed weak binding site

MT metal binding properties has been under investigation for many years. However a consensus has not been achieved about the mechanism of Zn^{2+} or Cd^{2+} binding to apo-MT and consequently the formation of α and β clusters. Most studies have shown similar stability constants for 7 Zn^{2+} or 7 Cd^{2+} binding to

metallothionein [149, 150]. In those studies, the method of using competing ligands, which have known stability constants with Zn^{2+} or Cd^{2+}, has been employed for the determination of Zn_7-MT stability constants. They have reported stability constants greater than 10^{10} and 10^{13} with $Zn^{2+}$and Cd^{2+}, respectively, at pH 7 and 25°. In contrast, Maret et al recently reported three different kinds of sites in Zn_7-MT with a difference of up to four orders of magnitude in their stability constants with Zn^{2+} [135]. They attributed the high affinity of metallothionein toward Zn^{2+} to the stability constant $10^{11.8}$ for the formation of the four-member cluster. On the other hand, they ascribed the capability of metallothionein in donating Zn^{2+} to other ligands under certain conditions, to a weakly bound Zn^{2+} in the 3-member cluster with a stability constant of $10^{7.7}$. The latter can pave the way for MT to donate at least 1 Zn^{2+} to proteins, which bind Zn^{2+} with a higher binding constant.

$$\text{Apo-MT} + 4Zn^{2+} \rightleftharpoons Zn_4\text{-MT} \qquad K_{1\text{-}4} = 10^{11.8} \quad \text{per } Zn^{2+} \qquad (17)$$

$$Zn_4\text{-MT} + Zn^{2+} \rightleftharpoons Zn_5\text{-MT} \qquad K_5 = 10^{10.9} \qquad (18)$$

$$Zn_5\text{-MT} + Zn^{2+} \rightleftharpoons Zn_6\text{-MT} \qquad K_6 = 10^{10.7} \qquad (19)$$

$$Zn_6\text{-MT} + Zn^{2+} \rightleftharpoons Zn_7\text{-MT} \qquad K_7 = 10^{7.7} \qquad (20)$$

The experimental determination of these stability constants began with the observation that the fluorescent Zn^{2+} sensor, Fluo-zin 3, reacts with Zn_7-MT to form a fluorescent Zn^{2+} product [135]. The Fluozin-3 structure includes a fluorophore linked to a set of amine and carboxylate metal binding ligands with a modest stability constant for Zn^{2+} at pH 7 of $10^{7.8}$ (**Figure 3.3**). Data in support of the weak stability constants were obtained from two similar experiments. In the first, binding

isotherms were fit to the titration of apo-MT with Zn^{2+} in the presence of FluoZin-3 and RhodZin-3. The second was based on competition between either FluoZin-3 or RhodZin-3 and MT for Zn^{2+}.

Besides their implications for metallothionein as a cellular participant in Zn^{2+} trafficking, the results presented by Maret and Krezel suggest that FluoZin-3 might be used to image the presence and intracellular location of Zn_7-MT. Considering the apparent centrality of MT-bound Zn^{2+} in cellular Zn^{2+} trafficking according to these authors and others, it was important to reexamine their determination whether Zn_7-MT contains a weak Zn^{2+} binding site.

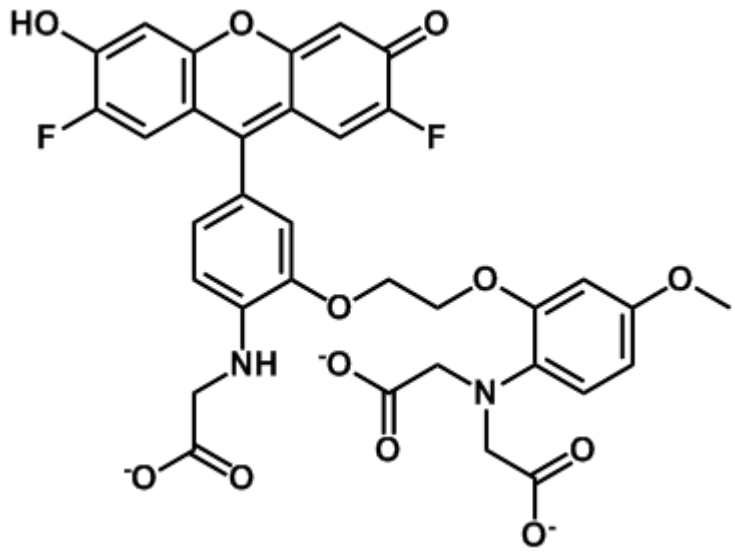

Figure 3.3. Chemical Structure of FluoZin-3, cell impermeant (2-[2-[2-[2-[bis(2-oxido-2-oxoethyl)amino]-5-methoxyphenoxy]ethoxy]-4-(2,7-difluoro-3-oxido-6-oxo-4a,9a-dihydroxanthen-9-yl)anilino]acetate)

3.1.4. Preparation of Zn_7-MT from Rabbit Liver

Zn_7-MT was prepared from rabbit liver as described in the methods section. Two peaks were obtained from DEAE chromatography, representing MT1 and MT2. In the anion exchange chromatography of MT1 and MT2 after loading the protein onto the HPLC column, an ionic gradient was employed to separate these isoforms. A typical ionic gradient, which was employed in the isoforms separation and depicted as conductivity versus the eluted volume, is shown in **Figure 3.4**. In **Figure 3.5** a chromatogram of MT1 and MT2 is shown as an example of several such separations, which was carried out during MT preparation. The MT2 fraction was characterized for protein content (220 nm absorbance), Zn^{2+} concentration (atomic absorption spectrophotometry) and sulfhydryl concentration (DTNB analysis). About 700-800 µg MT2/g liver was isolated and purified from rabbit liver in a typical MT preparation. The protein used in this study had a Zn^{2+}/MT ratio of 6.9±0.2, a SH/MT ratio of 20.5±0.5, and a SH/Zn^{2+} of 2.9±0.1. These values closely agree with the theoretical values of 7, 20, and 2.86, respectively.

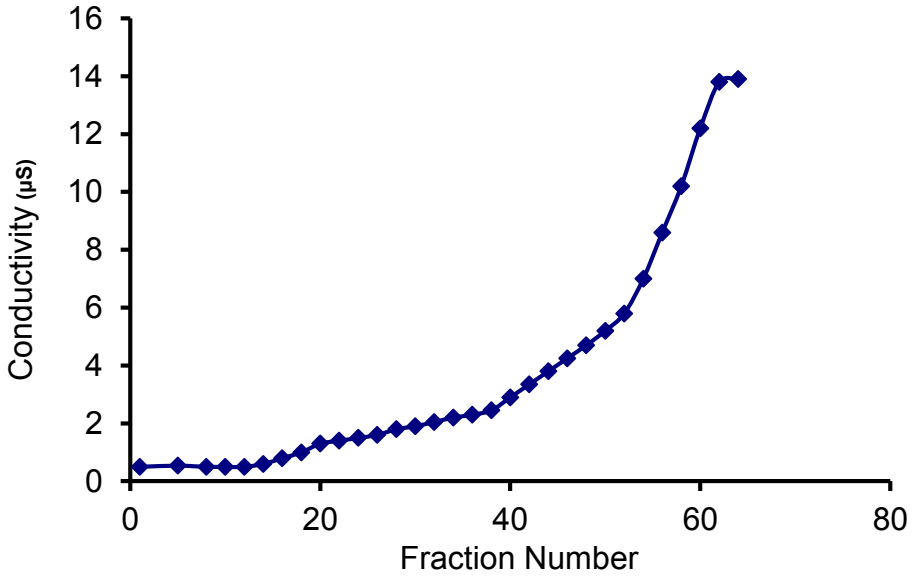

Figure 3.4. Graph of Conductivity Showing the Ionic Gradient Applied after MT pool loaded onto the Protein-Pak™ DEAE 5PW 7.5×75 mm Column. The separation of MT1 and MT2 took place in an applied ionic gradient with conductivity less than 3 µS.

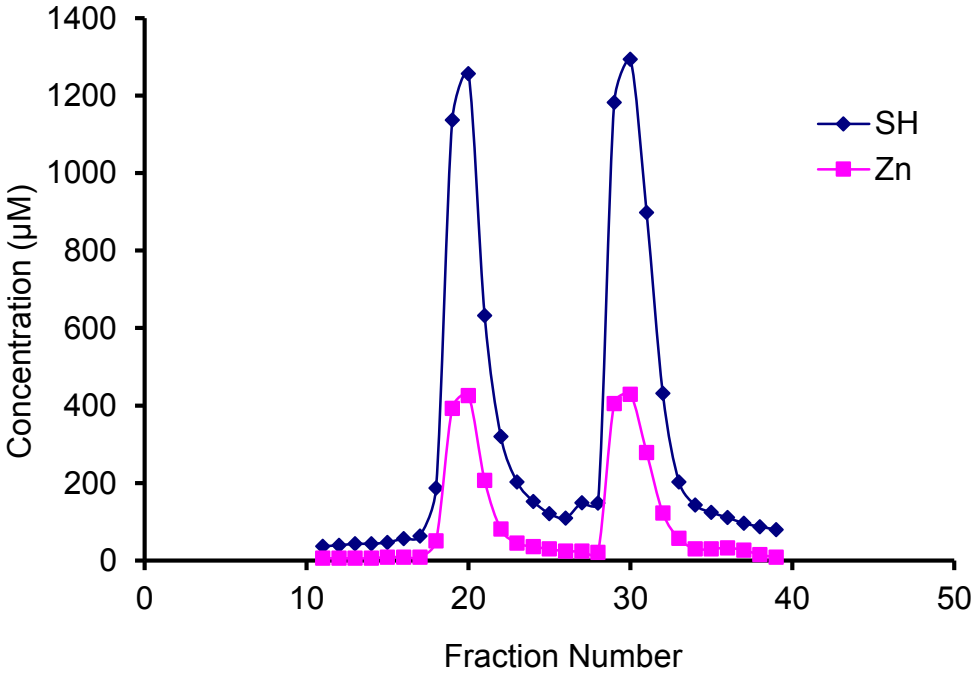

Figure 3.5. HPLC Chromatogram of MT1 and MT2 separated on the Protein-Pak™ DEAE 5PW 7.5×75 mm column

3.1.5. Preparation of Zn_7-MT* from Zn_7-MT

3.1.5. Preparation of Zn_7-MT* from Zn_7-MT

Maret et al prepared Zn_7-MT* by expressing human MT2 in *Escherichia coli* as an intein fusion protein without addition of metal ions to the growth medium [135]. The construct was purified by affinity chromatography and the intein was cleaved using 0.1 M DTT. The purified protein was acidified to pH 1 using 1.2 M HCl and purified by G-25 chromatography equilibrated with 0.01 M HCl (pH 2). Final neutralization was achieved by adding small amounts of apoMT to neutral reaction buffer in the presence of Zn^{2+}. In addition, PAGE electrophoresis on MT showed its high purity (>95%) based on runs with 2-10 µg of protein.

We subjected rabbit liver Zn_7-MT2 to acid conditions below pH 1, which released all of the bound Zn^{2+} and then restored the sample to pH 7.4. After this acid-base cycle the product, designated as Zn_7-MT*, retained its full complement of sulfhydryl groups as measured with DTNB. In addition, PAGE electrophoresis on MT and MT* showed that they migrated at the same rate on the gel, displaying one single band based on runs with 0.2-10 µg of protein (**Figure 3.6**). Moreover, MT and MT* were chromatographed over Sephadex G-15 to further test the quality of modified MT in comparison to MT. Collected protein fractions from this experiment exhibited a SH/Zn^{2+} ratio of 2.9±0.1 for both MT and MT* and appeared as single peaks in their chromatograms (**Figure 3.7a, b)**. These results showed that MT* did not undergo peptide cleavage, loss of metal or modification of sulfhydryl groups. Competing ligands such as FluoZin-3, NTA, and H_2KTS were then used to compare the Zn^{2+} binding properties of the native (MT) and modified (MT*) protein.

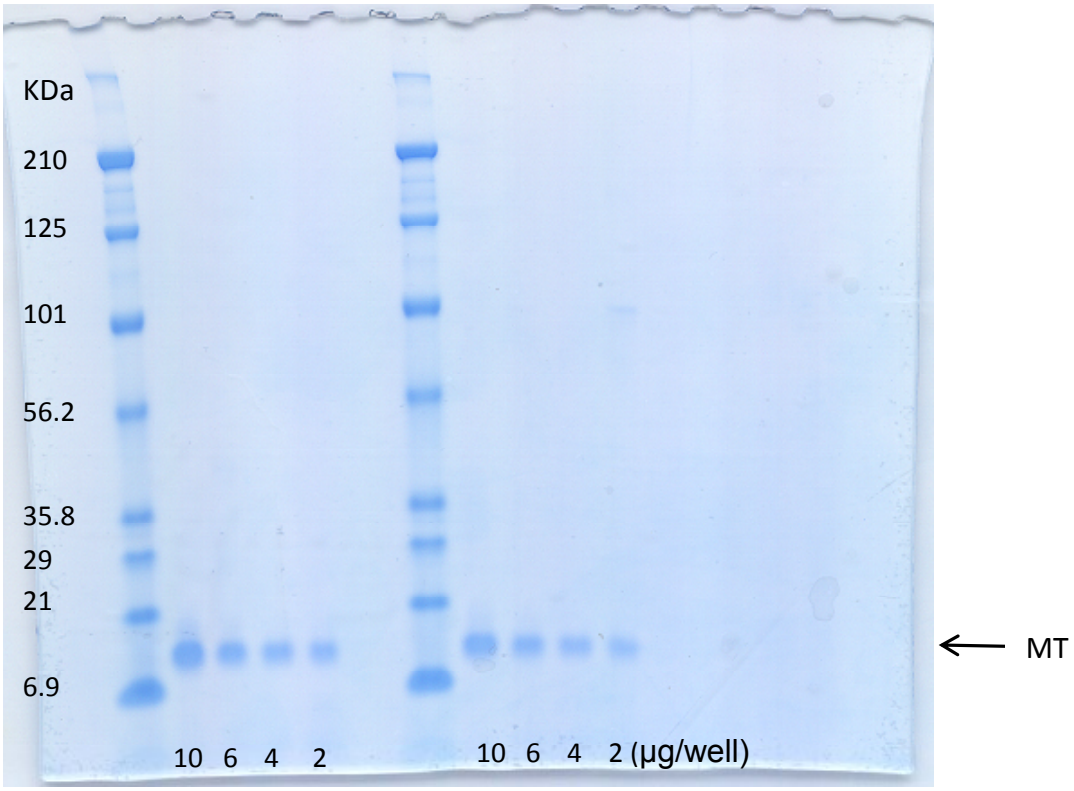

Figure 3.6. SDS-PAGE for MT and MT* run with 2-10 µg protein/well.

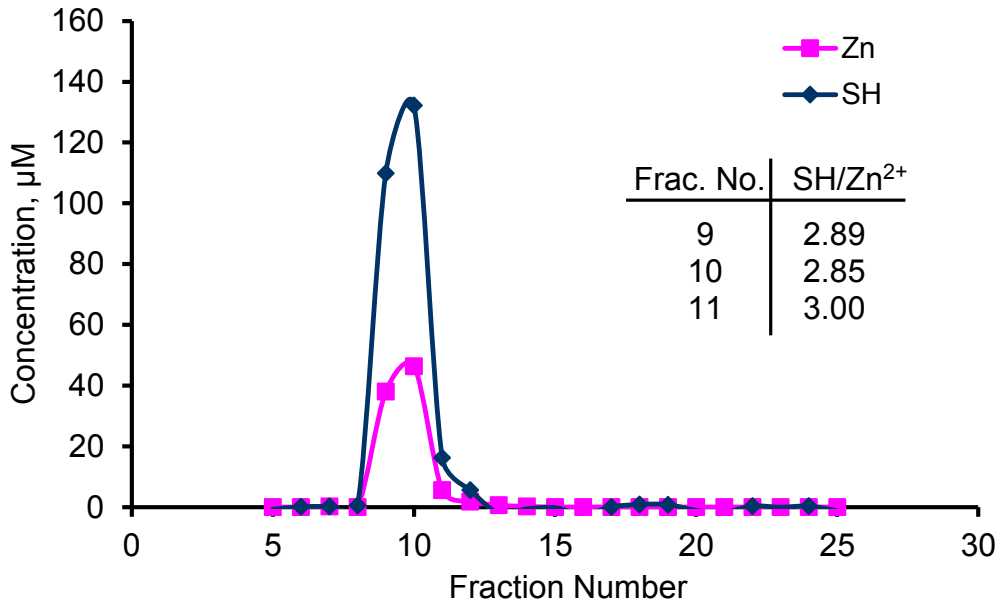

Figure 3.7a. Chromatogram of Zn_7-MT chromatographed over 30cm x 1.5 cm Sephadex G-15 column. SH and Zn^{2+} concentration and their corresponding ratios for 1-ml fractions are shown.

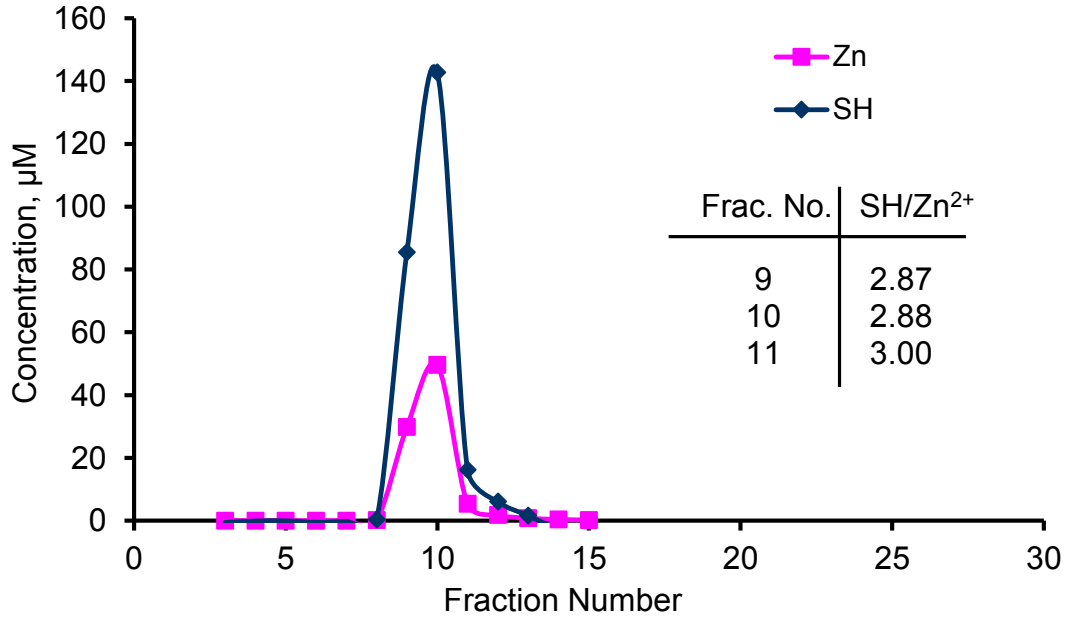

Figure 3.7b. Chromatogram of Zn_7-MT* chromatographed over 30cm x 1.5 cm Sephadex G-15 column. SH and Zn^{2+} concentrations and their corresponding ratios for 1-ml fractions are shown.

3.1.6. Characterization of Zn_7-MT and Zn_7-MT* Using Various Competing Ligands

3.1.6.1 FluoZin-3

Anaerobic reaction of excess FluoZin-3 with Zn_7-MT removed 0.22 μM Zn^{2+} equivalent to 0.14 moles Zn^{2+} per mole MT after a 120 min incubation period (**Figure 3.8a**). The nearly complete lack of reactivity alerted us to the fact that Zn_7-MT isolated from tissue at pH 7 did not behave as reported by Maret et al [135]. In comparison, Zn_7-MT* reacted with FluoZin-3 as described by these authors such that 1.0 ± 0.07 moles of Zn^{2+} per mole MT were extracted over the 1 h incubation period. Based on calculations using the weak stability constant suggested by Maret et al and concentrations of MT and FluoZin-3 used in this experiment, we expected removal of 0.81 moles Zn^{2+} per MT mole by FluoZin-3. Thus 20% more Zn^{2+} was removed than expected by FluoZin-3. This 20% excess reaction can be attributed to the removal of Zn^{2+} from sites with higher binding constants than $10^{7.8}$.

The kinetics of the Zn_7-MT* reaction were multi-phasic and could be fit to first order kinetic steps including two distinct phases and a possible third very rapid reaction phase that comprised about 67% of the overall reaction. (**Figure 3.8b**) This would be consistent with FluoZin-3 easily competing with the first Zn^{2+} binding site in the rapid phase. FluoZin-3 was in sufficient excess so that it would compete with the second and third Zn^{2+} sites, allowing for the appearance of one or possibly two slower phases.

In order to broadly establish the differential behavior of Zn_7-MT and Zn7-MT*, both proteins were reacted with other ligands that also have modest affinity for Zn^{2+}

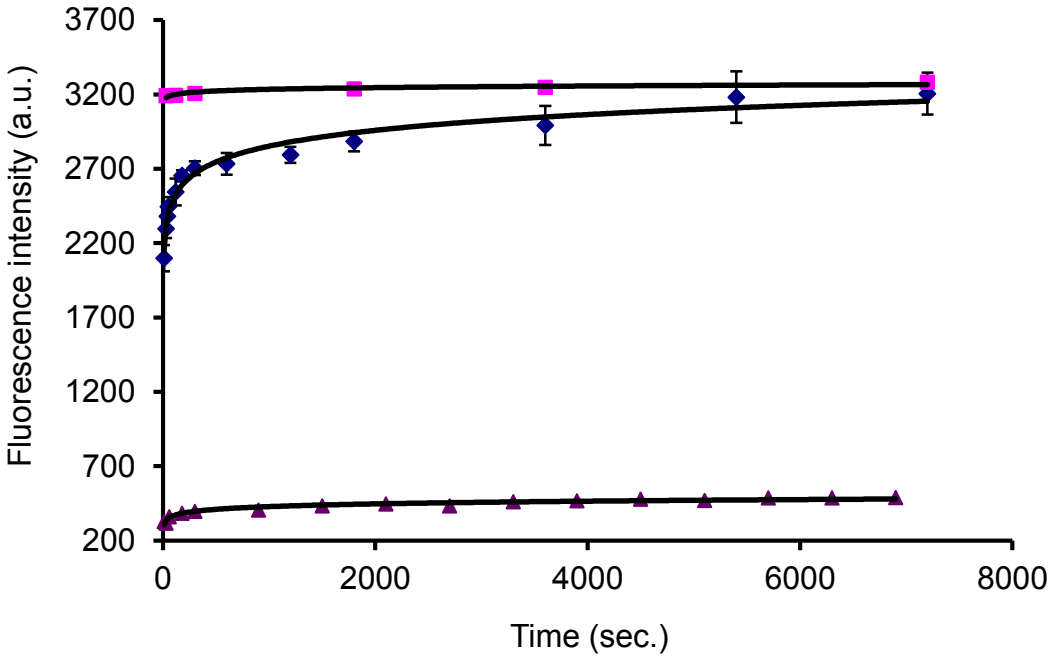

Figure 3.8a. Reaction of FluoZin-3 with $ZnCl_2$ (■), Zn_7-MT (▲) or Zn_7-MT*(♦). Conditions: 1.6 μM protein (11.2 μM Zn^{2+}), 5.0 μM FZ in anaerobic 50 mM Hepes buffer, containing 50 mM KNO_3, pH 7.4 at 25 ºC. $ZnCl_2$ concentration, 1.54 μM.

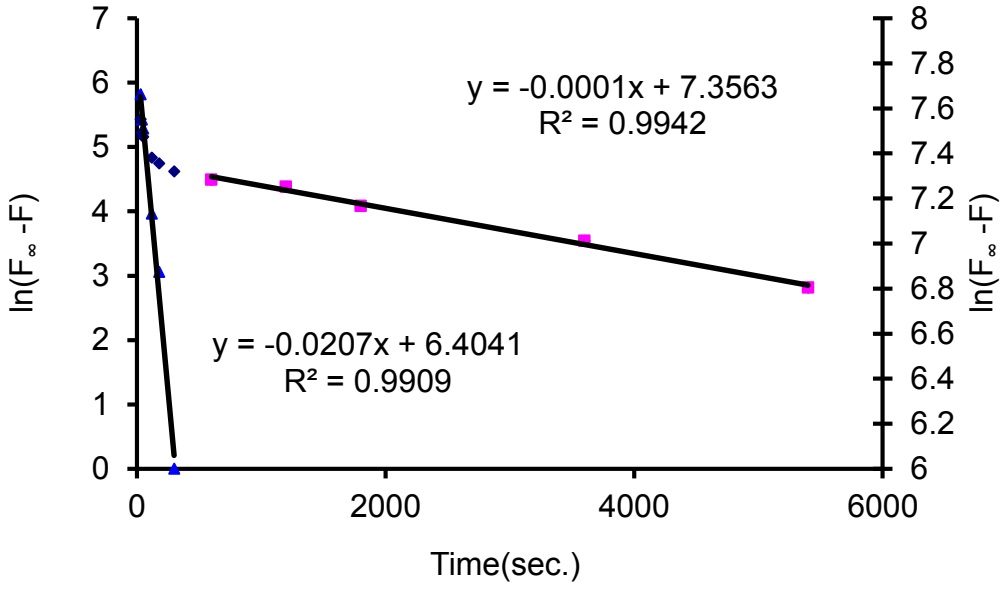

Figure 3.8b. Kinetic analysis of reaction of FluoZin-3 with Zn_7-MT*, the fast (▲) and slow (■) phases are shown. The very fast phase was not analyzed.

3.1.6.2. H_2KTS

A second ligand, H_2KTS, was employed to probe for a modestly bound Zn^{2+} ion in Zn_7-MT. H_2KTS forms a complex with Zn^{2+} that is readily detected, spectrophotometrically. **Figure 3.9** shows the chemical structure of H_2KTS. A stock solution of H_2KTS was diluted 10 times and titrated with standard solution of 8.5 mM $ZnCl_2$. **Figure 3.10** shows the titration curve for the above mentioned titration. Based on the data from titration curve, the concentration of H_2KTS stock solution and its extinction coefficient were calculated as 2.2 mM and 12,000 $M^{-1}Cm^{-1}$, respectively. K(H) for ZnKTS formation was calculated based on the following equation:

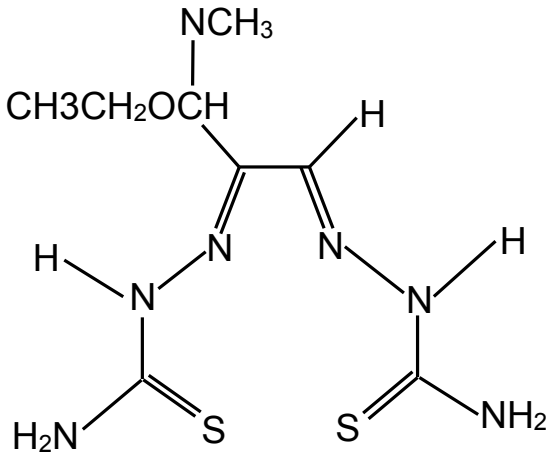

Figure 3.9. Chemical Structure of H_2KTS

$$K(H)=[Zn\text{-}Chelate]/([Zn^{2+}][bis(thiosemicarbazone)]_{all\ forms}) \quad (21)$$

The slope of 2.05 shows that two protons are associated with H_2KTS in very close agreement with the theoretical equation of pH dependence of K(H).

$$\log K(H)=2pH + C \quad (22)$$

In which *C* is a constant. The pH-dependent formation of ZnKTS was plotted versus pH and shown in **Figure 3.11**.

Reaction of H_2KTS with MT and MT* showed that they also react differently with this ligand. Only an insignificant fraction (0.01 mol Zn^{2+}/mol Zn_7-MT) of MT's complement of Zn^{2+} became bound to this competing ligand after 2 h incubation of 660 µM H_2KTS with 23 µM Zn_7-MT (161 µM Zn^{2+}) under anaerobic conditions (**Figure 3.12**). Based on calculation we expected removal of 0.61 mole Zn^{2+} per one mole of Zn_7-MT* by H_2KTS under the above mentioned conditions. After 2 h, 0.78 ± 0.06 mol Zn^{2+}/mol MT* was complexed by this ligand, most of it within 10 min, with the reaction still slowly proceeding at the end of this period.

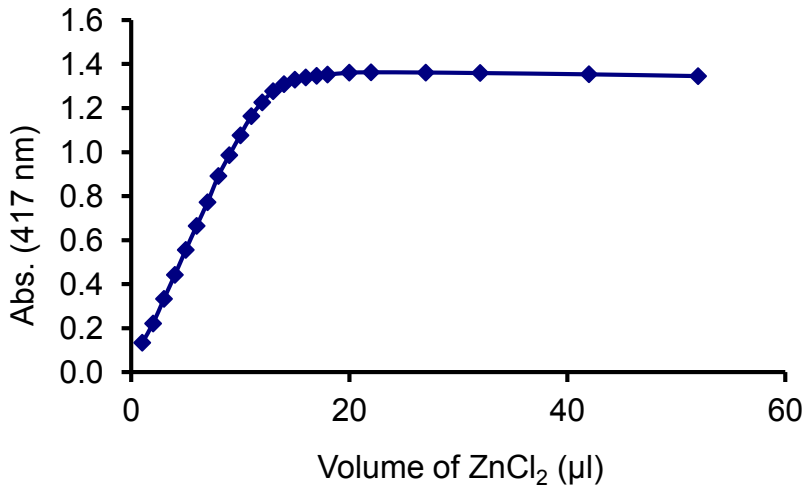

Figure 3.10. Standard curve of H_2KTS titration with Zn^{2+}

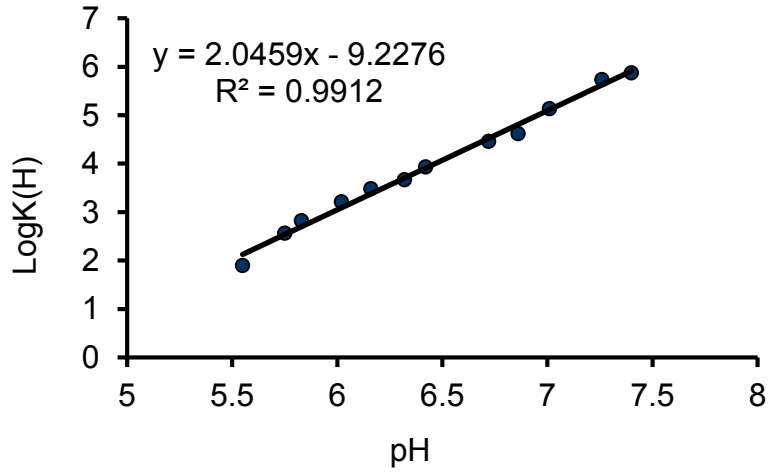

Figure 3.11. Plot of K (H) versus pH for ZnKTS formation

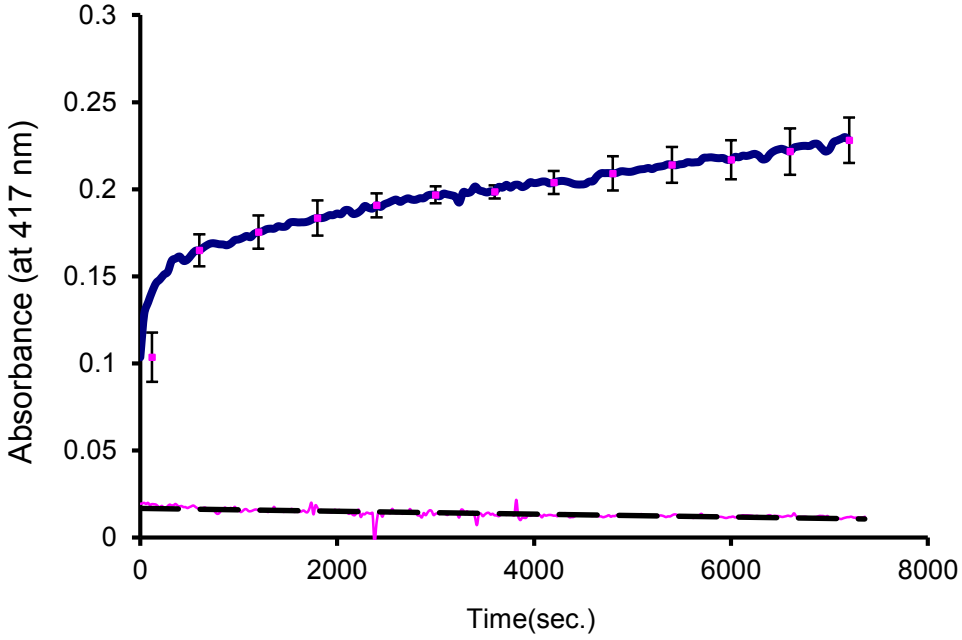

Figure 3.12. Reaction of H_2KTS with Zn7-MT (dashed line) or Zn7-MT* (solid line). Conditions: 23 µM protein (161 µM Zn^{2+}), 660 µM H_2KTS in 50 mM Hepes and100 µM TCEP, containing 50 mM KNO_3, pH 7.4 at 25 ºC.

3.1.6.3. NTA

Both Zn_7-MT and Zn_7-MT* were reacted with NTA following the approach used by Maret et al [135]. Samples were incubated anaerobically with NTA for 2 h and then chromatographed over Sephadex G-25 (**Figure 3.13** and **3.14**). The protein fractions were analyzed for Zn^{2+} and sulfhydryl concentration and their ratio used to assess the state of the protein. Zn_7-MT retained its native ratio of 2.9±0.1, whereas, the ratio of MT* protein increased to 3.5±0.2, consistent with the removal of 1 Zn^{2+} per mol MT* (20 SH: 6 Zn^{2+}).

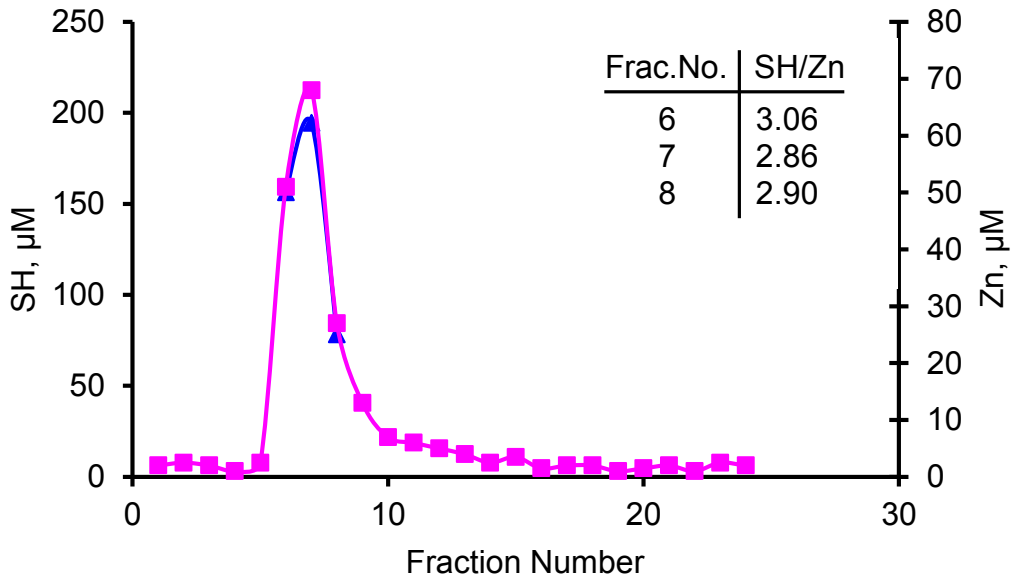

Figure 3.13. Reaction of NTA with Zn_7-MT
Conditions: 24 µM protein, 168 µM Zn^{2+}, 200 µM NTA in 50 mM Hepes and 480 µM TCEP, containing 50 mM KNO_3, pH 7.4 at 25 ºC. SH (▲); Zn (■).

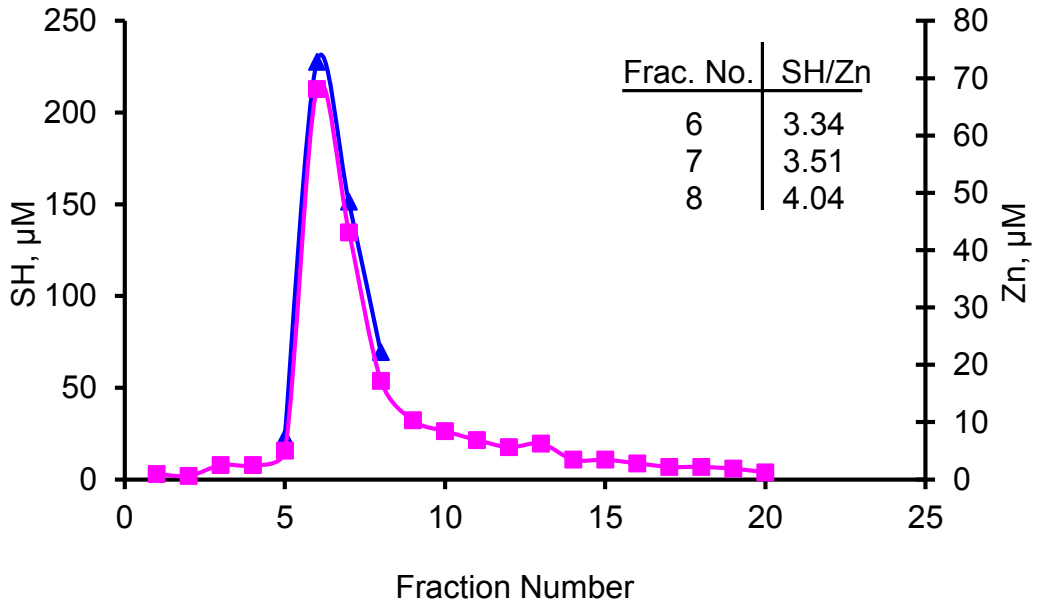

Figure 3.14 Reaction of NTA with Zn_7-MT*
Conditions: 24 µM protein, 168 µM Zn^{2+}, 200 µM NTA in 50 mM HEPES and 480 µM TCEP, containing 50 mM KNO_3, pH 7.4 at 25 ºC. SH (▲); Zn (■).

3.1.7. Acid-base Titration of Zn_7-MT

Zn_7-MT* was prepared by acidifying Zn_7-MT to about pH 0.4 and then restoring the pH to 7.4. It was of interest to examine the acid-base titration characteristics of this process. Typical acid-base titrations of Zn_7-MT spanning pH 7 to 2-3 display a single step of Zn^{2+} dissociation and re-association and are completely reversible. In contrast, with Zn_7MT* according to **Figure 3.15a**, during neutralization 2 steps are resolved. The first step follows the path of the acidification and accounts for 85% of the overall change in 215-nm absorbance (Zn-sulfhydryl bonding) or 6/7 of the bound Zn^{2+} assuming a linear relationship between Zn^{2+} and 215-nm absorbance. The second occurs between pH 5-7 and represents a weakly bound fraction of about 1 Zn^{2+} per mol MT*.

The following chemical equation, which assumes equal stability constants for all seven Zn^{2+} ions, represents the single-step acid titration.

$$Zn_7–MT + mH^+ \rightleftharpoons H_m–MT + 7Zn^{2+} \quad (23)$$

Where, m=20

However the base titration, which is two-step, can be shown by the following equations:

$$(H_{(m+n)} –MT^*) + 6\ Zn^{2+} + mOH^- \rightleftharpoons Zn_6–MT^*\text{-}H_n + mH_2O \quad ,m=18\text{-}19 \quad (24)$$

$$Zn_6–MT^*\text{-}H_n + Zn^{2+} + nOH^- \rightleftharpoons Zn_7–MT^* + nH_2O, \quad ,n=1\text{-}2 \quad (25)$$

For Cd_7-MT, a two-step acid titration curve was obtained indicative of a slight difference for stability constants of Cd^{2+} binding in three-member and four-member clusters (**Figure 3.15b**). Indeed Cd_4S_{11} showed a midpoint for titration at a lower pH 3.1 in comparison to Cd_3S_9, which displayed a midpoint at pH about 3.6. This difference became less significant for Cd_7-MT*, which instead showed a distinct step with a midpoint at a higher pH about 5 for 1 Cd^{2+}.

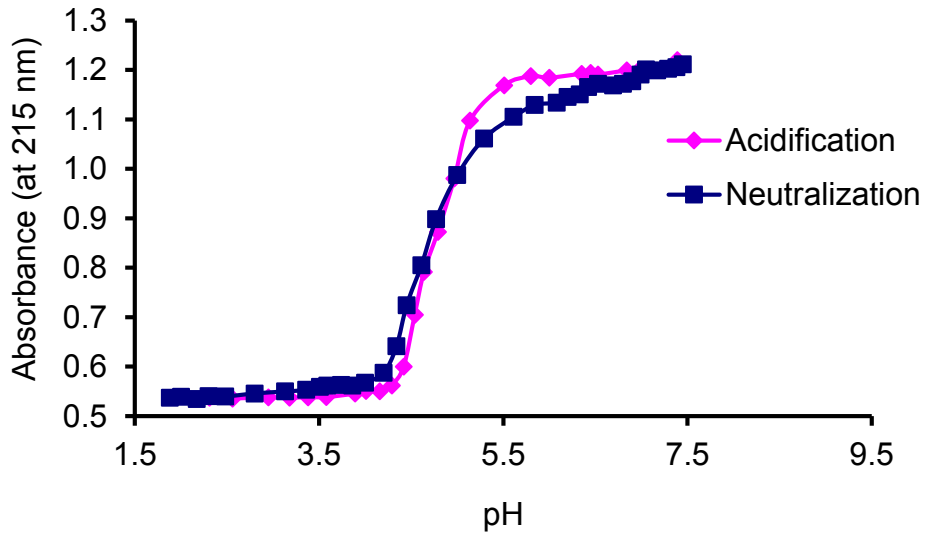

Figure 3.15a. Acid–base titration of Zn_7-MT. Acidification with HCl (♦) and neutralization with NaOH (■) in 5 mM Tris–Cl buffer, 0.1 M KCl at room temperature.

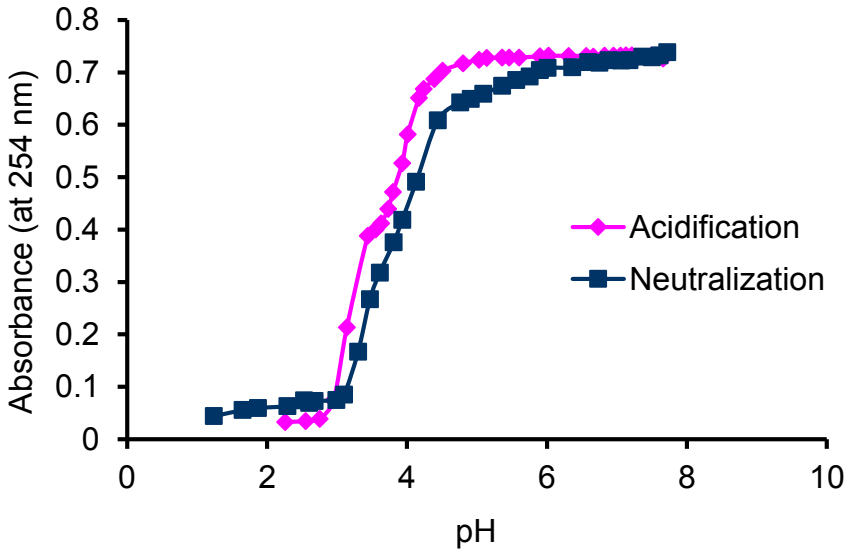

Figure 3.15b. Acid–base titration of Cd_7-MT. Acidification with HCl (♦) and neutralization with NaOH (■) in 5 mM Tris–HCl buffer, 0.1 M KCl at room temperature.

3.1.8 Kinetics and extent of reaction of Zn_7-MT with hydrogen ion

Zn_7-MT was incubated at pH 3, 2.7, 1.8, and 1.0 for a series of times, rapidly neutralized, and then reacted with FluoZin-3 as an indicator of the degree of conversion of Zn7-MT to Zn7-MT*. Like pH 0.4, the native samples reacted at pH 1.0 and 1.8 were converted to Zn7-MT* within 20 min. Indeed, at pH 1.0, the reaction was complete within 3 min, the quickest time for acidification and neutralization. At pH 2.7 and 3.0 the reactions were time dependent. For example, the fractional conversion to Zn_7-MT* after incubation at pH 2.7 for 20, 60, and 120 min was 0.68, 0.96, and 1.12 mol Zn^{2+}/mol MT, respectively. (**Figure 3.16a**) These values for pH 3.0 were 0.5, 0.6, and 0.8, respectively. (**Figure 3.16b**)

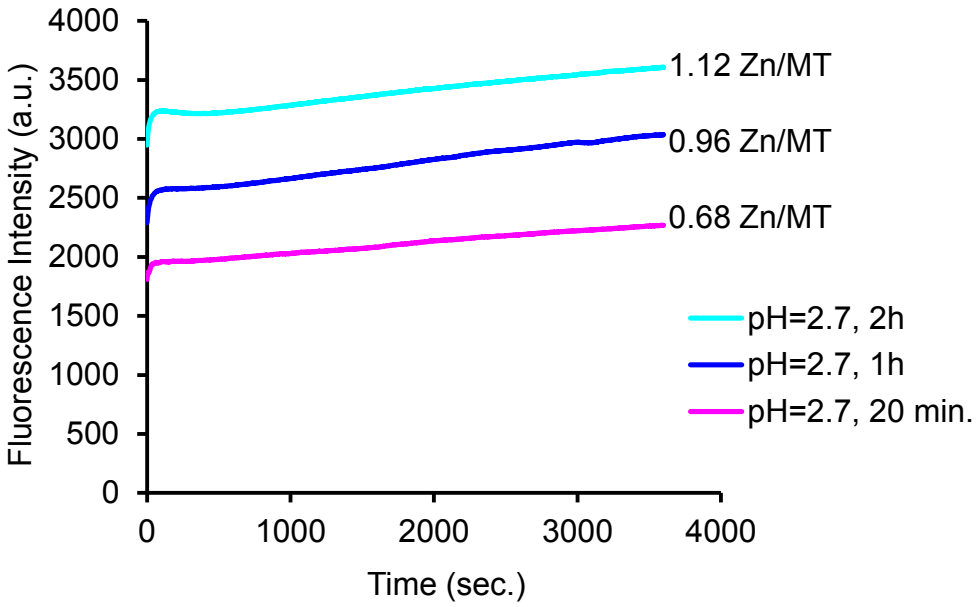

Figure 3.16a. Extent of reactivity of MT* with FluoZin-3 after its acidification to pH 2.7 for 20, 60, 120 min and reneutralizaion.

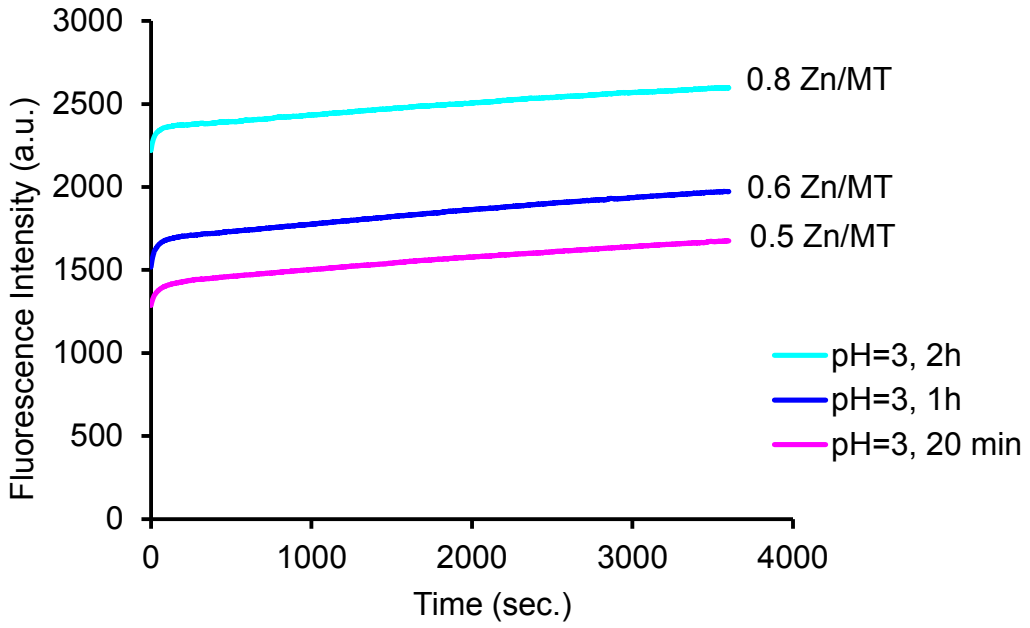

Figure 3.16b. Extent of reactivity of MT* with FZ after its acidification to pH 3 for 20, 60, 120 min and reneutralizaion

3.2. Reaction of proteome and Cell Supernatant with Cd^{2+} and Zn^{2+}

3.2.1. Introduction

The combination of all proteins working either in assembly or in discrete fashion in living cells, tissues, or organisms is called the proteome. The number of known proteins in the proteome is increasing as more research detects new proteins and finds their functions in living organisms. A significant portion of the proteome consists of proteins with at least one metal ion in their structure; therefore it is designated as the metalloproteome [151]. Metals in the metalloproteome have two major roles; they either take part in the determination and/or stabilization of protein structure or contribute directly to protein function, as in metalloenzymes. Among metals, transition metals play a crucial role in living

cells and their biological activities, despite their existence of trace amounts in living organisms. A transition metal with filled 3d orbitals, Zn^{2+} is the second most abundant transition metal ion in living organisms. It has a broad spectrum of functionality and a variety of structural binding patterns in proteins. Zn^{2+} is almost spectroscopically invisible; therefore, detecting and studying the role of Zn^{2+} in Zn-proteins requires more effort than needed for spectroscopically active-metal containing proteins such as iron and copper proteins.

Despite the significant amount of research that has been done on Zn^{2+} in living cells, Zn trafficking from outside the cell into the cytosol and its regulation inside the cell remain elusive. Previously, Zn-transporters as the suppliers of Zn^{2+} to the cell were largely the focus of study [152]; but the nature of Zn^{2+} species involved in Zn^{2+} trafficking from the external medium to the binding sites of metalloproteins were not addressed. Two main hypotheses suggest that either free Zn^{2+} or ligated Zn^{2+} is in play with Zn^{2+} transporter proteins of the cell membrane, which carry Zn^{2+} from outside the cell to the cell cytoplasm [152].

Previous studies have shown that pM to nM concentrations of free Zn^{2+} or very loosely bound Zn^{2+} exist in living cells [153] These low concentrations along with the relatively small K_m values of Zn-transporters (e.g. Zrt1, 10 nM and Zrt2, 100 nM) [154] imply that if free Zn^{2+} is assumed to be involved in the transport processes, Zn-transporters would not be efficient [155]. Furthermore, even 1 nmolar free Zn^{2+} would provide only 10% of the Zn demand of cells that divide every 24h, assuming cellular Zn-protein concentration of 100 μM and a highly

optimistic second-order rate constant of 10^8 $M^{-1}s^{-1}$ for the formation of the Zn-protein

$$Zn^{2+} + \text{apo-protein} \rightleftharpoons \text{Zn-protein} \quad (26)$$

The other hypothesis suggests that Zn^{2+} is transited among different binding sites and regulated within the cell through ligand substitution reactions analogous to what seen for copper trafficking [156]. Glutathione, metallothionein, and Zn-proteome are the major Zn-binding pools within the cell that may participate in the Zn^{2+} trafficking. However, the mechanism of this complex process and the explicit role of these cellular Zn^{2+} chelating agents are as yet too complicated to be fully understood.

The pernicious effects of Cd on human kidney function and bone integrity was first noticed in mid twentieth century upon people's exposure to occupational and environmental Cd contaminant in Sweden and Japan, respectively [79, 157]. The discovery of metallothionein as a sulfhydryl-rich protein that binds to Cd^{2+} tightly in living organism has formed the majority of the research about Cd^{2+} toxicity. The main documented function of metallothionein in the literature is also about its involvement in Cd^{2+} toxicity. Metallothioneins scavenge elevated amounts of Cd^{2+} in tissues and cells by binding tightly to it and therefore buffering it from interfering with hundreds of enzymes and thousands of proteins. Like all other proteins there is a balance between biosynthesis and biodegradation of metallothionein. The degredaded MT releases Cd^{2+}, which will be taken mostly by the newly synthesized apo-MT. Therefore, under steady state, Cd^{2+} cannot exist as free Cd^{2+} and will be tightly bound to MT.

$$\text{Cd-MT} \rightarrow Cd^{2+} + \text{amino acids} \rightarrow \text{Cd-MT} \qquad (27)$$

If the rate of biodegradation exceeds the rate of biosynthesis, the newly synthesized apo-MT would not be sufficient to take up the Cd^{2+} released from the biodegraded Cd-MT. Under such condition, other proteins and enzymes will take up Cd^{2+} and therefore their functions or structures will be impaired. In another scenario, even in the presence of MT, there might exist some sites in some proteins or enzymes, which bind Cd^{2+} that leads to cell injury.

Like Zn^{2+}, Cd^{2+} belongs to bio-reactive transition metal ions with filled d orbitals. Because of the similarity it shares with Zn^{2+} in its chemical properties, Cd^{2+} can mimic Zn^{2+} and play the role of its rival in binding to proteins and ligands in the cell. This simple-looking change in chemistry of cells upon their exposure to Cd^{2+}, can lead to a cascade of problems in physiological activities of cells that finally cause kidney, lung and liver failure. Cd has a bigger atomic and ionic size than Zn. In comparison, this property confers higher affinity on Cd^{2+} toward ligands that have sulfhydryl groups and lower affinity toward ligands with nitrogen moieties.

In order to study possible cellular reactions of Cd^{2+}, we used the extracted proteome from rabbit liver or LLC-PK1 cells as a model. We were curious to know what sites Cd^{2+} might bind to upon entrance into cells and whether apo-MT or Zn-MT was reactive with Cd^{2+} associated with these sites. Cd^{2+} was reacted with the proteome and after separation and purification of the product, reacted it with different ligands (fluorophores TSQ and ZQ_{ACID} , EDTA), apo-MT, and Zn_7-MT. In the following pages, results and explanation of these experiments are provided.

3.2.2. Reaction of Zn-proteome with Cd^{2+}

Zn-proteome from LL-CPK1 cells was used in this experiment. In order to isolate Zn-proteome from LL-CPK1 cells, cells were grown to confluence and harvested by scraping. Harvested cells were sonicated and centrifuged to extract the cell supernatant. Zn-proteome was separated from supernatant by Sephadex G-75 column chromatography and one-ml fractions were collected and pooled for analysis of its Zn^{2+} content. Details of these procedures are given in the chapter 2 methods. $CdCl_2$ was reacted with Zn-proteome for 30 min. at room temperature and the product solution loaded onto a Sephadex G-75 column. Collected fractions were analyzed for their Zn^{2+} and Cd^{2+} content by AAS. **Figure 3.17a, b** shows the chromatogram for the control proteome and sample proteome with Cd^{2+}/Zn^{2+} ratio of 0.65. All the Cd^{2+} reacted with the Zn-proteome and no Zn^{2+} was released. The proteome quantatively retained both metal ions. In all reactions up to a Cd^{2+}/Zn^{2+} ratio of 1, no Zn^{2+} was liberated, as indicated by the quantative retention of Zn^{2+} in the proteome and the lack of detectable Zn^{2+} in the low molecular weight region of the chromatogram. Data are summarized in **Table 2.3**. Clearly, Cd^{2+} binds within the proteome. Whether it reacted with Zn-containing sites could not be determined by this experiment. Cd^{2+} may have displaced Zn^{2+} from Zn-proteome (Cd-proteome•Zn) or bound adventitiously to protein ligands:

$$Cd^{2+} + \text{Zn-proteome} \rightleftharpoons \text{Cd-proteome•Zn or Zn-proteome•Cd} \qquad (28)$$

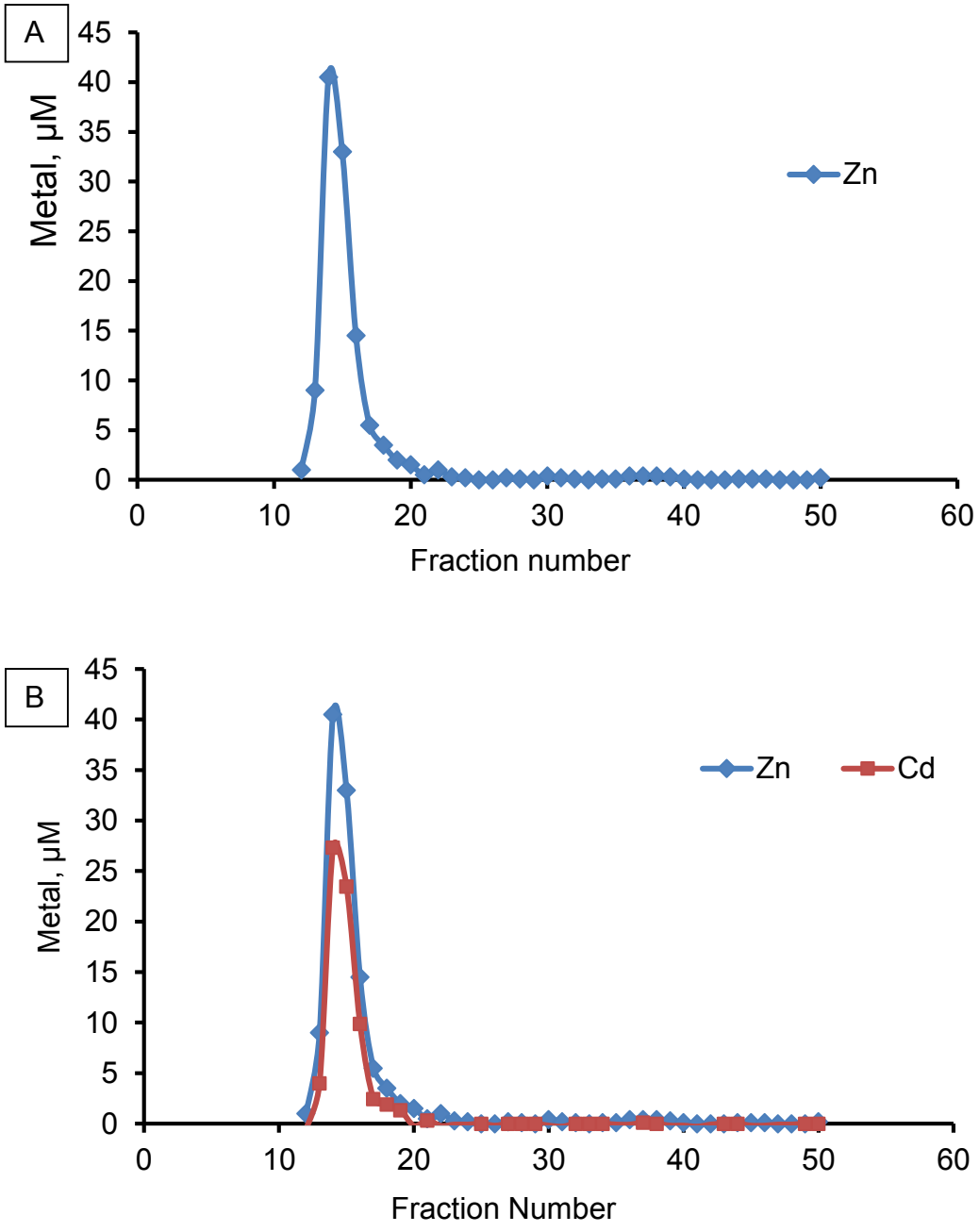

Figure 3.17a, b. Sephadex G-75 chromatography of Zn-proteome reacted with Cd^{2+}. Proteome contained 120 μM Zn^{2+} and was reacted with 80 μM $CdCl_2$ in Tris-HCl buffer, pH 7.4.

Table 3.1. Summary of data for the reaction between the proteome and $CdCl_2$

Reactants		**Products**	
Cd^{2+}	Zn-proteome	proteome	
Cd^{2+},µM	Zn^{2+}, µM	Zn^{2+},µM	Cd^{2+}, µM
80	120	110	75
25	45	44	23
25	30	28	22

3.2.3. Reaction of Cd-loaded proteome with fluorophores ZQ_{ACID} and TSQ

Two quinoline sulfonamide fluorophores; 6-Methoxy-(8-*p*-toluenesulfonamido) quinoline (TSQ) and 6-Methoxy-(8-*p*-toluenesulfonamido) quinolinoxy acetate (ZQ_{ACID}) (**Figure 3.18**) were used to study the effect of Cd^{2+} or excess Zn^{2+} on metal binding properties of the proteome. Zn fluorescent sensors are typically comprised of a metal-chelating ligand, which is connected to a fluorescent moiety that undergoes a change in fluorescent properties and displays fluorescence upon binding of Zn^{2+}. Studies show these fluorophores exhibit two distinct types of reactions with the zinc proteome [116, 128,129,131]. In one reaction designated as adduct formation; a ternary complex is formed with the participation of three moieties, the metal ion, protein, and fluorophore. In the other reaction, the ligand sequesters the metal ion from proteomic Zn^{2+} binding sites and a free complex of Zn^{2+} and the ligand with a stoichiometry of 1:2, respectively, is generated. Fluorescence spectroscopy of these complexes shows that upon an

excitation at 370 nm, ternary complexes exhibit a fluorescence emission with a λ_{max} at about 470 nm, whereas, free complex fluoresces with a λ_{max} at about 490 nm. ZQacid and TSQ quantum yields upon binding to Cd^{2+} are 33% those observed in their binding to Zn^{2+}.

Based on the above mentioned two different products involving TSQ and ZQ, possible reactions between fluorophore competing ligands (FL) and M-proteome•Zn can be deduced as follows:

$$2FL + Zn\text{-}Proteome \rightleftharpoons Proteome + Zn(FL)_2 \quad (29)$$

$$FL + M\text{-}proteome\bullet Zn \rightleftharpoons FL\text{-}M\text{-}proteome\bullet Zn \quad (30)$$

$$FL + M\text{-}proteome\bullet Zn \rightleftharpoons M\text{-}proteome\bullet Zn\text{-}FL \quad (31)$$

$$2FL + M\text{-}proteome\bullet Zn \rightleftharpoons M\text{-}proteome + Zn(FL)_2 \quad (32)$$

$$2FL + M\text{-}proteome\bullet Zn \rightleftharpoons proteome\bullet Zn + M(FL)_2 \quad (33)$$

$$2FL + M\text{-}proteome\bullet Zn \rightleftharpoons FL\bullet M\text{-}proteome\bullet Zn\text{-}FL \quad (34)$$

$M=Zn^{2+}$ or Cd^{2+}

FL= Fluorophore competing ligand (TSQ or ZQ_{ACID})

TSQ alone does not react with Zn-Proteome to produce $Zn(TSQ)_2$ and ZQ exhibits very small reactivity with it (≤ 5 %). TSQ and ZQ, overall, image only 10-20 % of the proteome Zn. In the following sections results of the reactions of TSQ and ZQ_{ACID} with Cd-treated (Zn)-proteome will be discribed first and then results of the reactions between these competing ligands and Cd-treated proteome will be discussed.

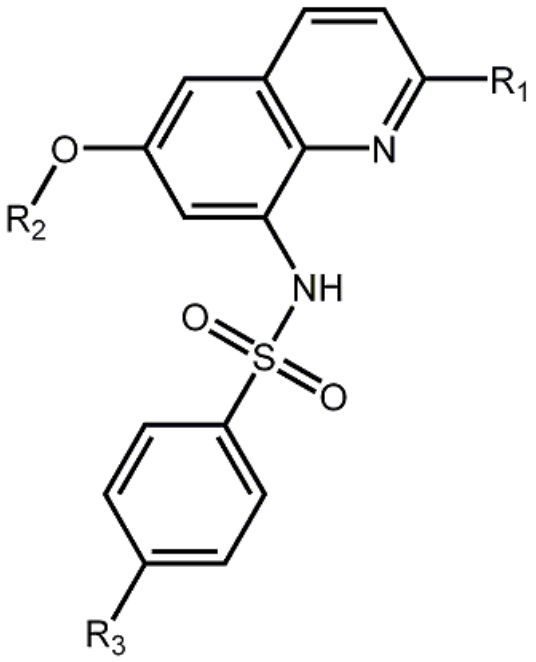

	TSQ	ZQ_{ACID}
R_1	-H	$-CH_3$
R_2	$-CH_3$	$-CH_2COOH$
R_3	$-CH_3$	$-CH_3$

Figure 3.18. Chemical structure of the two quinoline based fluorophores 6-Methoxy-(8-*p*-toluenesulfonamido) quinoline (TSQ) and 6-Methoxy-(8-*p*-toluenesulfonamido) quinolinoxy acetate (ZQ_{ACID}). Similarities and differences of these two molecules are shown. The chemical group R_2 in ZQ_{ACID} makes this fluorophore a negatively charged moiety in neutral aqueous solutions.

3.2.3.1 Reaction of Cd-loaded Proteome with TSQ

TSQ binds to Zn^{2+} or Cd^{2+} with a 2:1 ratio of the ligand to metal. Chelation of the metal cation takes place by nitrogen atoms of the quinoline and sulfonamide groups through donation of lone pair electrons to the metal cation. Therefore, TSQ exhibits higher binding constant with Zn^{2+} in comparison to Cd^{2+} because it prefers N ligation, whereas, Cd prefers S coordination.

Cd-treated proteome with Zn and Cd contents of 9 and 5 μM, respectively, was prepared and reacted with 15 μM of TSQ in 20 mM degassed Tris-HCl buffer, pH 7.4. The control solution consisted of Zn-proteome containing 9 μM Zn and 15 μM TSQ in the same buffer. Fluorescence spectral increases for sample and control solutions were observed over the course of time for 60 minutes after which the final flurorescence spectrum was recorded (**Figure 3.19**). Sample and control solutions were then loaded onto G-75 columns and the collected fractions were measured for their metal contents (**Figure 3.20a, b**) and fluorescence. Reaction of Cd^{2+}-treated proteome (sample) with TSQ displayed much more fluorescence emission when compared with Zn-proteome (control) that contained the same amount of metal (**Figures 3.19 and 3.21**). Considering that $Cd(TSQ)_2$ has only about 1/3 the quantum yield as its Zn^{2+} counterpart, this suggests that Cd^{2+} mobilizes Zn^{2+} within the proteome and makes much more Zn^{2+} accessible to the fluorophore. The λ_{max} emission for the reaction of TSQ with Cd-exposed proteome centered at 470 nm indicative of ternary complex formation (TSQ-Zn-proteome). Cd^{2+} reacted with the proteome without release of any significant Zn^{2+} **(Figure 3.17)**. The fluorescence spectrum indicates that many adventitious sites within the

proteome react with Zn^{2+} and TSQ to form ternary complexes. These results are consistent with the product of reaction- being Cd-proteome•Zn, in which both Cd^{2+} and Zn^{2+} are available for adduct formation with TSQ.

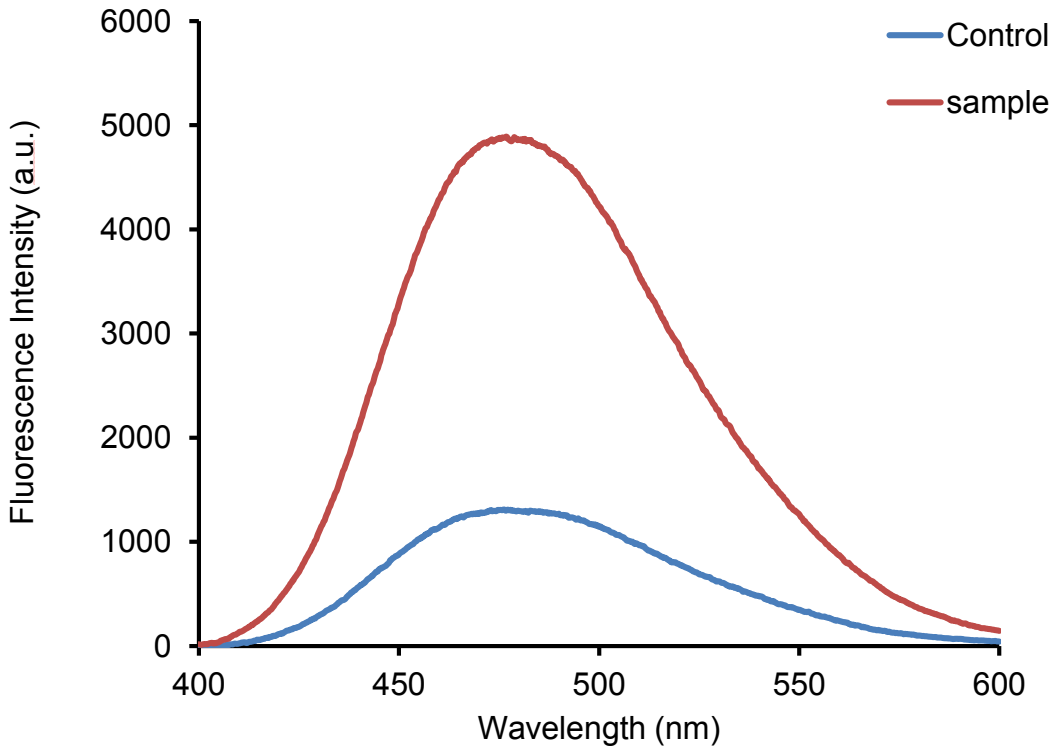

Figure 3.19. Fluorescence emission spectra of Zn-proteome and Cd^{2+} treated Zn-proteome reacted with TSQ. Control solution: Proteome (9 μM Zn^{2+}) reacted with 15 μM TSQ in 20 mM Tris buffer pH 7.4 in a total volume of 1 ml. Sample solution: Proteome (9 μM Zn^{2+}, 5 μM Cd^{2+}) was reacted with 15 μM TSQ in 20 mM Tris buffer pH 7.4 in a total volume of 1 ml. Fluorescence emission spectra were recorded at after 60 min. with an excitation at 370 nm.

A

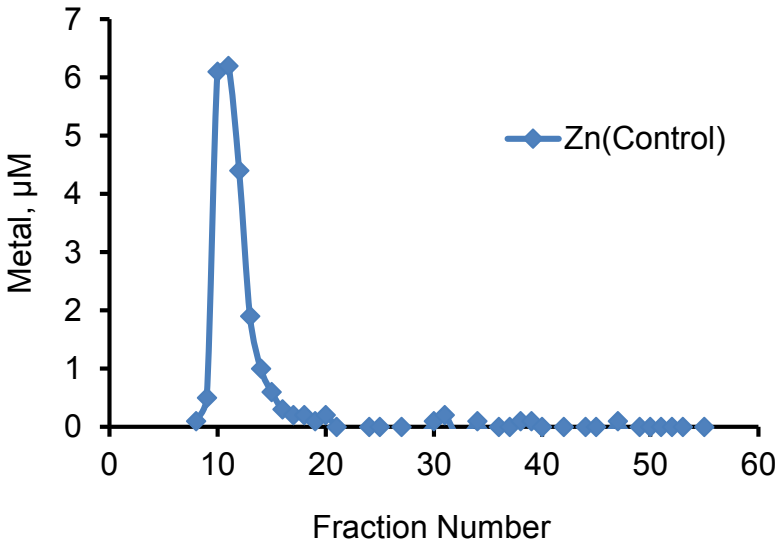

B

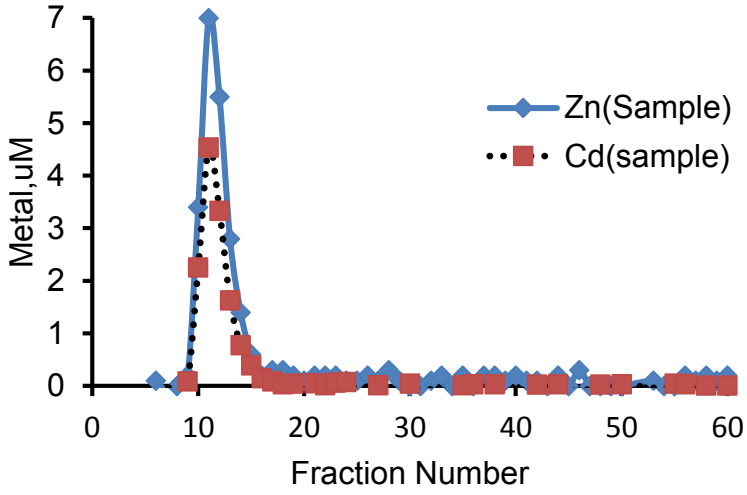

Figure 3.20a, b. Sephadex G-75 Chromatograms of reaction mixures for sample and control solutions (Figure 3.19).

Table 3.2. Summary of data for the reaction between TSQ and the proteome

Control	**Reactants**		**Products**	
	Zn-proteome	TSQ	TSQ-Zn-proteome	Cd, $Zn(TSQ)_2$
Zn^{2+} (μM)	9	0	9.0 ± 0.5 (n=3)	0
Cd^{2+} (μM)	0	0	0	0
Fluoresc., a.u. (λ_{max}, nm)	0	0	1300 ± 50 (470)	0
Sample	**Reactants**		**Products**	
	Cd-proteome•Zn	TSQ	TSQ-Zn,Cd-proteome	Cd, $Zn(TSQ)_2$
Zn^{2+} (μM)	9	0	9.0 ± 0.5	0
Cd^{2+} (μM)	5	0	5.0 ± 0.4	0
Fluoresc., a.u. (λ_{max}, nm)	0	0	4800 ± 100 (470)	0

3.2.3.2 Reaction of Cd-loaded Proteome with ZQ_{ACID}

In order to further investigate the phenomena taking place upon reaction of Cd^{2+} with the proteome, ZQ_{ACID} was used as another specific Zn-sensor. Like TSQ, ZQ_{ACID} binds to Zn^{2+} or Cd^{2+} with a 2:1 ratio of the ligand to metal and prefers binding to Zn^{2+} over Cd^{2+}. $Zn(ZQ_{ACID})_2$ displays a fluorescent emission with a λ_{max} at 490 nm. ZQ_{ACID} also makes ternary complexes with Zn-proteome with a λ_{max} at about 470 nm [129].

Zn-proteome containing 4.5 μM Zn^{2+} (as control) and Cd-treated proteome containing 4.5 μM Zn^{2+} and 3.2 μM Cd^{2+} (as sample) were reacted with 15 μM ZQ_{ACID} in degassed Tris-HCl buffer pH 7.4. The fluorescence emission spectrum of each reaction mixture was recorded for 60 minutes (**Figure 3.21a, b**) using excitation at 370 nm. To separate proteins from low molecular weight species, Amicon centrifugal filtraters were employed. Sample and control solutions were concentrated to a very small volume using Amicon 30 kDa cut off filters and control and sample filtrates were collected as low molecular weight moieties and their fluorescence measured (**Figure 3.22a, b**). Tris-HCl buffer was added to restore control and sample concentrated proteomes to their initial volumes. Their fluorescence spectra were also recorded (**Figure 3.23a, b**). The significant increase of fluorescence emission from the control to the sample solution (**Figure 3.21a, b**) indicates an enhanced metal availability in the proposed Cd-proteome•Zn product for reaction with ZQ_{ACID}. The dominating λ_{max} at about 480 nm (**Figure 3.23a, b**) shows that ZQ both form ternary adducts with Cd-proteome and also 1:2 metal to ligand complexes. The λ_{max} emission at 490 nm for the

sample filtrate confirms that the sample also contained low molecular weight, free complex $M(ZQ_{ACID})_2$.

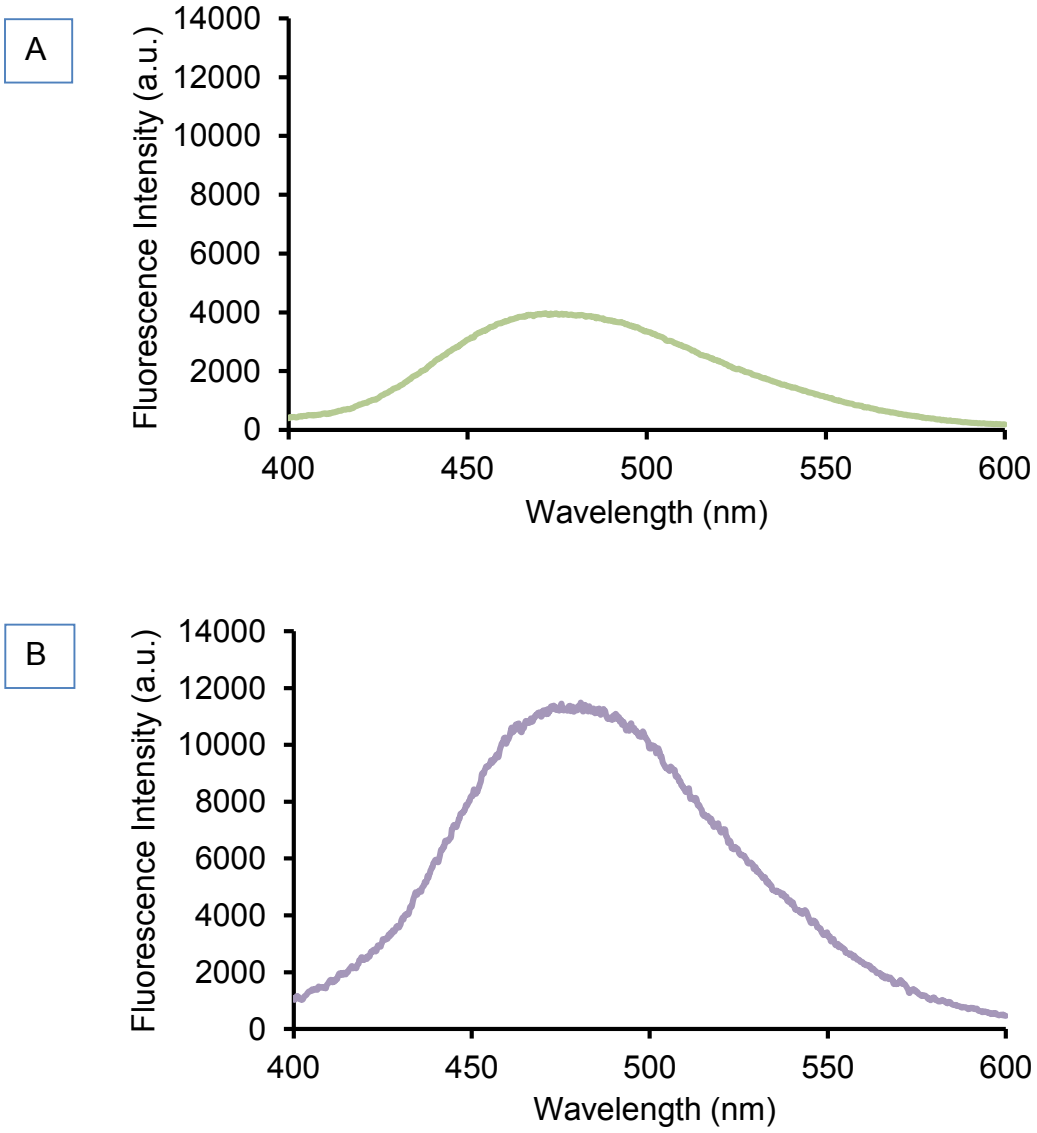

Figure 3.21a, b. Fluorescence spectra of Zn-proteome and Cd^{2+} treated Zn proteome reacted with ZQ_{ACID}. A. Spectrum of Zn-proteome containing 4.5 µM Zn^{2+} reacted with 15 µM ZQ_{ACID} in 20 mM degassed Tris-HCl buffer pH 7.4. B. Spectrum of Cd^{2+} exposed Zn-proteome containing 4.5 and 3.2 µM Zn^{2+} and Cd^{2+}, respectively, reacted with 15 µM ZQ_{ACID} in 20 mM Tris-HCl buffer pH 7.4. Fluorescence emission spectra were recorded after 60 minutes with an excitation at 370 nm.

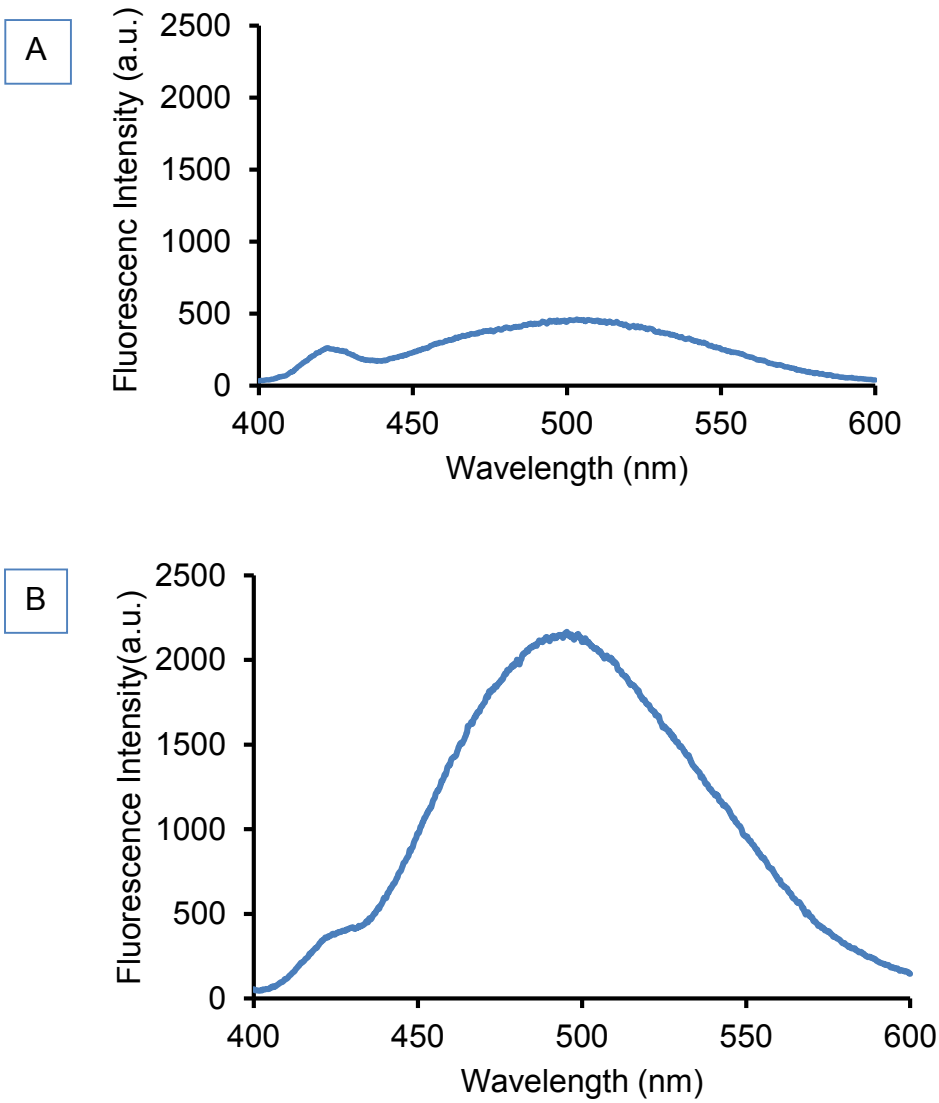

Figure 3.22a, b. Fluorescence emission spectra of the filtrate from centrifugal separation of control (A) and Cd^{2+} exposed sample (B) in figure 3.21.

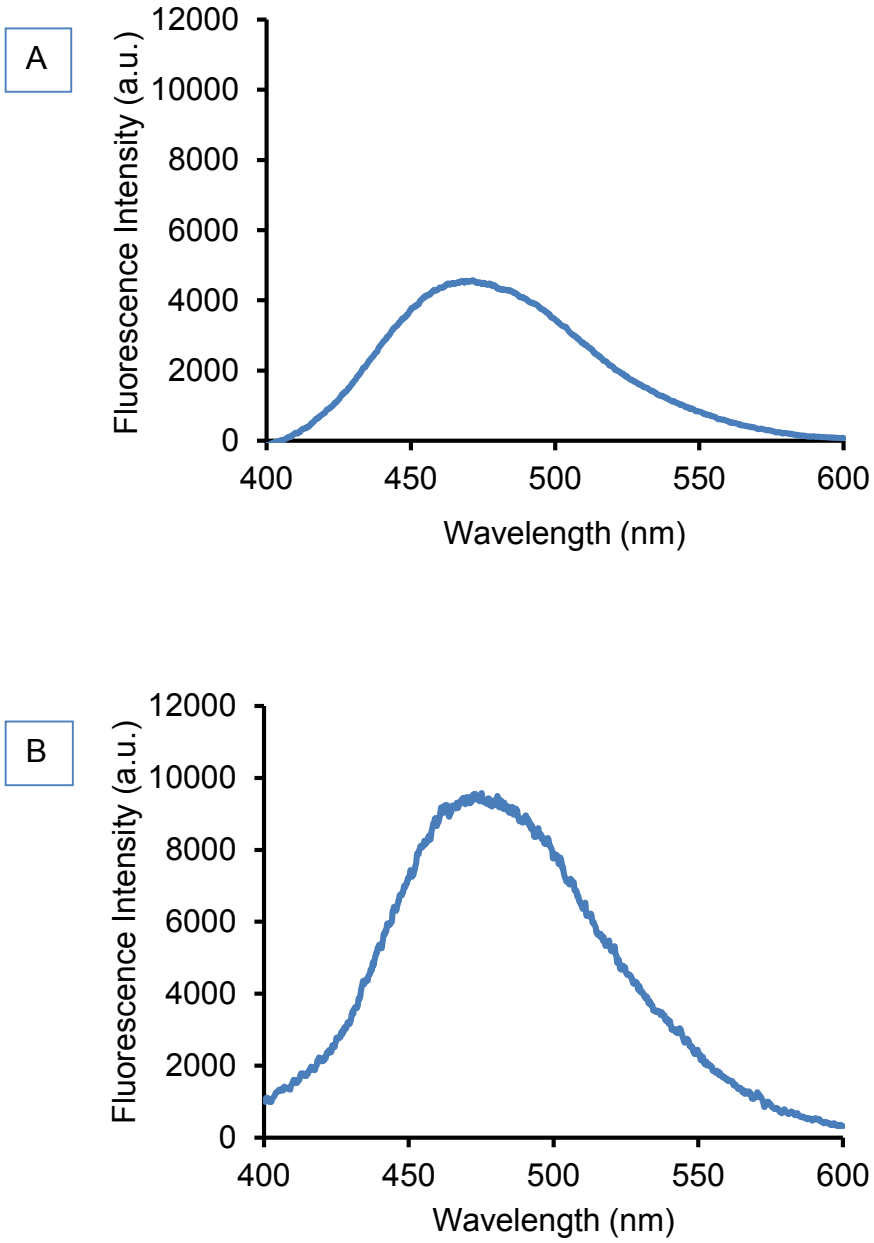

Figure 3.23a, b. Fluorescence emission spectra of the retentates from centrifugal separation of control (A) and Cd^{2+} exposed sample (B) in Figure 3.21.

Table 3.3. Summary of data for the reaction between ZQ_{ACID} and the proteome

Control	**Reactants**		**Products**	
	Zn-proteome	ZQ_{ACID}	ZQ-Zn-proteome	Cd, $Zn(ZQ_{ACID})_2$
Zn^{2+} (μM)	4.5	0	4.0 ± 0.4 (n=3)	0.5±0.2
Cd^{2+} (μM)	0	0	0	0
Fluoresc., a.u. (λ_{max}, nm)	0	0	4500 ±100 (467)	450 (492)
Sample	**Reactants**		**Products**	
	Cd-proteome•Zn	ZQ_{ACID}	ZQ_{ACID}-Zn, Cd-proteome	Cd, $Zn(ZQ_{ACID})_2$
Zn^{2+} (μM)	4.5	0	2.0 ± 0.3	2.5 ± 0.3
Cd^{2+} (μM)	3.2	0	3.2 ± 0.2	0.0 ± 0.2
Fluoresc., a.u. (λ_{max}, nm)	0	0	9400 ± 100 (470)	2100 ± 50 (492)

These results confirm the finding with TSQ that upon reaction of Zn-proteome with Cd^{2+}, Zn^{2+} is labilized. In this case this is seen directly through the formation of $Zn(ZQ)_2$. ZQ bind Zn^{2+} more strongly than TSQ. As a result, $Zn(ZQ)_2$ forms whereas $Zn(TSQ)_2$ did not. Indeed, the concentration of mobilized Zn^{2+} is only 75% of the Cd^{2+} added to the proteome. So the Cd–Zn exchange process is at least semi-quantative by this measure. Interestingly, no $Cd(ZQ)_2$ was detected in the filterate, indicating significant stability of Cd-proteome species.

3.2.4. Reaction of Cd-loaded proteome with EDTA

Previous studies have shown that EDTA can sequester about 30% of Zn^{2+} from Zn-proteome upon 30-minute incubation with it [158]. The question is: Does Cd-treated (Zn)-proteome exhibit the same behavior? Based on our hypothesis about the increase of Zn^{2+} labiality in Zn•proteome incubated with Cd^{2+}, we expected a higher extent of reactivity with EDTA than seen in control Zn-proteome. In order to answer the question, EDTA was reacted with both Zn-proteome and Cd-treated (Zn)-proteome and their G-75 chromatograms were compared to reveal their corresponding extent of reactivity with EDTA. Cd-treated (Zn)-proteome containing 44 μM Zn^{2+} and 22 μM Cd^{2+} was reacted with 86 μM EDTA in degassed 20 mM Tris-HCl buffer, pH 7.4, 0.1 M KCl and incubated for 60 minutes before loading onto a G-75 column. A control solution of Zn-proteome (44 μM Zn) was prepared with all concentrations and conditions similar to those of the Cd-treated sample. Sephadex G-75 Chromatography of the reaction mixtures was carried out to separate proteome and EDTA. Collected fractions for both control and sample solutions were then analyzed for their Zn^{2+} and Cd^{2+} contents. Chromatograms showing metal contents of control and sample fractions obtained from the G-75 column are depicted in **Figure 3.24a, b**. Integration of chromatograms, shows transfer of 13 μM (30%) Zn and 26 μM Zn (60%), and 6 μM Cd (60%) from proteome to EDTA for control and sample solutions, respectively. The higher sequestration of metal from Cd-loaded (Zn)-proteome when compared to the control solution of native Zn-proteome, indicates a boosted lability of Zn^{2+} in Cd-

exposed (Zn)-proteome. Thus, the results are consistent with proteomic Cd-Zn exchange reaction leading to Cd-proteome•Zn.

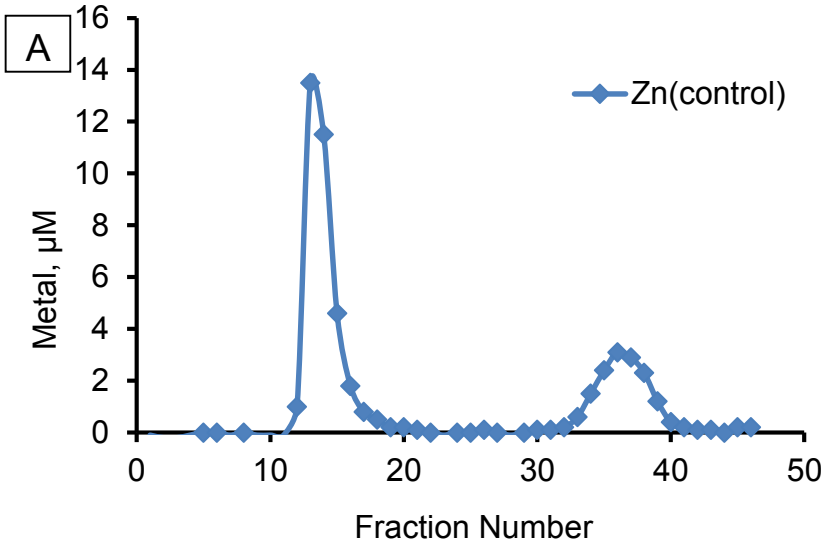

Figure 3.24a. Sephadex G-75 chromatography of the reaction mixture of EDTA and Zn-proteome. Proteome containing 44 µM Zn^{2+} was reacted with 86 µM EDTA in 20 mM Tris, 0.1 M KCl buffer, pH 7.4. Reaction time was 60 min.

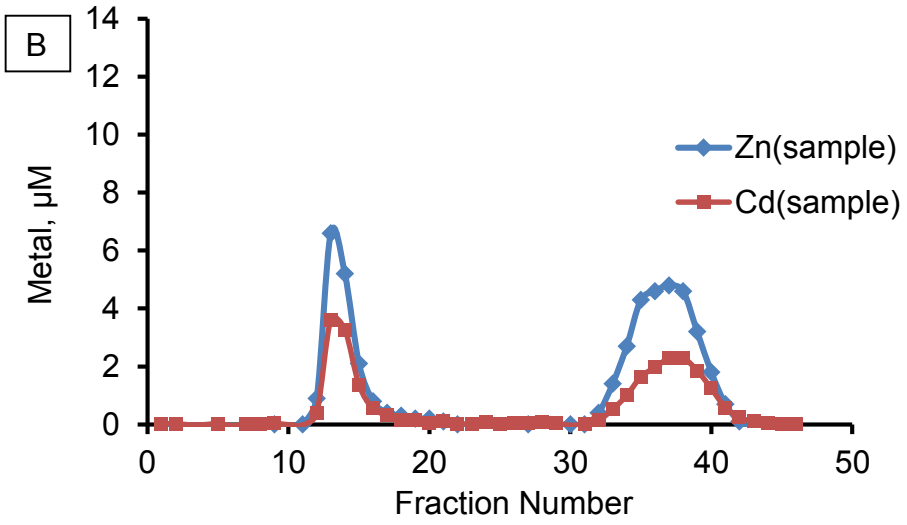

Figure 3.24b. Sephadex G-75 chromatography of the reaction mixture of EDTA and Cd-loaded proteome. Proteome containing 44 µM Zn^{2+} and 22 µM Cd^{2+} was reacted with 86 µM EDTA in 20 mM Tris, 0.1 M KCl buffer, pH 7.4. Reaction time was 60 min.

Table 3.4. Summary of data for the reaction between proteome and Cd-loaded proteome with EDTA

Control	**Reactants**		**Products**	
	Zn-proteome	EDTA	Zn-proteome	Zn-EDTA
Zn^{2+} (μM)	44	0	31±1 (n=3)	13±1
Cd^{2+} (μM)	0	0	0	0
Sample	**Reactants**		**Products**	
	Cd-proteome•Zn	EDTA	Cd-proteome•Zn	Zn,Cd-EDTA
Zn^{2+} (μM)	44	0	18±1	26±1
Cd^{2+} (μM)	22±1	0	16±2	6±2

3.2.5. Reaction of Cd-loaded Proteome with apo-MT

Chelators such as EDTA, EGTA, and TPEN, regardless of their binding constant with Zn^{2+}, react with proteome and sequester about 30% of Zn^{2+} from it [158]. In contrast to the above mentioned chelators, apo-MT, which has a high binding constant with Zn^{2+}, has been observed to remain almost inert in the presence of susceptible proteome, only chelating less 0-10% of the total Zn^{2+}. The above mentioned observations led us to test the reactivity of apo-MT with the hypothesized Cd-proteome•Zn to better understand the properties of Cd-loaded proteome. In this study, 4 μM apo-MT (28 μM Zn^{2+} binding sites) was reacted with Zn-proteome containing 28 μM Zn^{2+} (control) or Cd-proteome•Zn containing 28

μM Zn^{2+} and 23 μM Cd^{2+} (sample) in 10 mM Tris buffer, pH 7.4, 0.1 M KCl. After running sample and control solutions over a Sephadex G-75 column and analyzing metal content of 1 ml collected fractions, their corresponding chromatograms were obtained (**Figure 3.25a, b, c**). Integration over concentrations of Zn^{2+} and Cd^{2+} peaks for the HMW and LMW regions of sample and control chromatograms shows that in comparison with the chelation of 0-10% of Zn^{2+} in Zn-proteome by apo-MT, metal chelation increased drastically when Cd-proteome•Zn reacted with apo-MT. 73% of Cd^{2+} (17 μM) and 40% of Zn^{2+} (11 μM) were sequestered from Cd-proteome•Zn by this limiting concentration of apo-MT. These results indicate that upon reaction of Cd^{2+} with Zn-proteome, much of its Zn^{2+} underwent a rearrangement in binding sites that leads to a higher lability of Zn^{2+} in the proteome. In addition, most of the Cd^{2+} that had hypothetically replaced Zn^{2+} in native Zn-binding sites was reactive with apo-MT. The fact that some Cd-proteome survived in the presence of apo-MT suggests that some Cd-proteome is stable in the presence of apo-MT. Thus, the results support the hypothesis that Cd^{2+} displaces Zn^{2+} from native Zn-binding sites in Zn-proteome to form Cd-proteome•Zn.

$$m\ \text{Cd-Proteome•Zn} + \text{apo-MT} \rightleftharpoons m\ Cd_{(1-\delta)}\text{-proteome•}Zn_{(1-\Delta)} + Cd_{m\delta}\text{-MT•}Zn_{(m\Delta)} \quad (35)$$

$$m(\delta+\Delta)=7$$

In this equation δ, Δ parameters represent the fraction of Cd^{2+} and Zn^{2+} loss from Cd-proteome•Zn, respectively. m is the factor to normalize sum of δ and Δ to 7, which is MT capacity for Zn^{2+} and/or Cd^{2+} uptake.

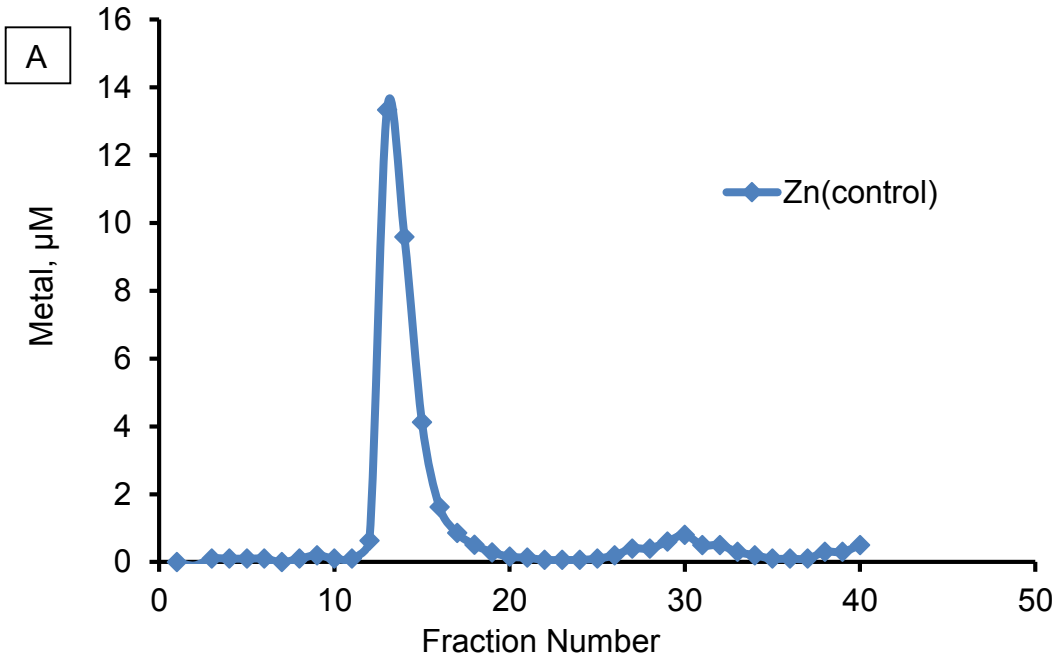

Figure 3.25a. Sephadex G-75 chromatography of the reaction mixture of apo-MT and Zn-proteome. Proteome containing 28 µM Zn^{2+} reacted with 4 µM apo-MT (28 µM Zn^{2+}) in 20 mM Tris, 0.1 M KCl buffer, pH 7.4. Reaction time was 60 min.

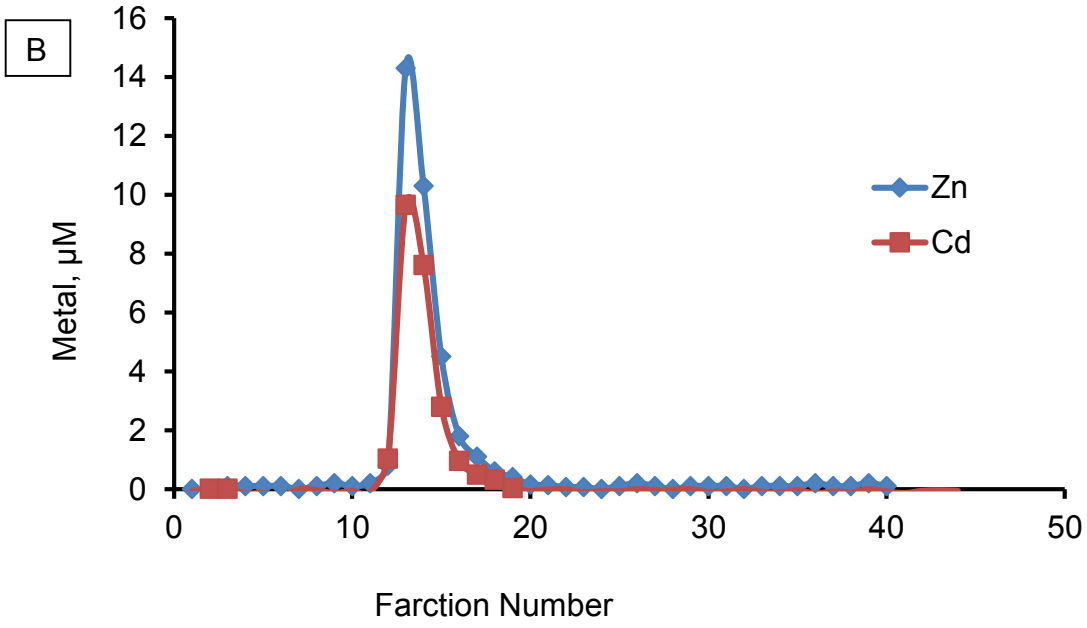

Figure 3.25b. Sephadex G-75 chromatogram of Cd-loaded proteome containing 28 µM Zn^{2+} and 23 µM Cd^{2+}.

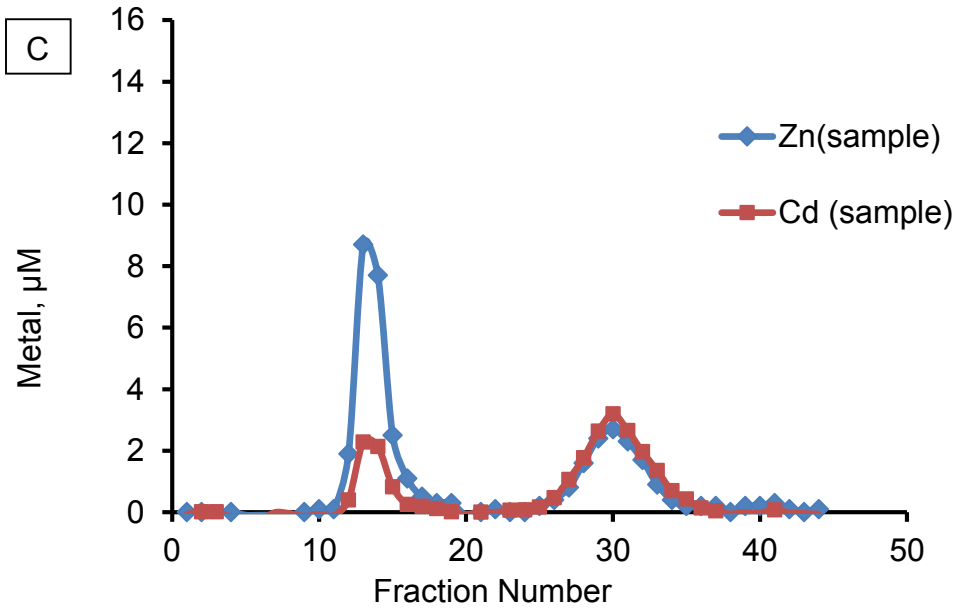

Figure 3.25c. Sephadex G-75 chromatography of the reaction mixture of apo-MT and Cd-loaded proteome. Proteome containing 28 µM Zn^{2+} ± 23 µM Cd^{2+} reacted with 4 µM apo-MT (28 µM Zn^{2+} or Cd^{2+} binding capacity) in 20 mM Tris, 0.1 M KCl buffer, pH 7.4. Reaction time, 60 min

Table 3.5. Summary of data for the reaction between the proteome and Cd-loaded proteome with apo-MT

Control	**Reactants**		**Products**	
	Zn-proteome	Apo-MT	Zn-proteome	Zn-MT
Zn^{2+} (µM)	28	0	28±1 (n=3)	3±1
Cd^{2+} (µM)	0	0	0	0
Sample	**Reactants**		**Products**	
	Cd-proteome•Zn	Apo-MT	Cd-proteome•Zn	Cd, Zn-MT
Zn^{2+} (µM)	28	0	17±1	11±1
Cd^{2+} (µM)	23±1	0	6±2	17±2

3.2.6. Reaction of Cd-loaded Proteome with Zn_7-MT

Based on our finding (part 3.2.1), Cd^{2+} reacts with the (Zn)-proteome and does not cause any release of Zn^{2+} from the proteome pool. Cd-loaded protein in turn exhibits more reactivity with competing ligands (parts 3.2.2-4) when compared to native proteome. We hypothesized that the reaction of Cd^{2+} with the proteome involved displacement of Zn^{2+} from Zn-proteome by Cd^{2+} and binding of Zn^{2+} again to the proteome. Zn-proteome and Cd-treated (Zn)-proteome were reacted with Zn_7-MT as control and sample reactions, respectively, to test our hypothesis.

A sample solution of Cd-proteome•Zn with respective Zn^{2+} and Cd^{2+} concentrations of 44 µM and 23 µM was reacted with 8 µM Zn_7-MT in10 mM Tris buffer, pH=7.4, KCl=0.1M, in 1 ml total volume. A control solution of 1 ml Zn-proteome was reacted with Zn_7-MT under the same conditions as above. Sample and control solutions were run over G-75 columns equilibrated with 10 mM degassed Tris buffer, pH 7.4. One ml sample and control fractions were collected and analyzed by AAS to assess Zn^{2+} and Cd^{2+} contents. Chromatograms obtained for control and sample (**Figure 3.26a, b, c**) show that an exchange of Cd^{2+} and Zn^{2+} takes place between Cd-proteome•Zn and Zn_7-MT. Integration of the second peak in **Figure 3.26c** for Cd^{2+} (fractions 22-32) indicates an uptake of about 17 nmol by MT, equal to the concentration of 17 µM in the loaded sample. The same amount of Zn^{2+} was sequestered from Zn_7-MT and was taken up by Cd-proteome•Zn. The metal ion exchange reaction between Cd-proteome•Zn and Zn_7-MT can be shown by the following chemical equation:

$$m\ Cd\text{-}Proteome\bullet Zn + Zn_7\text{-}MT \rightleftharpoons m\ Cd_{(1-\delta)}\text{-}proteome\bullet Zn_{(1+\delta)} + Cd_{m\delta},\ Zn_{(7-m\delta)}\text{-}MT \quad (36)$$

In this reaction, δ is the parameter ranging from 0-1.0 that describes the extent of metal ion exchange. By comparing the total amount of Cd^{2+} in the Cd-proteome•Zn with the amount taken up by metallothionein, the δ parameter in the exchange reaction can be obtained. The high value for δ (=0.73) is an indicative of efficient exchange of Cd^{2+} for Zn^{2+} in MT and Zn^{2+} for Cd^{2+} in the proteome. These results are consistent with the fact that the majority of intracellular Cd^{2+} is accumulated into MT.

In vitro ^{113}Cd NMR study on rabbit liver MT has shown a strikingly similar metal exchange reaction to reaction 36 between Zn_7-MT and Cd_7-MT [159].

$$m\ Zn_7\text{-}MT\ +\ n\ Cd_7\text{-}MT \rightleftharpoons (m+n)\ Cd_{(7n/m+n)},Zn_{(7m/m+n)}\text{-}MT \quad (37)$$

This result also broadens the potential for this reaction to sequester Cd^{2+} in MT beyond an earlier Cd-Zn exchange reaction that has also seen between Zn-MT and Cd-carbonic anhydrase and Cd-tramtrack Zn-finger peptide [160, 161].

The amount of Cd^{2+}, which stays bound to the proteome in the presence of MT, is hypothesized to contribute to the toxicity in cells. For example, the down-regulation of Sp1 transcription factor activity continues even as MT synthesis is induced and much of the Cd^{2+} localizes in the MT pool. In vitro, Cd^{2+} readily competes with Zn^{2+} for binding to Sp1 and in the process inhibits its ability to bind to *SGLT1* and *2* promoter sites [162].

$$3Cd^{2+} + Zn_3\text{-Sp1} \rightleftharpoons Cd_3\text{-Sp1} + 3\,Zn^{2+} \qquad (38)$$

An approximate equilibrium constant calculated on the basis of this reaction is 10, indicating a small preference for binding of Cd^{2+} to the protein [80]. This probably reflects the stronger affinity of Cd^{2+} than Zn^{2+} for the two thiolate ligands in the binding site. Neither Zn_3-Sp1 nor Cd_3-Sp1 should be stable in the presence of apo-MT. The fact that the Sp1 remains functionally down-regulated in the presence of induced MT is consistent with in-vitro experiments suggesting that Cd_3-Sp1 converts to Cd_n-Sp1 (n=1-3) that binds Cd^{2+} with much larger affinity.

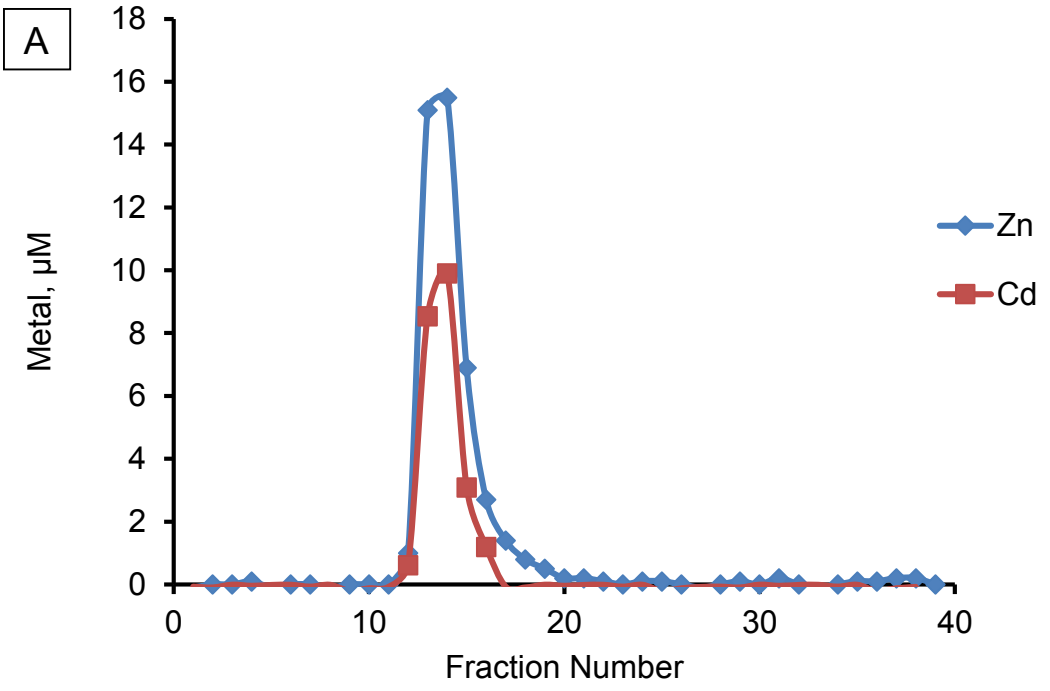

Figure 3.26a. Sephadex G-75 chromatography of Zn-proteome reacted with Cd^{2+}. Zn-proteome containing 44 µM Zn^{2+} was reacted with 25 µM Cd^{2+} and ran over Sephadex G-75 column. One-ml fractions were analyzed with AAS for their Zn^{2+} and Cd^{2+} content.

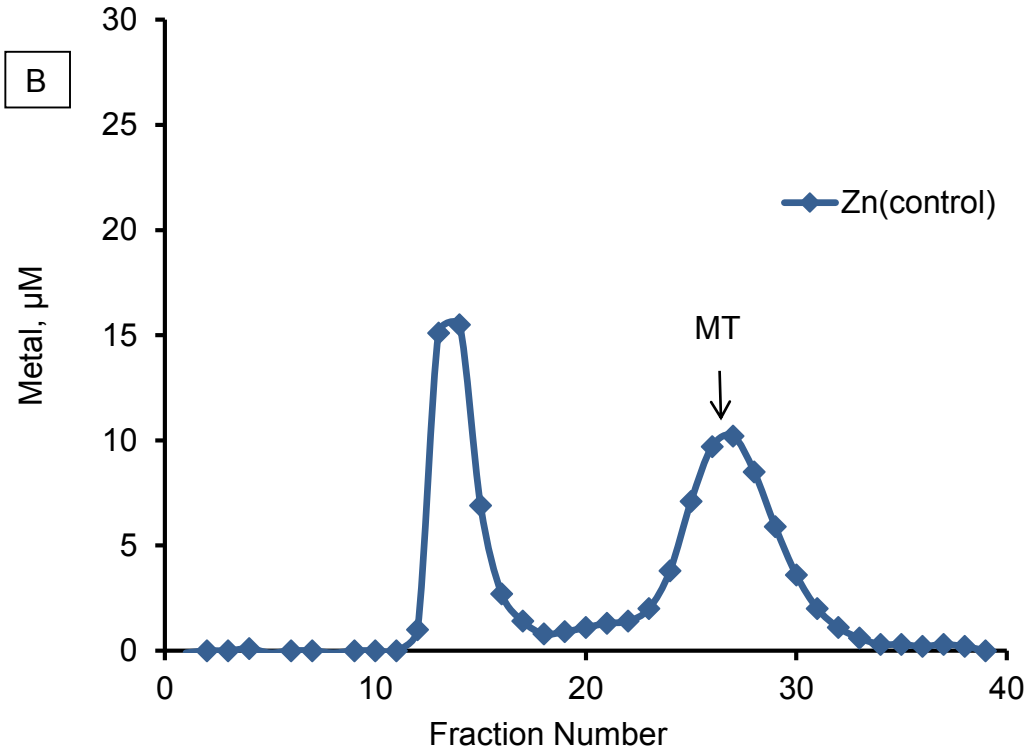

Figure 3.26b. Control Solution: Sephadex G-75 chromatography of the reaction of Zn-MT and Zn-proteome. Proteome containing 44 µM Zn^{2+} reacted with Zn_7-MT (56 µM Zn^{2+}) in 20 mM Tris, 0.1 M KCl buffer, pH 7.4. Reaction time, 60 min.

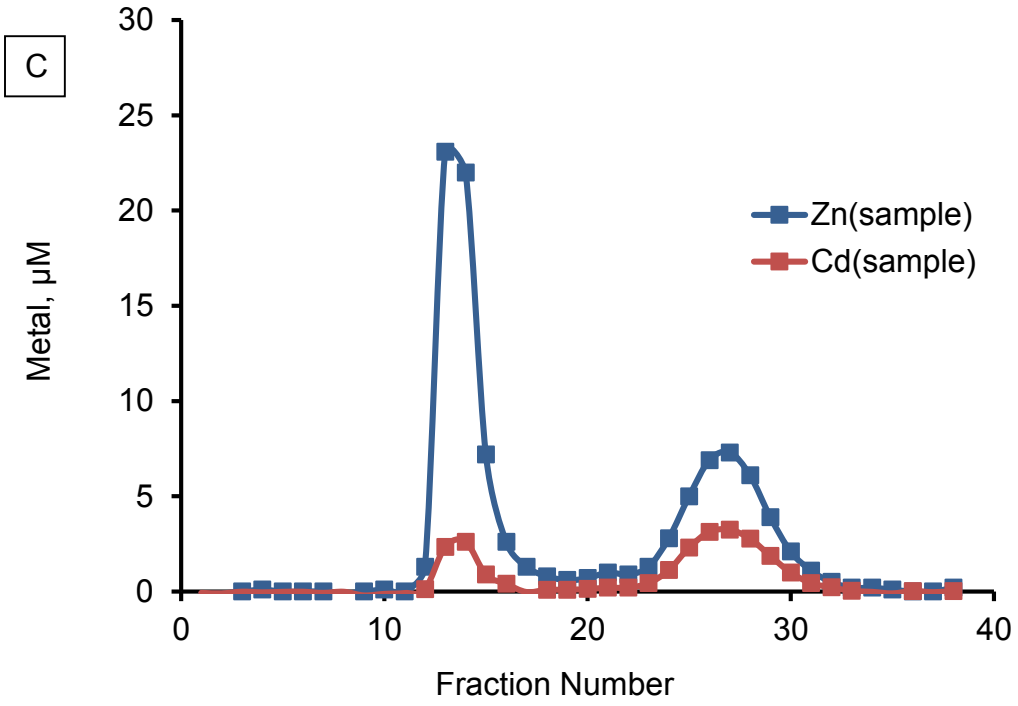

Figure 3.26c. Sephadex G-75 chromatography of the reaction of Zn-MT and Cd-loaded proteome**. Sample Solution**: Proteome containing 44 µM Zn^{2+} ± 23 µM Cd^{2+} reacted with Zn_7-MT (56 µM Zn^{2+}) in 20 mM Tris, 0.1 M KCl buffer, pH 7.4. Reaction time, 60 min

Table 3.6. Summary of data for the reaction between the proteome and Cd-loaded proteome with Zn_7-MT

Control	**Reactants**		**Products**	
	Zn-proteome	Zn_7-MT	Zn-proteome	Zn-MT
Zn^{2+} (µM)	44	56	44±2 (n=3)	56±2
Cd^{2+} (µM)	0	0	0	0
Sample	**Reactants**		**Products**	
	Cd-proteome•Zn	Zn_7-MT	Cd-proteome•Zn	Cd, Zn-MT
Zn^{2+} (µM)	44	56	60±3	38±2
Cd^{2+} (µM)	23±2	0	6±1	17±2

3.2.7. Reaction of Zn-loaded proteome with ZQ_{ACID}

Proteome extracted and isolated from the cytosol of LL-CPK_1 cells (containing 5.5 μM Zn^{2+}) was reacted with 5.5 μM of Zn^{2+} in 20 mM degassed Tris-HCl buffer, pH 7.4 KCl 0.1 M. The product was loaded onto a G-75 column and collected fractions corresponding to the high molecular weight region were pooled, analyzed for their Zn^{2+} and labeled as Zn-proteome•Zn. No free Zn^{2+} was detected in the low molecular weight region indicative of binding all Zn^{2+} to the proteome. This was further confirmed from the Zn^{2+} content of the pooled Zn-proteome•Zn (containing 11 nanomoles Zn^{2+}).

$$\text{Zn-proteome} + Zn^{2+} \rightleftharpoons \text{Zn-proteome•Zn} \qquad (39)$$

Pooled Zn-proteome•Zn was concentrated to its initial volume of 1 ml using 30 kDa cut off Amican filter. Zn-proteome and Zn-proteome•Zn containing 5.5 μM Zn^{2+} each, were reacted with 26 μM ZQ_{Acid} in 1 ml 20 mM degassed Tris-HCl buffer pH 7.4 and KCl =0.1 M as control and sample solutions, respectively. Fluorescence emission (excitation at 370 nm) intensity for control and sample solutions was recorded between 400-600 nm for about 2 hours starting immediately after mixing of reactants with an excitation at 370 nm. Figures **3.27a** and **3.27b** show control and sample spectra recorded over a course of 110 minutes. Fluorescence emission at 470 nm and 490 nm was depicted versus time in figure **3.28a** and **3.28b** for control and sample solutions. Fluorescence intensities of about 5000 units at 470 nm and 490 nm for the sample solution versus intensities of about

3000 units for the control solution indicate that Zn^{2+} was more labile and reactive in Zn-Proteome•Zn than in native Zn-Proteome.

Not only the extent of reaction differs from control solution to the sample solution but also their kinetics of reaction are different. Contribution of the 50% external Zn^{2+} in Zn-proteome•Zn to the kinetics of the sample reaction is evident from kinetics analysis of control and sample reactions. A comparison of **Figures 28a** and **28b** shows that the kinetics of the sample reaction consists of three phases of reactions. However, the control reaction exhibits a biphasic reaction of fast and slow reactions. The phase I in the sample reaction which is totally absent for the control reaction, can be ascribed to to the Zn^{2+} added to the proteome.

In order to have enough Zn^{2+} in the proteome to be detectable in atomic absorption spectroscopy, the above mentioned reactions were done with higher amounts of proteome and ZQ_{Acid}. Proteome containing 20 μM Zn^{2+} were used for this part of the experiment for both control and sample reactions. The product of the control and sample solutions were run over G-75 columns and 1ml collected fractions were analyzed for their Zn^{2+} and fluorescence intensities. **Figure 3.29** shows chromatograms of control and sample solutions. Integration of the Zn^{2+} in the low molecular weight region of the chromatogram shows sequestration of 12% and 28% of Zn^{2+} by ZQ_{Acid} from the control and sample proteome, respectively. **Figures 3.30a1-b2** show the fluorescence spectrum of control and sample fractions recorded between 400-600 nm with an excitation at 370 nm. Fluorescence spectra for fractions of the high molecular regions of the chromatogram exhibit the characteristic λ_{max} 470 nm indicative of adduct formation

and low molecular weight fractions give a λ_{max} at 490 nm implying free complex formation of ZQ_{Acid} and Zn^{2+}. Summation of fluorescence intensities at 490 nm in the low molecular region of the chromatograms for the control and sample solutions gives similar fractional amounts of 0.12 and 0.28 of total Zn^{2+} sequestered from Zn-proteome and Zn-proteome.Zn by ZQ_{Acid}. Integration of fluorescence intensities for the high molecular region of the sample in comparison to that of the control show that adduct formation in the sample proteome is more facilitated and more Zn^{2+} can be accessed by ZQ_{Acid} for adduct formation.

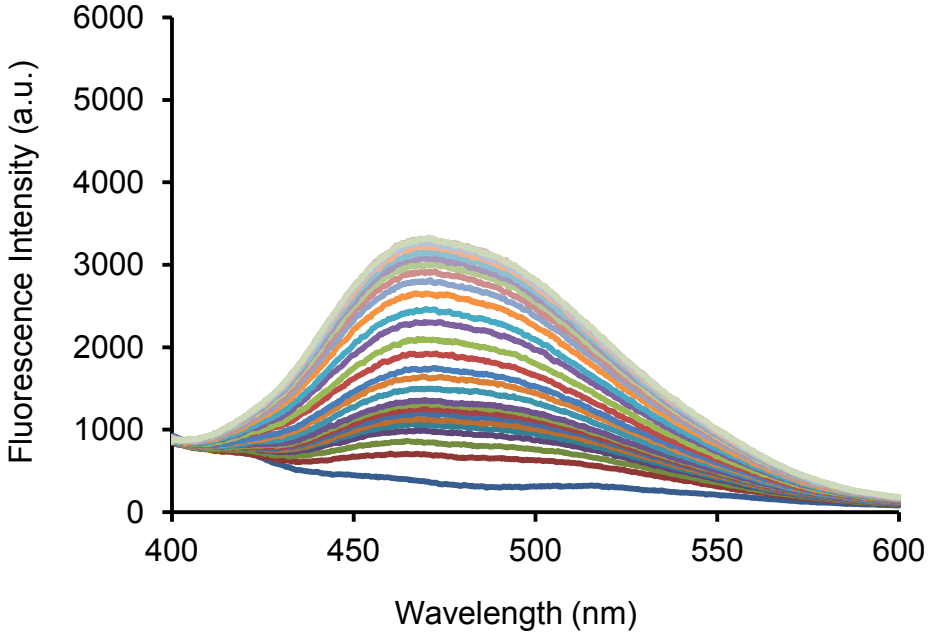

Figure 3.27a. Fluorescence spectrum for control solution of reaction between Zn-proteome and ZQ_{Acid}. Emission spectrum with a λ_{max} at about 470 nm and a shoulder at 490 nm is indicative of formation of both ZQ_{Acid}-Zn-proteome adduct and the free complex $Zn(ZQ_{Acid})_2$ in this reaction.

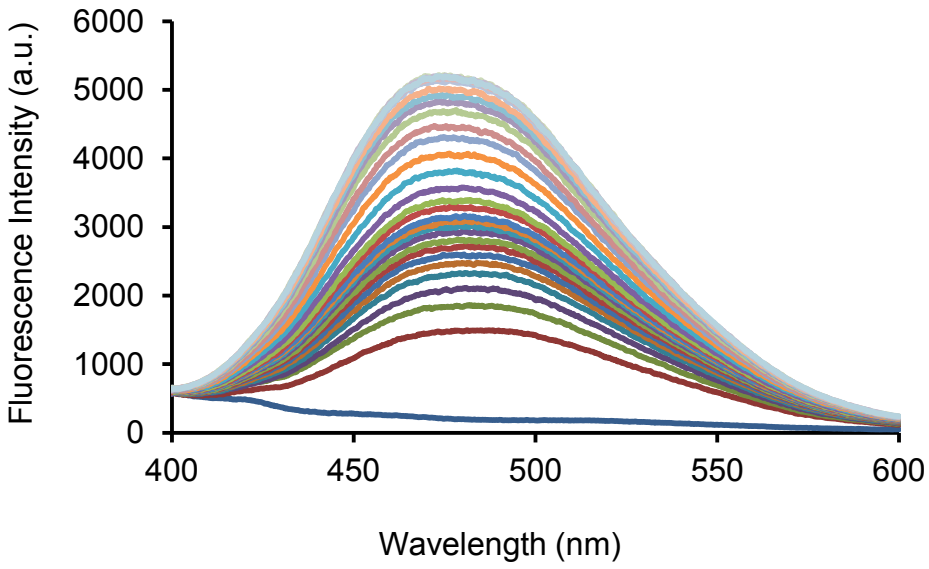

Figure 3.27b. Fluorescence spectrum for the sample solution of the reaction between Zn-proteome and ZQ_{Acid}. Higher fluorescence intensity for the sample in comparison to the control solution indicates a higher reactivity between Zn^{2+} from Zn-proteome.Zn and ZQ_{Acid}.

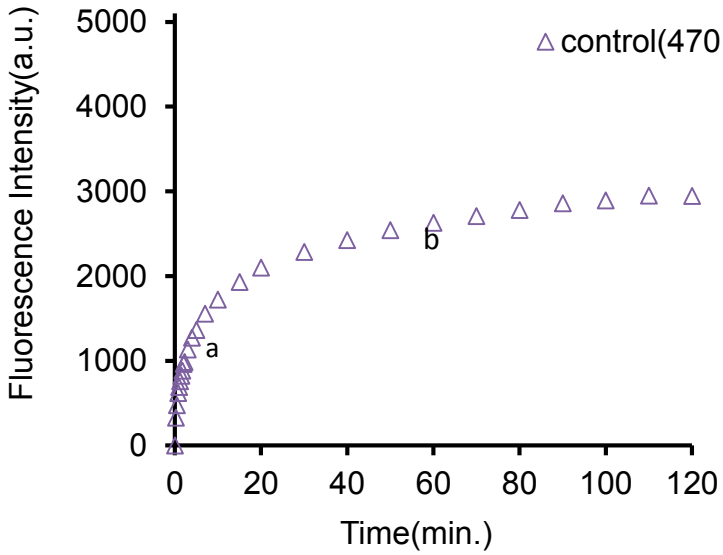

Figure 3.28a. Diagram of fluorescence intensities at 470 nm versus time for the control reaction (Figure 3.27a). Zn-proteome containing 5.5 µM Zn^{2+} reacted with 26 µM ZQ_{Acid} in 20 mM degassed Tris-HCl buffer pH 7.4.

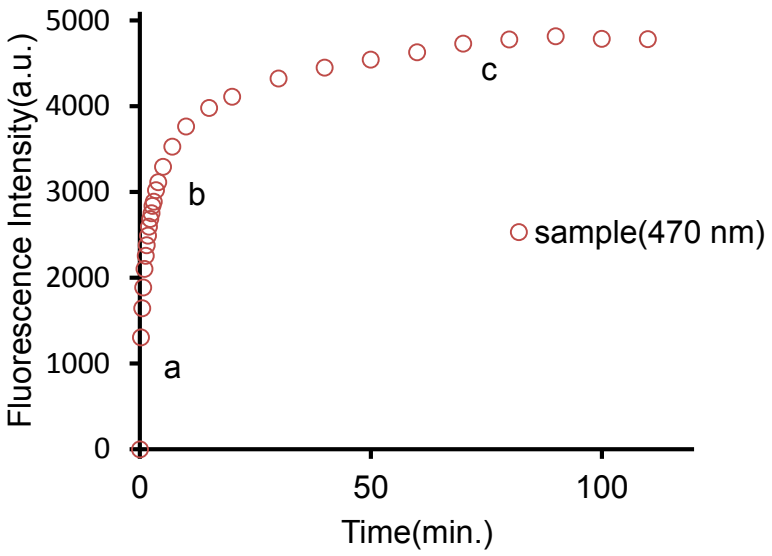

Figure 3.28b. Diagram of fluorescence intensities at 470 nm versus time for the sample reaction (Figure 3.27b). Zn-Proteome•Zn containing 5.5 μM Zn^{2+} reacted with 26 μM ZQ_{Acid} in 20 mM degassed Tris-HCl buffer pH 7.4.

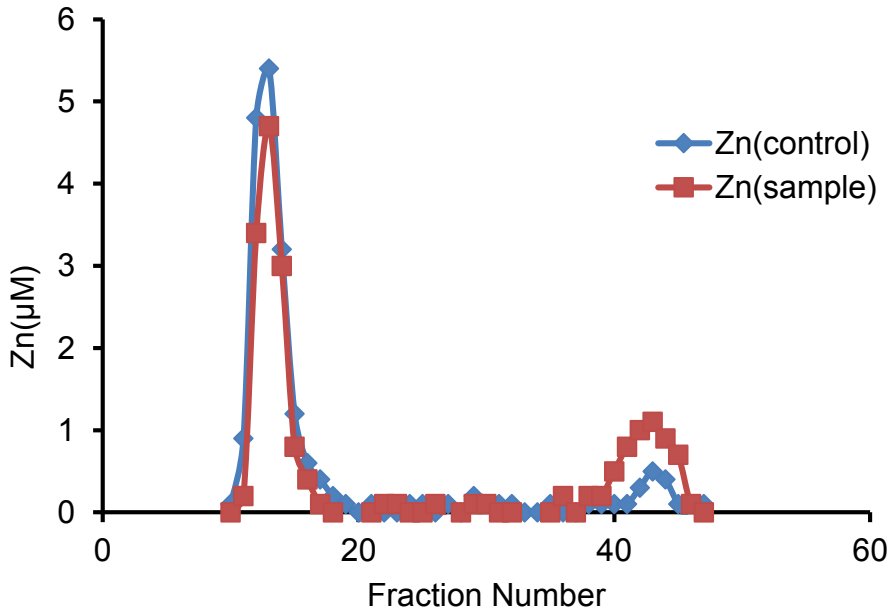

Figure 3.29. Sephadex G-75 chromatography of Zn-proteome reacted with ZQ. Control (10 μM) Zn^{2+} as Zn-proteome) and Sample (10 μM Zn-proteome and 10 μM Zn^{2+} reacted with 50 μM ZQ). Reaction time, 60 min.

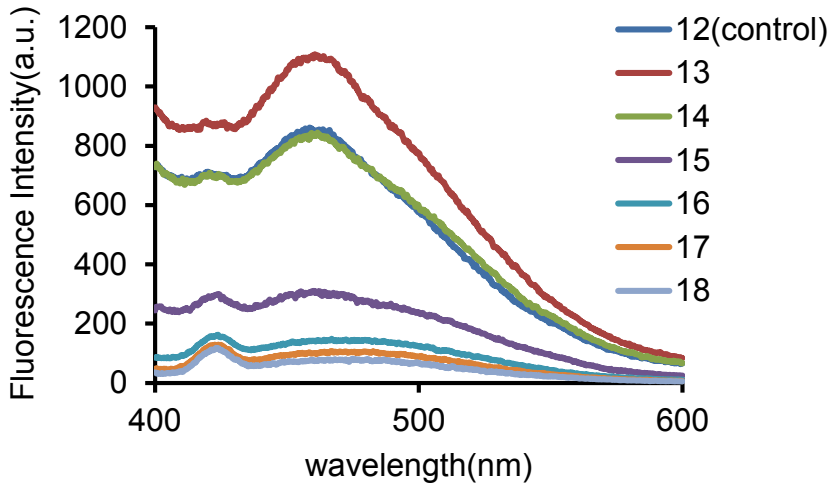

Figure 3.30a1. Fluorescence spectra of the control fractions corresponding to the high molecular weight region of the chromatogram.

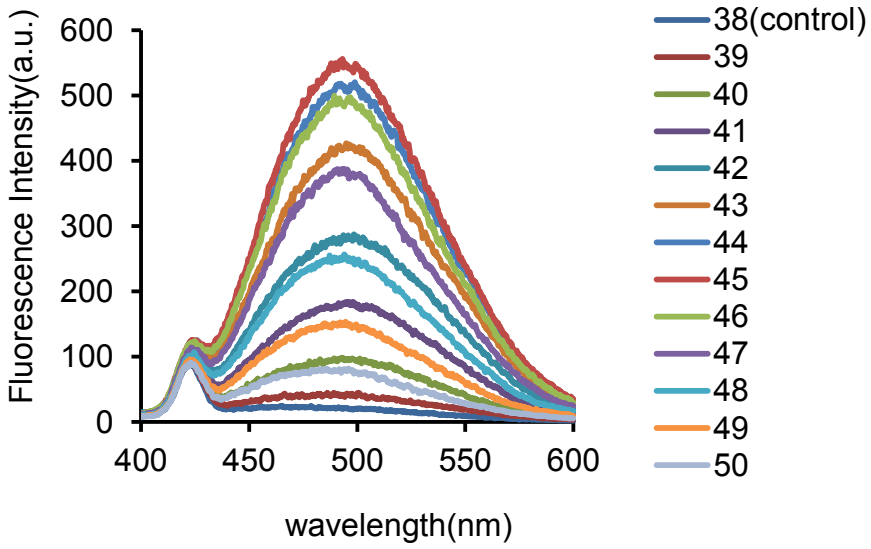

Figure 3.30a2. Fluorescence spectra of the control fractions corresponding to the low molecular weight region of the chromatogram.

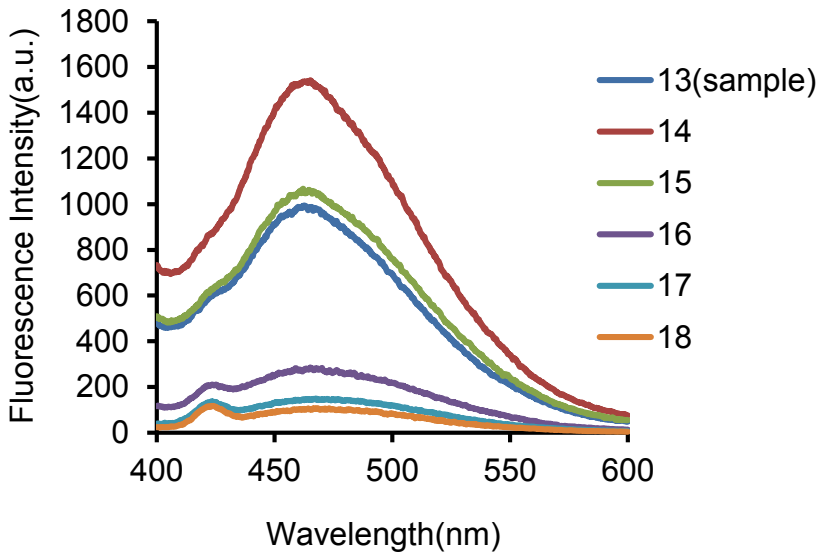

Figure 3.30b1. Fluorescence spectra of the sample fractions corresponding to the high molecular weight region of the chromatogram. λ_{max} at 470 nm indicates the adduct formation between ZQ_{Acid} and Zn-proteome (ZQ•Zn-proteome).

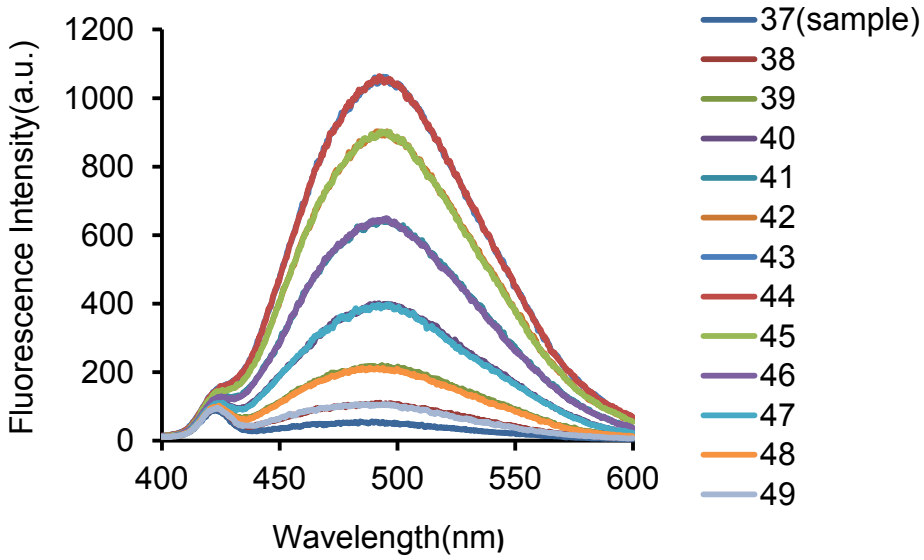

Figure 3.30b2. Fluorescence spectra of the sample fractions corresponding to the low molecular weight region of the chromatogram. λ_{max} at 490 nm indicates sequestration of Zn^{2+} from the proteome by ZQ_{Acid} and the free complex $Zn(ZQ_{Acid})$ formation.

3.2.8. Reaction of Zn-loaded proteome with TSQ

Zn-proteome and Zn-proteome•Zn containing 5 μM Zn^{2+} each, was reacted with 18 μM of TSQ in 1 ml degassed 20 mM Tris-HCl buffer pH 7.4 as control and sample solutions, rspectively. Emitted fluorescence intensity was recorded for 45 minutes starting immediately after mixing reactants of both control and sample solutions. Figures **3.31a** and **3.31b** show fluorescence spectra recorded over 45 minutes for control and sample solutions. Fluorescence intensities for control and sample reactions recorded at 470 nm are plotted versus time in **Figure 3.32**. Excitation wave length was 370 nm and fluorescence emission was recorded between 400 to 600 nm. Similar to the results from the reaction of ZQ with Zn-proteome•Zn, the fluorescence intensity for the sample solution was higher than that of the control solution. Moreover, fluorescence spectra exhibited the characteristic λ_{max} at 470 nm indicative of formation adduct complexes. The higher fluorescence intensities for the sample solution in comparison to the control solution arise from both kinetic and thermodynamic reasons. Thermodynamically, TSQ can compete with binding sites within Zn-proteome•Zn that bind to Zn^{2+} loosely and therefore, sequester Zn^{2+} and upon binding to it gives rise to higher fluorescence. Kinetically, there is more Zn^{2+} accessible for TSQ to react with and form adducts complexes. Three phases of reaction are deducible from the kinetics of the sample reaction with TSQ (**Figure 3.32**). About 35% of the overall reaction for the sample takes place in the first phase of the reaction within the mixing time.

Control and sample solutions then were loaded onto a Sephadex G-75 column and collected fractions were analyzed for their fluorescence intensities.

Figures 3.33a and **3.33b** show fluorescence emission spectrum of control and sample fractions corresponding to the high molecular weight region of their chromatogram. No fluorescence emission was detected in fractions corresponding to the low molecular weight region of the separation profile. This observation implies that no detectable Zn^{2+} was sequestered from the proteome by TSQ either in control or in sample solutions. The control experiments were undertaken to characterize how the Zn^{2+} mobilized from native binding sites by Cd^{2+} would associate with the proteome as observed by ZQ and TSQ. Despite the fact that the amounts of Zn^{2+} in the native proteome and the Zn-loaded proteome were the same, the fluorescence response for the sample is almost three times of that from the control. These results confirm that the mobilized Zn^{2+} from the proteome associates with other sites within the proteome and exhibit more lability in the reaction with the fluorophore compared to the native sites that results in a higher fluorescence response.

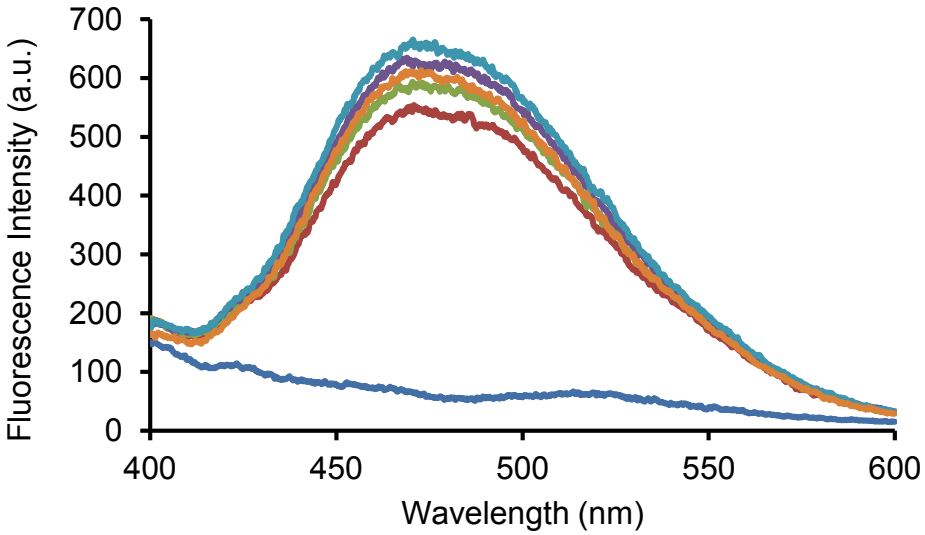

Figure 3.31a. Fluorescence spectrum for the control solution of the reaction between Zn-proteome and TSQ. Zn-proteome containing 5 μM Zn^{2+} reacted with 20 μM TSQ in 20 mM degassed Tris-HCl buffer pH 7.4, KCl 0.1 M. Fluorescence intensities were recorded with an excitation at 370 nm.

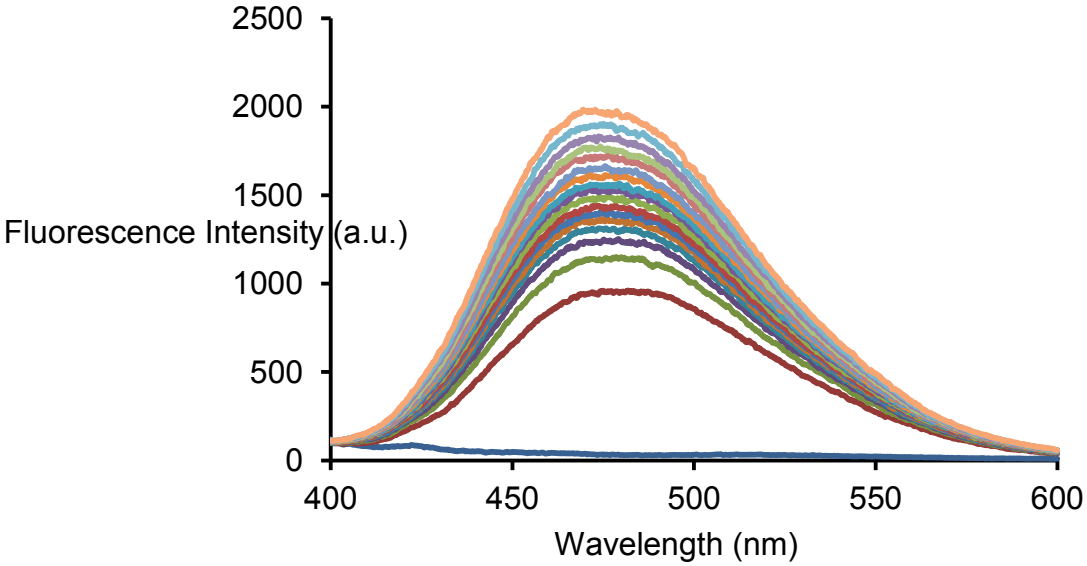

Figure 3.31b. Fluorescence spectrum for the sample solution of the reaction between Zn-loaded proteome and TSQ. Zn-proteome•Zn containing 5 nanomoles Zn^{2+} reacted with 20 nanomoles TSQ in 20 mM degassed Tris-HCl buffer pH 7.4, KCl 0.1 M.

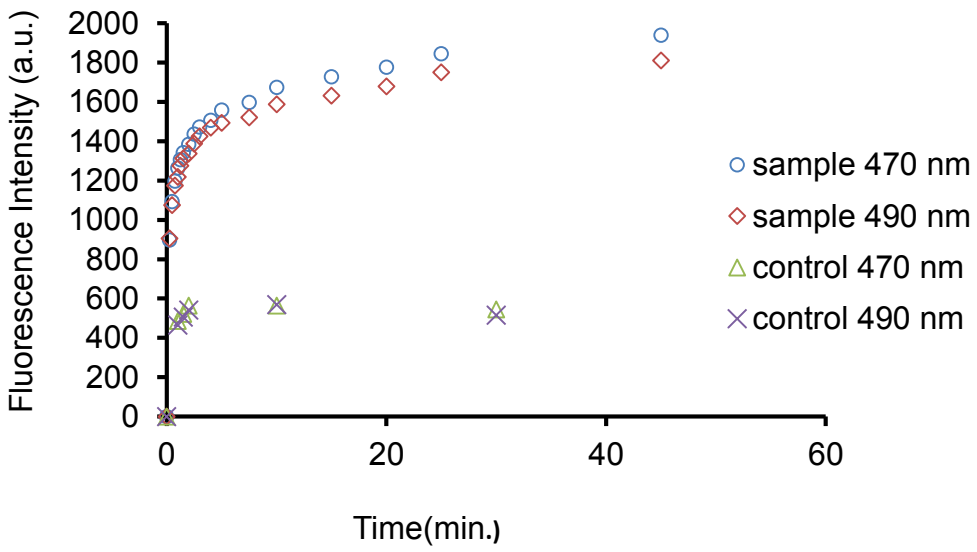

Figure 3.32. plot of fluorescence intensities at two wavelengths 470 and 490 nm versus time for control and sample solutions. Sample reaction displays three phases of reactions.

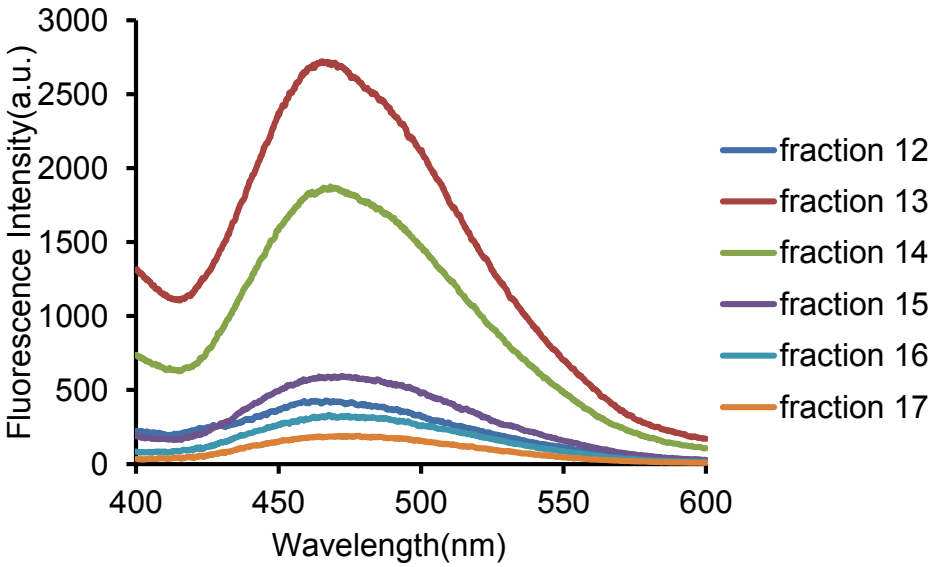

Figure 3.33a. Fluorescence spectra of the control fractions corresponding to the high molecular weight region of the control chromatogram.

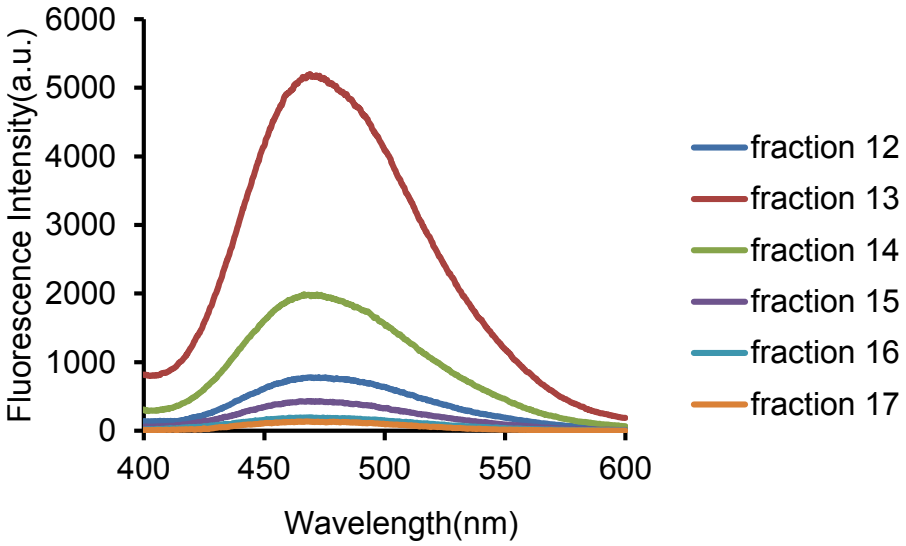

Figure 3.33b. Fluorescence spectra of the sample fractions corresponding to the high molecular weight region of the sample chromatogram. λ_{max} at 470 nm indicates the adduct formation between TSQ and Zn-proteome (TSQ-Zn-proteome).

3.3. The study of Zn^{2+} binding to the proteome using the weak Zn^{2+} chelating agent, Zincon

3.3.1. Introduction

The concentration of free Zn^{2+} in cells is not enough so that free Zn^{2+} is considered as an effective species in Zn^{2+} trafficking. Therefore, it was hypothesized that proteome bound zinc would account for such processes. The ligands, ZQ and TSQ that we have employed for ligand substitution reactions with the proteome so far had moderate to strong affinities toward Zn^{2+} and also readily form adduct species. Zincon (ZI), a colorimetric indicator of zinc, has a low Zn^{2+} binding constant and recently has been used to observe proteomic binding of Zn^{2+} [153]. From titration of HT-29 cell homogenate with Zn^{2+} in the presence of ZI, Maret and Krezel have concluded that there exists a considerable concentration of unoccupied Zn^{2+} binding sites in the cell lysate. They also hypothesized that such sites provide a cellular buffering capacity for Zn^{2+}. Because of some concern, we revisited their experiment. In the present work, LL-CPK_1 cell proteome and supernatant were titrated with Zn^{2+} in the presence of ZI. Zn-ZI was also used to titrate proteome, TSQ, and some model proteins such as bovine serum albumin (BSA), and Zn-carbonic anhydrase (Zn-CA) for further supporting information.

3.3.2. Titration of the proteome with Zn^{2+} in the presence of ZI

ZI has a weak binding affinity for Zn^{2+} with a binding constant of $10^{4.9}$ at pH 7.4 and 25°C. Upon binding to Zn^{2+}, it displays an absorbance spectrum with a

λ_{max} at 620 nm, characteristic of Zn-ZI species. **Figure 3.34** shows chemical structure of ZI.

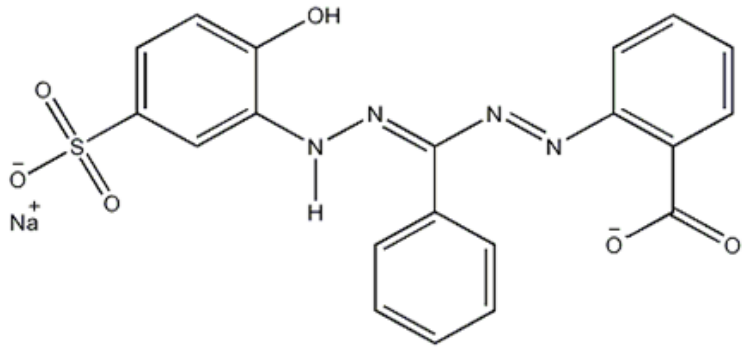

Figure 3.34. Chemical structure of ZI.

Proteome isolated from LL-CPK$_1$ cells containing 3.2 μM Zn^{2+} was reacted with 100 μM ZI without exhibiting a significant and observable absorbance at 620 nm. In other words, ZI did not undergo ligand substitution reaction with the proteome pool to sequester Zn^{2+} from it. In contrast, the addition of Zn^{2+} to proteome in the presence of ZI resulted in a progressive enhancement of absorbance at 620 nm. The titration curve consisted of two parts that qualitatively matched the published titration by Maret and Krezel. The first part (part I), in which no increase in the absorbance at 620 nm was detected, represented the initial phase of the titration. During this stage, ZI was unable to compete with the proteins that bind to Zn^{2+} (**Figure 3.35**). The absorbance increased in the second part (part II) of the curve; Maret interpreted this latter behavior as showing that after the

endpoint of part I, ZI competed efficiently with cellular binding sites to form Zn-ZI. But the slope of this process is substantially smaller than that obtained in the titration of ZI with Zn^{2+}. Moreover, the absorbance spectra measured during the titration of proteome were red-shifted to 640 nm (**Figure 3.36**). These two observations suggested that the second phase of the titration of proteome was not simply the result of the reaction of ZI with Zn^{2+}.

We hypothesized that similar to some other Zn^{2+} chelators such as TSQ and ZQ, ZI forms an adduct complex with Zn^{2+} and proteome.

$$\text{Proteome} + \text{ZI} + Zn^{2+} \rightleftharpoons \text{ZI-Zn-Proteome} \qquad (40)$$

The binding sites of proteome that are involved in the formation of the ternary adduct are those to which Zn^{2+} binds adventitiously. The curvature of part II of the titration was consistent with continued, though less powerful, binding of Zn^{2+} to proteome sites as proteome•Zn in competition with those sites that accommodated Zn^{2+} and ZI.

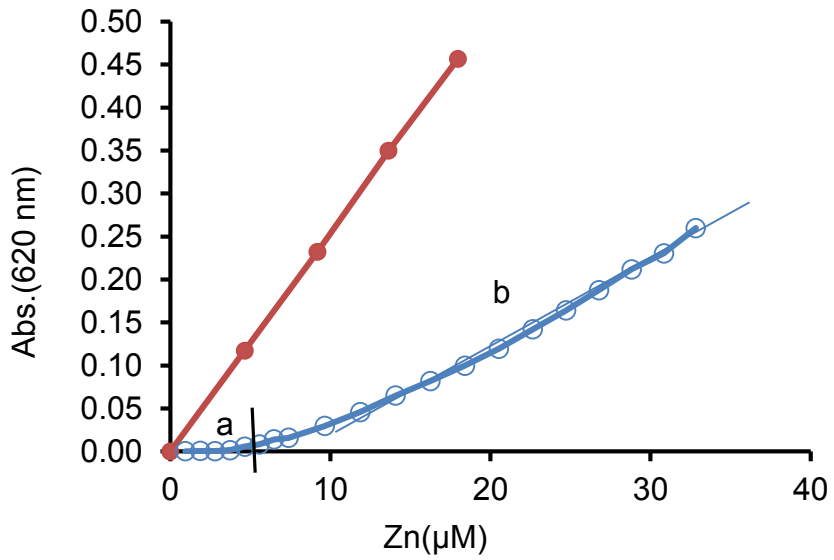

Figure 3.35. Titration of cell proteome with Zn^{2+} in the presence of ZI. Conditions: proteome containing 3.2 μM Zn^{2+} and 90 μM ZI titrated with Zn^{2+} in degassed Tris-HCl buffer, pH 7.4 at room temperature.

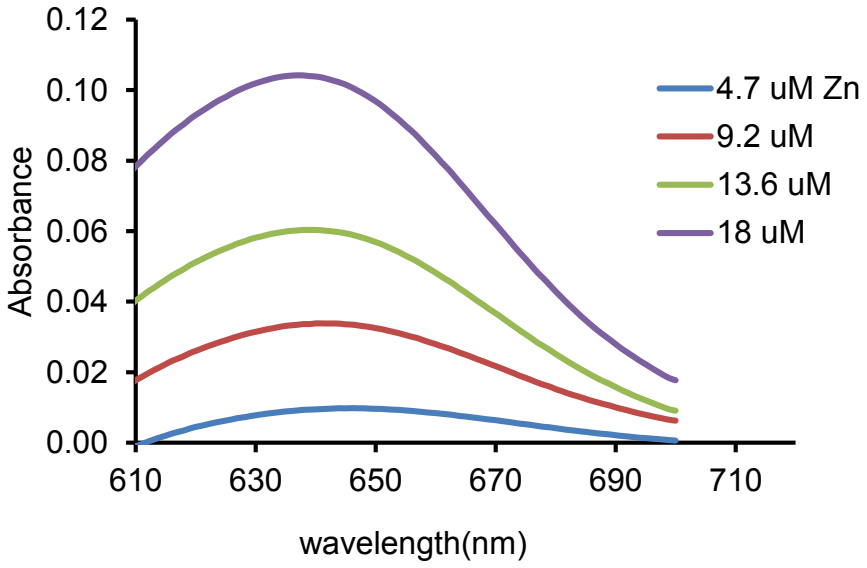

Figure 3.36. Absorbance spectra of cell proteome titrated with Zn^{2+} (Figure. 3.35) in the presence of ZI

In order to test this hypothesis, the product of the proteome titration was run over a Sephadex G-75 column. The resultant chromatogram (**Figure 3.37**) showed that proteome, ZI, and Zn^{2+} migrated together during the chromatographic separation, supportive of the hypothesis that ternary adduct formation had occured (reaction 40). ZI alone was also incubated with proteome for 30 min and chromatographed over Sephadex G-75. To detect the location of ZI in the eluate, 5 nanomoles Zn^{2+} was added to each 1 ml fraction and its absorbance at 220 nm was measured. According to the chromatogram depicted in **Figure 3.38**, ZI itself did not associate significantly with proteome and was readily separated from proteome and appeared in the low molecular weight region of the elution profile. Thus, the presence of Zn^{2+} is necessary for ZI to be eluted with the proteome. In other words ZI is only associated with the proteome when it forms the ternary adducts, ZI-Zn-proteome, involving extra Zn^{2+} that had been added to the proteome.

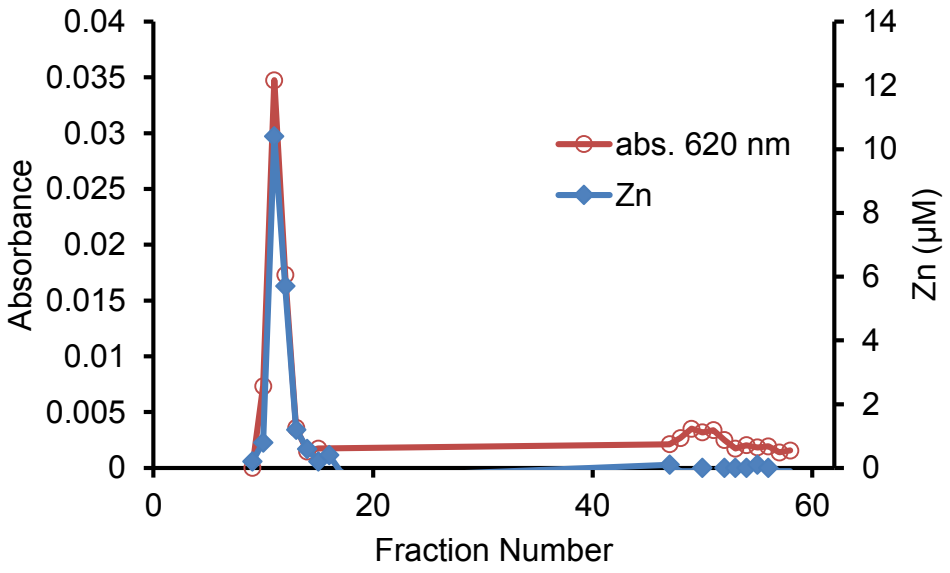

Figure 3.37. Sephadex G-75 chromatography of the reaction mixture in **Figure 3.35.**

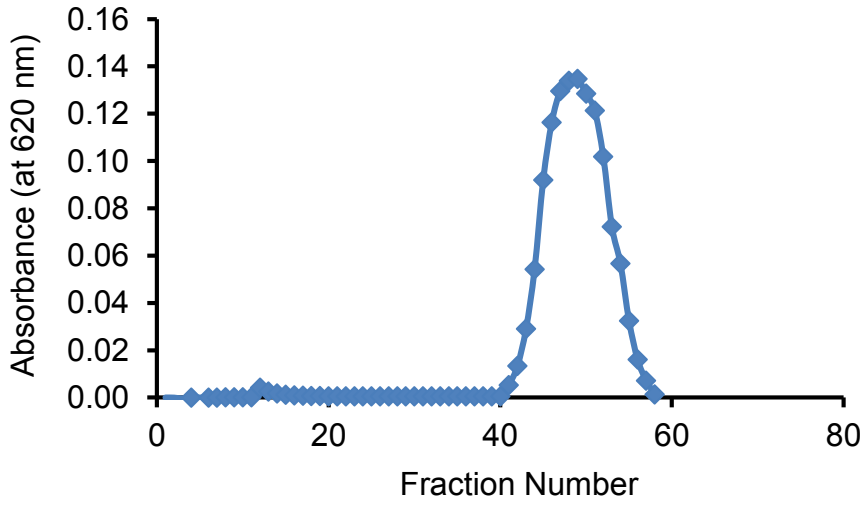

Figure 3.38. Sephadex G-75 chromatogram obtained from the mixture solution of proteome and ZI. 5 nmoles Zn^{2+} were added to fractions 40 to 60 to locate ZI in the chromatogram.

3.3.3. Titration of the LL-CPK$_1$ Cell Supernatant with Zn^{2+} in the Presence of ZI

The previous experiment was repeated using the entire cell supernatant that contained both the proteome and glutathione and similar results were obtained (**Figure 3.39a, b**). The experiment was also performed in a different way: cells supernatant was titrated with Zn-ZI. Upon this titration, results qualitatively similar to those obtained in previous experiment and depicted in **Figure 3.40a, b** were observed. At first, the spectral intensity was quenched; later as the absorbance increased the spectrum of Zn-ZI, characterized by a wavelength maximum at 620 nm, was replaced by a spectrum with a shoulder at about 640 nm.

We hypothesized that proteome initially underwent a ligand substitution reaction with Zn-ZI at sites inaccessible to ZI for ternary adduct formation.

$$\text{Proteome} + \text{Zn-ZI} \rightleftharpoons \text{Zn-Proteome} + \text{ZI} \qquad (41)$$

After completion of this part of the titration for this part, Zn-ZI started to associate with other sites to form ternary adduct complexes. This reaction was revealed by the shift in λ_{max} of Zn-ZI (620 nm) to 640 nm and by a different extinction coefficient of the new product.

$$\text{Proteome} + \text{Zn-ZI} \rightleftharpoons \text{ZI-Zn-Proteome} \qquad (42)$$

The product solution then was chromatographed on Sephadex G-75 and the resulted chromatogram showed that both Zn^{2+} and ZI migrated with the proteome after completion of the titration (**Figure 3.41**).

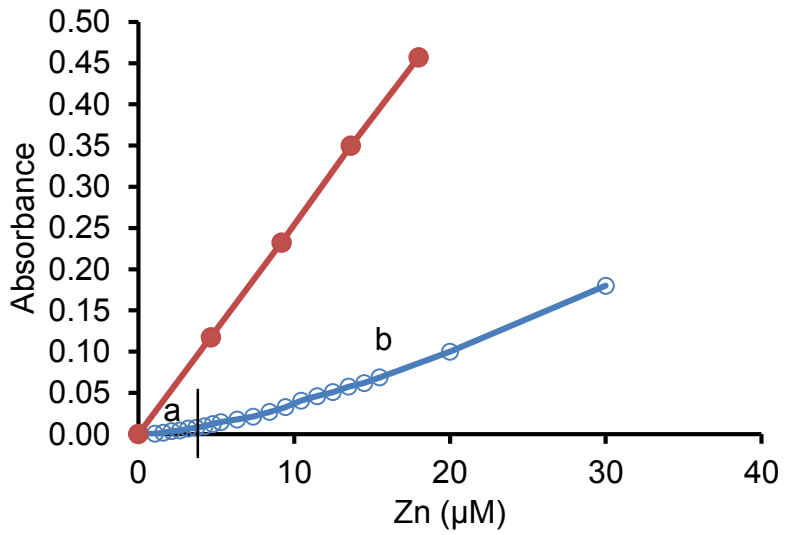

Figure 3.39a. Titration of cell supernatant with Zn^{2+} in the presence of ZI. Supernatant containing 2.4 μM Zn^{2+} and 80 μM ZI titrated with Zn^{2+} in degassed Tris-HCl buffer, pH 7.4 at room temperature.

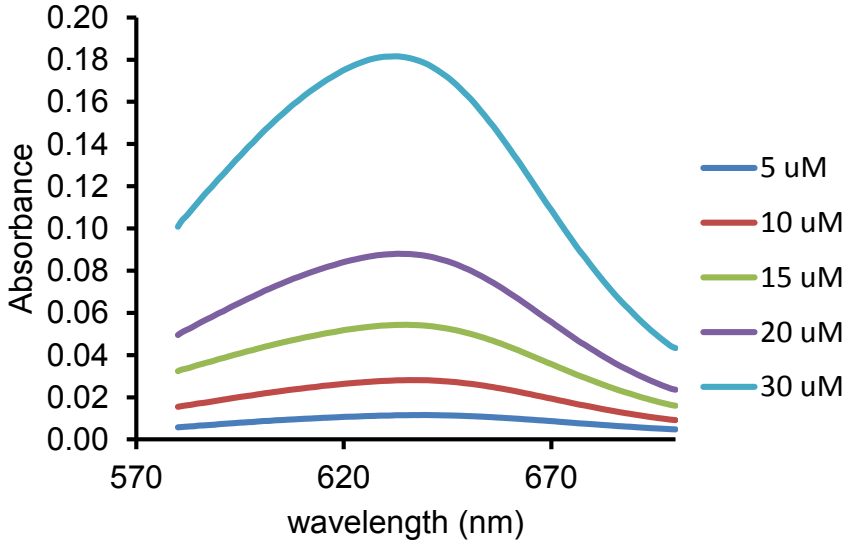

Figure 3.39b. Absorbance spectra of titrating mixture in **Figure 3.39a** displaying a λ_{max} absorbance at 640 nm

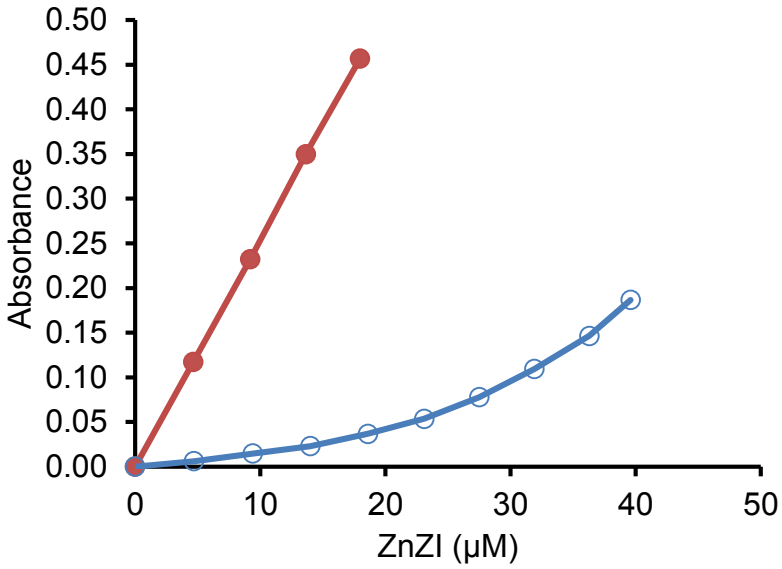

Figure 3.40a. Titration of cell supernatant with ZnZI. Supernatant containing 2.4 μM Zn^{2+} titrated with ZnZI in degassed Tris-HCl buffer, pH 7.4 at room temperature.

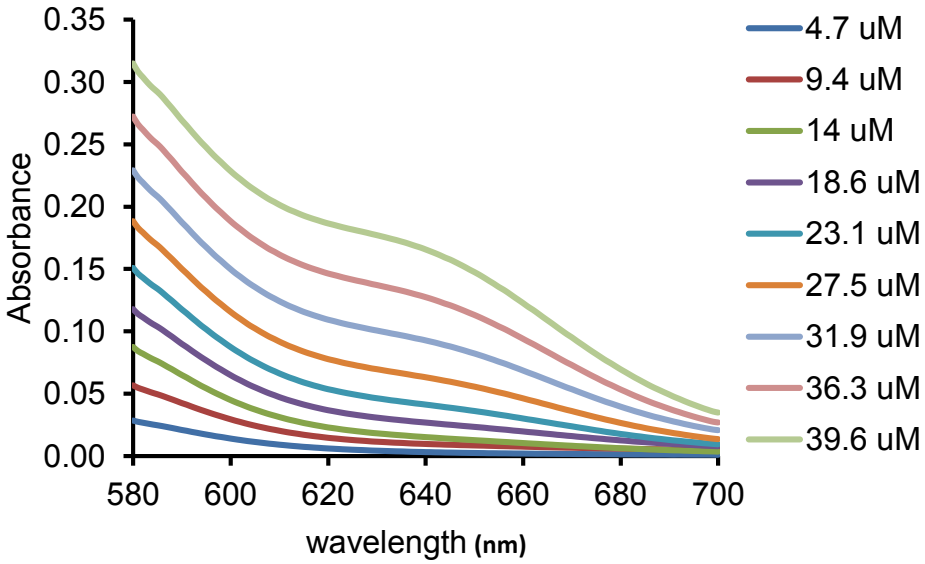

Figure 3.40b. Absorbance spectra of the cell supernatant titrated with Zn-ZI. The shoulder seen in the spectra exhibits a red-shift from the maximum absorbance at 620 to 640 nm.

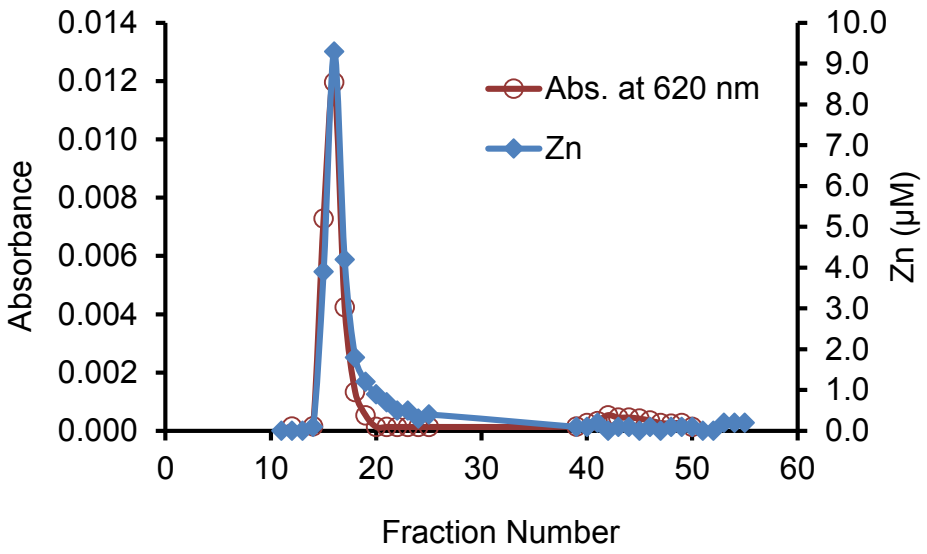

Figure 3.41. Sephadex G-75 chromatography of the reaction mixture in **Figure 3.40a**.

3.3.4. Reactions of Zn-ZI with model proteins

Several model proteins such as bovine serum albumin (BSA), carbonic anhydrase (CA), and trypsin were employed to further investigate the reactions of Zn^{2+} and ZI or Zn-ZI with the proteome. BSA served as a model protein with unoccupied Zn^{2+} binding sites [163]. Similar to the reaction of Zn-ZI with the proteome, BSA reacted with Zn-ZI and the resulted absorbance spectra exhibited a shift in λ_{max} from 620 nm to 640 nm (**Figures 3.42, 43**). The chromatogram obtained from running the product solution on a Sephadex G-75 column further confirmed the formation of ternary adduct complex (**Figures 3.44, 45**). In contrast, two other proteins, carbonic anhydrase and trypsin did not show any reaction with Zn-ZI indicated by lack of change in λ_{max} in their absorbance spectra. The former is a Zn-protein without unoccupied Zn^{2+} binding sites and the latter has neither Zn^{2+} nor documented Zn^{2+} binding sites.

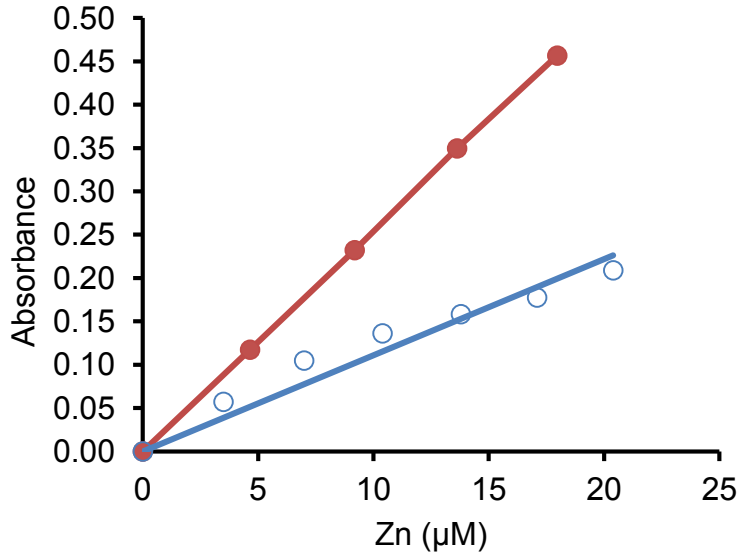

Figure 3.42. Titration of BSA with ZnZI. 16.5 μM BSA was titrated with ZnZI in degassed Tris-HCl buffer, pH 7.4 at room temperature

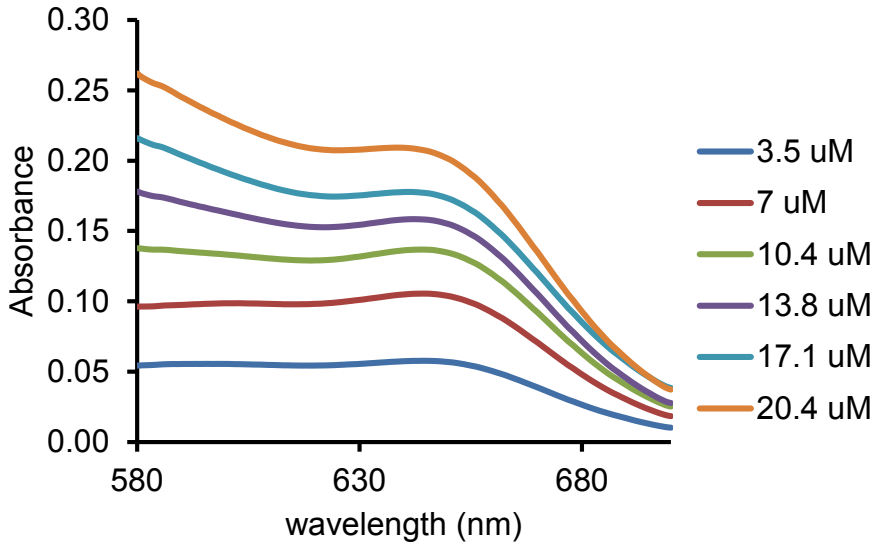

Figure 3.43. Absorbance spectra of the titration of BSA with ZnZI. 16.5 μM BSA was titrated with ZnZI in degassed 20 mM Tris-HCl buffer pH 7.4 at room temperature

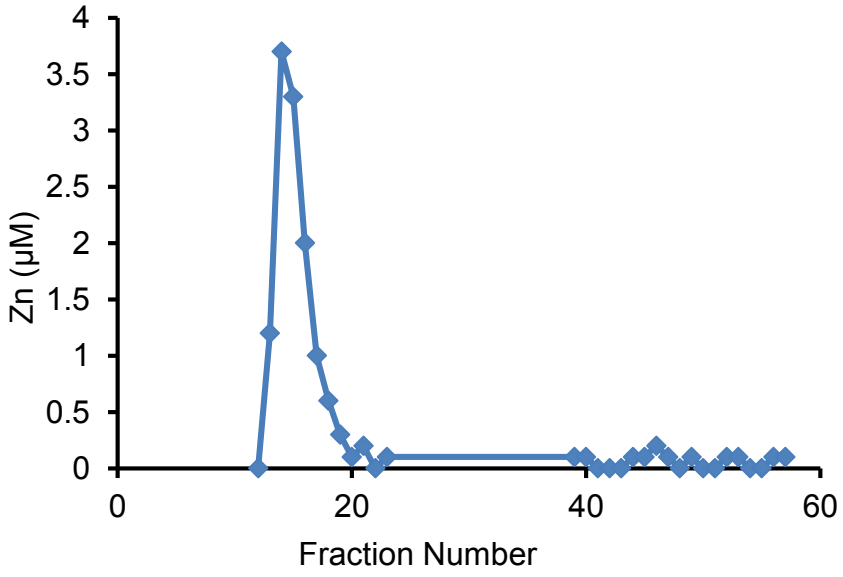

Figure 3.44. Sephadex G-75 Chromatogram of the reaction mixture of BSA and Zn-ZI

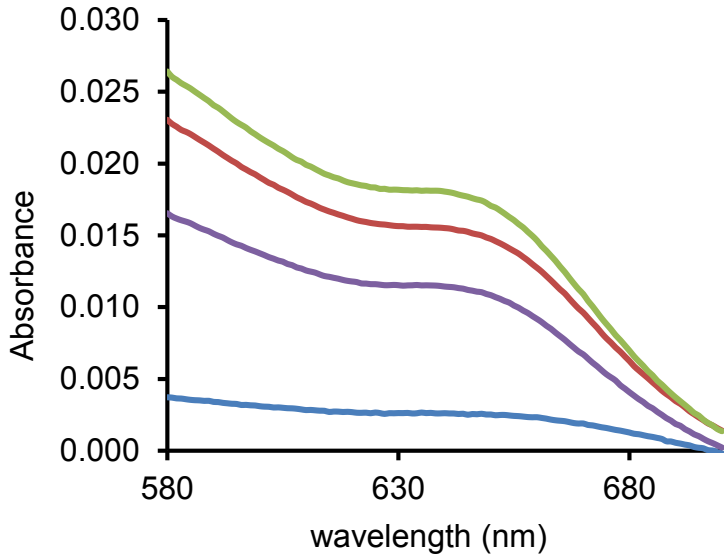

Figure 3.45. Absorbance spectra of fraction solutions (fractions 12-15) eluted in the high molecular part of the chromatogram shown in **Figure 3.44**. Any absorbance spectra were not obtained in the other parts of the chromatogram.

3.3.5 Model adduct formation: TSQ-Zn-ZI

In order to give more support to the conclusion that Zn-ZI was able to form ternary adducts with Zn^{2+} binding sites, the reaction of Zn-ZI with TSQ was investigated. TSQ forms ternary adducts with Zn^{2+} complexes and proteins displaying a fluorescence spectrum with a λ_{max} emission at 470 nm [116]. Reaction of 0-150 μM TSQ with 30 μM Zn-ZI resulted in a fluorescent product with a fluorescence emission λ_{max} at 470 nm. As more TSQ was reacted with Zn-ZI, the fluorescence emission spectrum was red-shifted exhibiting an emission λ_{max} at 490nm (**Figure 3.46**). The fluorescence emission λ_{max} at 470 was ascribed to the ternary adduct complex that forms initially when TSQ reacted with Zn-ZI.

$$\text{Zn-ZI} + \text{TSQ} \rightleftharpoons \text{TSQ-Zn-ZI} \qquad (43)$$

Upon addition of more TSQ and as the concentration of TSQ-Zn-ZI increased the following reaction occurred between these two species:

$$\text{TSQ-Zn-ZI} + \text{TSQ} \rightleftharpoons \text{ZI} + \text{Zn(TSQ)}_2 \qquad (44)$$

As a result of the formation of $Zn(TSQ)_2$ in reaction 42, the emission λ_{max} shifted from 470 nm to 490 nm.

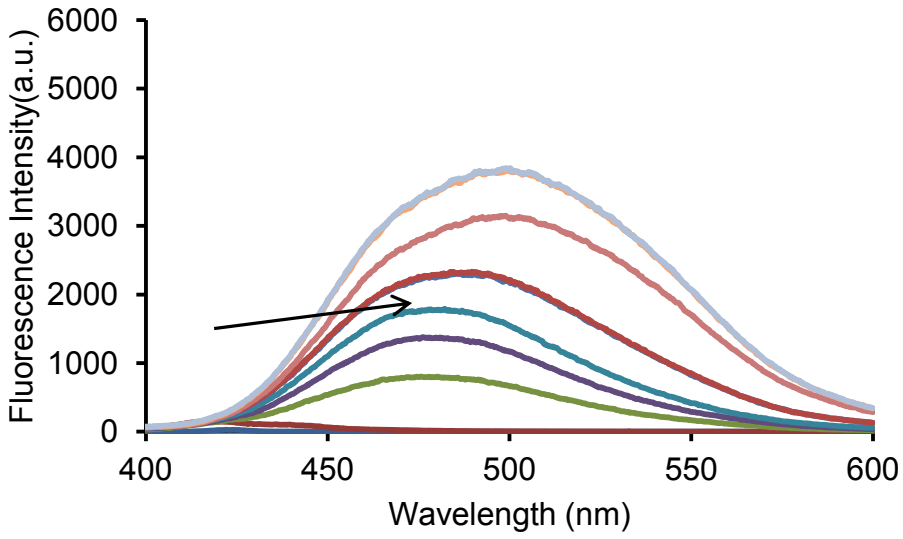

Figure 3.46. Fluorescence emission spectra of the titration of 30 μM ZnZI with 15 mM TSQ, adding 15 μM at a time in degassed 20 mM Tris-HCl buffer pH 7.4

4. Discussion

Zn, the second most abundant metal in human body, plays a significant role in a myriad of different physiological activities as the catalytic and structural cofactor for thousands of enzymes and proteins [5, 6, 7].The system of chemical reactions in living organism that leads to cellular influx, distribution, and efflux of metal ions is defined as metal ion metabolism or trafficking. Chemical reactions that might be involved in Zn trafficking is summarized below:

$$Zn^{2+} + p_1 \rightleftharpoons Zn\text{-}p_1 \qquad (45)$$

$$Zn\text{-}p_1 + p_2 \rightleftharpoons Zn\text{-}p_2 + p_1$$

$$\vdots$$

$$Zn\text{-}p_{n-1} + p_n \rightleftharpoons Zn\text{-}p_n + p_{n-1}$$

Where p_1 through p_{n-1} represent proteins that regulate Zn^{2+} and may consist of Zn-transport proteins, chaperone proteins or group of proteomic sets “proteome”. Final set of bindings of Zn^{2+} to proteins occurs in Zn-p_n.

Despite the good understanding achieved during the last decade about Zn^{2+} transport into and out of the cell interior and intracellular compartments [152], our knowledge about the trafficking of Zn^{2+} to cell organelles and proteins remains premature. External or internal metal ions, which are chemically similar to Zn^{2+} may disrupt or interfere with the process of Zn^{2+} trafficking and make complications. We hypothesize that toxicity of heavy metal such as Cd, Pb, and Hg that disrupt normal physiological activities and lead to pathological conditions

stems from their interference with normal Zn trafficking. Cd^{2+} can react with proteins involved in Zn trafficking and impairs this important process through affecting normal functions of Zn proteins.

$$Cd^{2+} + p_i \rightleftharpoons Cd\text{-}p_i \quad (46)$$

$i=1,..n$

We hypothesize that Cd^{2+} displaces Zn^{2+} from Zn proteins and then the displaced Zn^{2+} binds to other proteins adventitiously:

$$Cd^{2+} + Zn\text{-}p \rightleftharpoons Cd\text{-}p + Zn^{2+} \quad (47)$$

$$Cd\text{-}p + Zn^{2+} \rightleftharpoons Cd\text{-}p\bullet Zn \quad (48)$$

Among Zn proteins, metallothionein has been studied for more than a half century and its significant contribution to Zn trafficking and localization and disruption of heavy metal toxicity is evident [162]. Two other important participants in Zn trafficking and heavy metal toxicity are the cell proteome and glutathione. Understanding Zn^{2+} and Cd^{2+} binding and exchange properties of the above mentioned candidates will help better understand heavy metals toxicity and Zn trafficking in the cell and its compartments.

Metallothionein's involvement in Zn trafficking and prevention of toxicity depends on its metal binding properties. Previous studies have shown that apo metallothionein binds to seven Zn^{2+} or Cd^{2+} with a single high binding constant of $10^{11.2}$ and $10^{14.2}$ and forms Zn_7-MT or Cd_7-MT, respectively [135]. Zn_7-MT and Cd_7-MT has also been observed to react with each other and form Zn, Cd-MT [79, 159]. These observations bring these questions to mind: how does the stable Zn_7-MT

contribute to zinc trafficking and even more stable Cd_7-MT exhibit reactivity with Zn_7-MT? In contrast to previous studies, a relatively recent study has shown evidence for multi-step binding of Zn^{2+} to MT using the competing fluorophore ligand, FluoZin-3. This multi-step binding includes a low binding constant of $10^{7.7}$ for the binding of the seventh Zn^{2+} to MT. The authors attributed the reactivity of Zn_7-MT and therefore its contribution to zinc trafficking to this low binding constant.

The reaction of FluoZin-3 with Zn_7-MT was re-examined because of the discrepancy seen between results from the recent study and the previous studies, which showed concerted binding of seven Zn^{2+} ions to the two Zn-thiolate clusters in MT with a single high binding constant [135]. In our studies freshly prepared Zn_7-MT from rabbit liver (petering lab.) did not exhibit significant reactivity with FluoZin-3 as well as ligands with weak to moderate affinity toward Zn^{2+} such as H_2KTS and NTA (**Figures 3.13 and 3.14**). Titration of Zn_7-MT with HCl also showed a single step pH dependent dissociation curve characteristic of a single dissociation constant, consistent with previous studies (**Figure 3.15**).

The high stability constant found for the binding of Zn^{2+} in Zn_7-MT observed in our laboratory compared with the low binding constant for 1 Zn^{2+} in the protein used by Maret and Krezel confirmed that these proteins were different. This difference originates in the different methods of protein preparation conducted in the two groups. Maret and Krezel had prepared their Zn_7-MT from an expression vector for human thionein, isoform 2, in *E coli*. Their purification process of the protein included step acidification to pH 1 followed by Sephadex G-25 chromatography at pH 2 to remove all metals, followed by the addition of $7Zn^{2+}$/MT

at pH 7 to constitute the holoprotein. In contrast, we separated Zn_7-MT from rabbit liver, induced using Zn^{2+} injections, under neutral pH conditions in all steps of the protein preparation.

We found that acidification and neutralization of Zn_7-MT converts the protein to Zn_7-MT* that shares similar Zn^{2+} binding properties with that from Maret's laboratory. Whereas, Zn_7-MT showed little reactivity with competing ligands FluoZin-3, H_2KTS, NTA, and ZI, these ligands were able to sequester about 1 Zn^{2+} per molecule of the Zn_7-MT*. Furthermore, the pH dependent titration curve for Zn_7-MT was not reversible when titrated to very low pH, indicative of the difference between Zn^{2+} binding properties of Zn_7-MT and Zn_7-MT*.

Dissociation of Zn^{2+} from Zn_7-MT upon acidic titration of the protein exhibited a smooth absorbance vs. pH curve centered at pH 4; however, re-association of Zn^{2+} with apo-protein showed a two-step curve. The first step shared the same pattern with the dissociation reaction curve up to pH 5. The second step, which included 15% of the curve, laid between pH 5 and 7, and was responsible for the 1 Zn^{2+} per mole of the protein with low binding constant. Faster conversion of the native protein to the modified form took place at lower pH. The conversion reaction took 20 min or less to be completed at pH 2 or lower. However, at pH 3 the incubation time must be extended to obtain the same extent of conversion to MT*. Since Zn^{2+} is almost or fully dissociated from the protein at pH ≤ 3 at the same rate, the main reaction that converts MT to MT* involves changes in the apo-MT structure. These changes consequently influence the subsequent re-association reaction of Zn^{2+} with modified MT* that happens as protein is restored to pH 7.

Conditions for restoration of Zn_7-MT* to Zn_7-MT were not found in a preliminary survey. Neither moderate heating nor urea treatment of Zn_7-MT* altered its reactivity with competing ligands. These preliminary findings implied that some structural property of the protein backbone might change at low pH, which is preserved within the protein structure even after neutralization of the protein environment. This modification affects the protein folding about one of its two metal clusters. It is unknown to us what sort of structural changes might occur in the protein upon acidification.

One possibility is cis-trans isomerization of peptides bonds. The barrier energy for the cis-trans interconversion of X-proline (where X represents any amino acid) peptide bond arises from its partial double bond nature. Previous studies have shown that cis-trans isomerization of peptide bonds can be catalyzed under strong acidic conditions [164, 165]. Protonation of the carbonyl oxygen [166] or the amide nitrogen of X-proline peptide bond ruptures the double bond and favors the single bond resonance structure. The single amide bond can speed up the cis-trans interconversion. We hypothesize that in mild to strong acidic conditions (pH ≤ 3), the cis-trans isomerization of the key peptide bond along the protein backbone converts MT to MT*. The conserved proline 38 in the α-domain of MT is a candidate site for the acid-catalyzed conformational change [135, 167]. Upon metal ion liberation under acidic conditions, MT peptide also loses its conformational stability, so the cis-trans interconversion reaction can be further facilitated. Finally, neutralization can lock the peptide bond in place as the amide-bind undertakes its planar partial double bond character. Such an isomerization

could alter protein folding. Since Zn-thiolate clusters occupy the interior of each domain of the protein, any change in peptide folding might directly result in modification of one the clusters.

In addition to the inherent interest in the understanding of Zn_7-MT* and the nature of its conversion and modification from Zn_7-MT in vitro, it would be particularly significant to know if it can be formed in vivo under some other conditions. Examples of in vivo conformational changes under certain conditions are: (i) Change in configuration of His-Pro amide linkage catalyzed by protonation of the imidazole group near pH 7 [168] and (ii) Cis-trans isomerization of proteins peptide bond catalyzed by the enzyme peptidylprolyl isomerase [166]. If such reaction can take place in vivo, with a probable involvement of thiolate protonation, then Maret's and Krezel's argument over participation of Zn_7-MT* in Zn^{2+} trafficking with companions that have a wide range of equilibrium affinities for Zn^{2+} may be physiologically relevant. This would be especially interesting considering previous reports suggesting presence of an unsaturated pool of metallothionein in many cells and the unsaturated MT could be the preferential MT species for Zn trafficking reactions [135, 147, 169].

In terms of toxicity of heavy metals (such as cadmium and mercury) to cells, if one weak binding site exists in the metallothionein for Zn^{2+} under physiological conditions, there might be similar site for its counterparts Cd_7-MT and Cd_n, $Zn_{(7-n)}$-MT. This can imply that Cd-MT would not remain inert site of binding Cd^{2+} and, instead, contributes to the toxicity of cells.

Most cellular Cd^{2+} is bound to MT in the steady state conditions. Previous studies have demonstrated that cells without significant amount of MT when exposed to Cd^{2+} exhibit biosynthesis of MT after 4 hours and the majority of Cd^{2+} will be placed in the MT pool after 24h [170]. Because during the first 4 hours cells do not have significant amount of MT, one expects the Cd^{2+} will bind to other sites during that period and that such sites are located within the proteome. We decided to study the mechanism of this process in vitro and explore the role the proteome plays in the metal trafficking.

We hypothesized that Cd^{2+} would be particularly reactive with members of the Zn-proteome. Reaction of Cd^{2+} with the proteome extracted from rabbit liver or LLC-PK_1 cells resulted in binding of Cd^{2+} and mobilization of Zn^{2+}, which remained non-specifically associated with the proteome after chromatographing the reaction mixture over sephadex G-75 column (**Figures 3.17a,b**). The fact that Cd^{2+} apparently exchanged with protein-bound Zn^{2+} under stoichiometric conditions, suggested that much of the Zn^{2+} in the proteome was associated with sites that contained sulfhydryl ligands and prefer Cd^{2+} to Zn^{2+} and that these sites thermodynamically and kinetically favor the metal exchange reaction. We hypothesized that the released Zn^{2+} binds to the proteome adventitiously and therefore it should be readily available for reaction with competing ligands [170].

If binding of Cd^{2+} to the proteome increases the lability of Zn^{2+} within the proteome, we should be able to test it by reacting the Cd-treated Zn-proteome with competing ligands. In particular, fluorescent ligands that are sensitive to Zn^{2+} can be useful for the characterization of this ligand substitution reaction. TSQ and

ZQ_{Acid} bind to free Zn^{2+} with a ratio of 2:1 and exhibit fluorescence with a λ_{max} at 490 nm upon an excitation wavelength at 370 nm. Previous studies have shown that upon reaction of proteome with TSQ, TSQ-Zn-proteome species form. With ZQ, both ZQ-Zn-proteome and a small amount of $Zn(ZQ)_2$ are generated. Reaction of Cd-treated Zn-proteome with TSQ and ZQ_{Acid} displayed much more fluorescence emission when compared with Zn-proteome (control) that contained the same amount of metal (**Figures 3.19 and 3.21a, b**). Considering that $Cd(TSQ)_2$ and $Cd(ZQ)_2$ have only about 1/3 the quantum yield as their Zn^{2+} counterparts, this suggests that Cd causes a rearrangement in the distribution of Zn^{2+} within the proteome and makes Zn^{2+} accessible to the fluorophore. The λ_{max} emission for all these reactions were centered at 470 nm indicative of ternary complex formation (sensor-Zn-proteome) with a shoulder at 480 nm for ZQ sensor indicative of the formation of both free complex species and adduct of this sensor with the proteome. Zn^{2+} reacted with the proteome without release of any significant Zn^{2+} **(Figure 3.17a, b)**, indicative of presence of many available sites within the proteome to react with Zn^{2+} or similar metal ions; also, another confirmation for presence of free Zn^{2+} in cells with only pico molar concentrations. Similar to the reaction for Cd-treated Zn-proteome, Zn-proteome•Zn exhibited more fluorescence emission when compared to Zn-proteome, consistent with the hypothesis of redistribution of Zn^{2+} within the proteome upon reaction with free metal ions.

In vitro reaction of Zn_7-MT with Zn^{2+}, Cd-proteome exhibited a Cd-Zn exchange reaction (51a) similar to the Cd-Zn exchange reaction between Zn_7-MT and Cd_7-MT (51b) found earlier by Otvos et al [159].

$$Cd^{2+} + \text{Zn-proteome} \rightleftharpoons \text{Cd-proteome} + Zn^{2+} \quad (49)$$

$$\text{Cd-proteome} + Zn^{2+} \rightleftharpoons \text{Cd-proteome•Zn} \quad (50)$$

$$m\ \text{Cd-Proteome•Zn} + Zn_7\text{-MT} \rightleftharpoons m\ Cd_{(1-\delta)}\text{-proteome•}Zn_{(1+\delta)} + Cd_{m\delta},Zn_{(7-m\delta)}\text{-MT} \quad (51a)$$

$$m\ Zn_7\text{-MT} + n\ Cd_7\text{-MT} \rightleftharpoons (m+n)\ Cd_{n/(n+m)},Zn_{(7-n)/(m+n)}\text{-MT} \quad (51b)$$

The results (**Figures 3.26a-c**) show that the metal ion exchange reaction between Zn_7-MT and the Zn, Cd-proteome is an efficient process. Most of the Cd^{2+} that was initially bound within the proteome accumulates in the metallothionein pool and, therefore, its contribution to the toxicity effects is diminished. The amount of Cd^{2+} that remains bound with the proteome would contribute to the Cd^{2+} toxicity. For example, the down-regulation of Sp1 transcription factor activity continues even after MT synthesis is induced and much of the Cd^{2+} localizes in the MT pool [170]. Still, to the extent that reaction (51a) occurs, and proteome Cd^{2+} shifts to MT as MT Zn^{2+} moves to the proteome, Cd^{2+}-Zn^{2+} exchange at native proteomic binding sites may occur and result in restoration of native function to the proteins. This hypothetical reaction was proposed many years ago [149]; these results provide encouragement for the hypothesis

Apo-MT did not exhibit significant reactivity with the Zn-proteome. On the other hand, it was able to sequester both Zn^{2+} and Cd^{2+} from Cd-proteome•Zn and

form Zn, Cd-MT (**Figures 3.26a-c**). This result is in agreement with the fact that there exists a considerable amount of apo-MT, which can coexist with the Zn-proteome in many cell types. And also implies that the mechanism under which apo-MT may acquire metal from native Zn-proteome and Cd-proteome•Zn should be different. In other words, the mechanism of ligand substitution reaction of apo-MT and Cd-proteome•Zn includes sequestration of adventitously bound Zn^{2+} because of its lability. One possible route in this mechanism can be formation of Zn_7-MT first and then Cd^{2+}-Zn^{2+} metal exchange reaction between Zn_7-MT and Zn, Cd-MT that supplies the majority of metal sites in MT pool with Cd^{2+}.

$$\text{Apo-MT} + m\ \text{Cd-Proteome•Zn} \rightleftharpoons Zn_7\text{-MT} + m\ \text{Cd-proteome•Zn}_{(m-7)/m} \quad (52a)$$

$$m\ \text{Cd-Proteome•Zn}_{(m-7)/m} + Zn_7\text{-MT} \rightleftharpoons m\ \text{Cd}_{(1-\Delta)}\text{-proteome•Zn}_{(m-7+m\Delta)/m} + \text{Cd}_{m\Delta}\text{-MT•Zn}_{(7-m\Delta)} \quad (52b)$$

To obtain more information about unoccupied metal binding sites within the proteome, LL-CPK_1 cell lysate was titrated with $ZnCl_2$ in the presence of ZI, which binds to Zn^{2+} with a low binding constant. The titration curve depicted in **Figure 3.35** consists of two parts. The first part, which corresponds to the addition of 10 μM Zn^{2+}, shows an absence of absorbance at 620 nm implying that proteome outcompetes ZI for binding to Zn^{2+}. The second part of the titration curve displays an increasing absorbance at 620 nm upon addition of Zn^{2+}. The y-axis intersection of these two parts of the curve was originally considered as the concentration of unoccupied Zn^{2+} binding sites of the proteome [153]. If ZI simply binds to Zn^{2+} in the second part of the reaction, we would expect to get a slope (extinction coefficient) similar to that observed in the titration of ZI by Zn^{2+}. However, two

different slopes are observed. This suggests the possibility that Zn-ZI, itself, interacts with metal binding sites to form ZI-Zn-proteome adducts (reaction 42).

Zn^{2+} sensors such as TSQ and ZQ exhibit fluorescence emission spectra blue-shifted from the spectra of $Zn(TSQ)_2$ and $Zn(ZQ)_2$ upon reacting with the proteome and forming sensor-Zn-proteome adducts. To further demonstrate the formation of such adduct species, we conducted gel chromatography separations and observed that the fluorophore sensor migrated with the proteome. A similar approach was used to investigate the hypothesis that ZI-Zn-proteome adducts form during the second phase of the reaction of ZI and Zn-proteome with Zn^{2+}.

Spectra of the mixture for the second part of the titration exhibited a λ_{max} absorbance at 640 nm (**Figure 3.36**), a red-shift from the λ_{max} absorbance for Zn-ZI (620 nm). The red-shifted spectra suggest that the product was not Zn-ZI species. Sephadex G-75 chromatography showed that the absorbing product, containing both Zn^{2+} and ZI, was not free Zn-ZI species because it was eluted with the proteome not the small molecular weight fractions (**Figure 3.37**). Moreover, ZI that was added to the proteome was readily separated from the proteome indicating that the organic ligand had little affinity for proteome environments (**Figure 3.38**). The added Zn^{2+} was key to converting ZI into a structure that associated with the proteome. We hypothesized that Zn-ZI form ternary adducts with proteome that contains unoccupied Zn^{2+} binding sites. Similar results were obtained when supernatant was titrated with Zn^{2+} in presence of ZI or with Zn-ZI (**Figures 3.39a, b**). With additional evidence that Zn-ZI did not react with a model protein, trypsin that neither contains Zn^{2+} nor a documented Zn^{2+} binding site, the

hypothesis that Zn-ZI formed adducts with adventitious Zn^{2+} binding sites within proteome was strengthened.

Because the adduct formation properties of the fluorophore, TSQ, are well established, its reaction with Zn-ZI was investigated. Although the hypothesized product, TSQ-Zn-ZI did not display a shift in its absorbance spectrum, its fluorescence emission spectrum was blue-shifted to 470 nm, characteristic of adduct complex formation (**Figure 3.46**). We ascribed the shift in the absorbance spectrum to a property coming from the interaction of Zn-ZI with the protein structure.

Next, the reaction of Zn-ZI with BSA was studied. BSA has a well-studied binding site for Zn^{2+} that might accommodate the Zn-ZI complex. Reaction of BSA with Zn-ZI resulted in the formation of BSA-Zn-ZI adduct that was confirmed by the appearance of a red shift in its absorbance spectrum and its co-migration during gel chromatography (**Figures 3.42-45**). In contrast, two other proteins, carbonic anhydrase and trypsin did not show any reaction with Zn-ZI indicated by lack of change in λ_{max} in their absorbance spectra. The former is a Zn-protein without unoccupied Zn^{2+} binding sites and the latter has neither Zn^{2+} nor documented Zn^{2+} binding sites

This set of findings indicates that there is a large concentration of metal ion binding sites within the proteome available for reaction with Zn^{2+} that enters the cell. We hypothesize that upon transport of Zn^{2+} from outside to inside the cell; it can bind to a myriad of available Zn^{2+} binding sites within the Zn-proteome. It does so in preference to GSH. Thus, Zn trafficking, the regulated movement or transfer

of Zn from the cell or compartment membrane to find sites of binding in Zn-metalloproteins, may be intimately linked to the presence of the large pool of unsaturated Zn binding sites. The binding constants for Zn^{2+} binding to these sites, which are not comparable to those of original Zn^{2+} binding sites within proteome can facilitate transit of Zn^{2+} from one protein to another and contribute to Zn^{2+} regulation. Similar reactions can occur between the cell-imported Cd^{2+} and proteome. Cd^{2+} may first bind to the proteome adventitiously and then binds to specific Zn-binding sites upon Cd^{2+}-Zn^{2+} exchange reactions with Zn-proteins in the proteome. The latter leads to an increase in the concentration of adventitiously bound Zn^{2+} to the proteome within the cell. The excess Zn^{2+} may be taken up by newly synthesized apo-MT and forms Zn_7-MT. The elevated amount of Zn_7-MT helps the cell get relieved from some of Cd^{2+} toxicity by taking part in an exchange reaction with Cd-proteome or proteome·Cd. These reactions in turn, produce Cd-MT and restores some native Zn-proteins within the proteome.

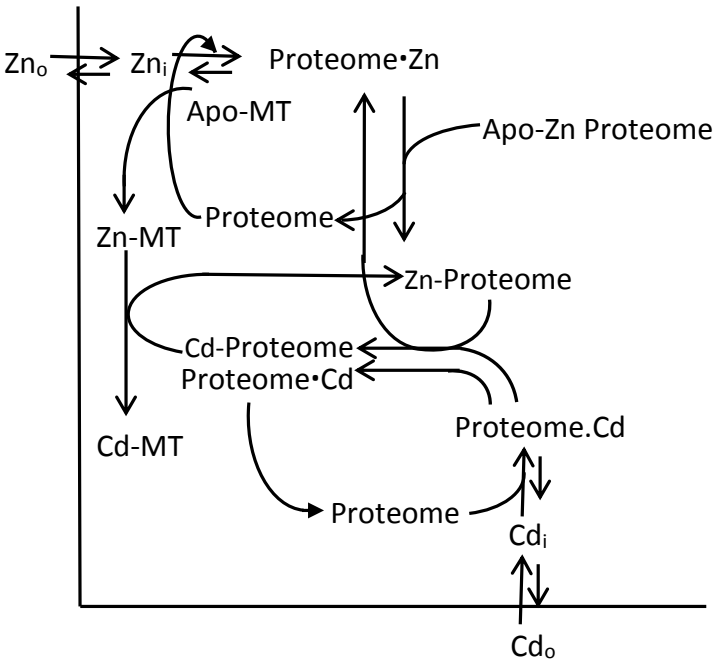

Figure 4.1. Schematic Zn^{2+} and Cd^{2+} trafficking and regulation in the cell.

In vivo studies on Zn^{2+} proteome and looking at Zn^{2+} proteome in individual organelles can expand these Zn^{2+} regulation studies and help better understand these complex processes. Further separation methods such as NSDS-PAGE and LA-ICPMS can be employed to look at the proteome at protein levels in the study of Zn^{2+} trafficking. Studying the proteome at protein levels will also pave the way to better understand the effects of Cd^{2+} and other toxic metals in Zn^{2+} regulation and their contribution to toxicity.

References

1. Kemsley, J., MERGING METALS INTO PROTEOMICS. *Chemical & Engineering News Archive* **2011,** *89* (50), 28-30.

2. Maret, W.; Li, Y., Coordination dynamics of zinc in proteins. *Chemical Reviews* **2009,** *109* (10), 4682-4707.

3. Dong, J.; Atwood, C. S.; Anderson, V. E.; Siedlak, S. L.; Smith, M. A.; Perry, G.; Carey, P. R., Metal binding and oxidation of amyloid-beta within isolated senile plaque cores: Raman microscopic evidence. *Biochemistry* **2003,** *42* (10), 2768-2773.

4. Kepp, K. P., Bioinorganic Chemistry of Alzheimer's Disease. *Chemical Reviews* **2012,** *112* (10), 5193-5239.

5. Miao, X.; Sun, W.; Miao, L.; Fu, Y.; Wang, Y.; Su, G.; Liu, Q., Zinc and Diabetic Retinopathy. *Journal of Diabetes Research* **2013,** *2013*.

6. Andreini, C.; Banci, L.; Bertini, I.; Rosato, A., Zinc through the three domains of life. *Journal of Proteome Research* **2006,** *5* (11), 3173-3178.

7. Moult, J.; Melamud, E., From fold to function. *Current Opinion in Structural Biology* **2000,** *10* (3), 384-389.

8. Tomat, E.; Lippard, S. J., Imaging mobile zinc in biology. *Current Opinion in Chemical Biology* **2010,** *14* (2), 225-230.

9. Kelleher, S. L.; McCormick, N. H.; Velasquez, V.; Lopez, V., Zinc in specialized secretory tissues: roles in the pancreas, prostate, and mammary gland. *Advances in Nutrition (Bethesda, Md.)* **2011,** *2* (2), 101-111.

10. Ciavardelli, D.; Consalvo, A.; Caldaralo, V.; Vacri, M. L. D.; Nisi, S.; Corona, C.; Frazzini, V.; Sacchetta, P.; Urbani, A.; Ilio, C. D.; Sensi, S. L., Characterisation of element profile changes induced by long-term dietary supplementation of zinc in the brain and cerebellum of 3xTg-AD mice by alternated cool and normal plasma ICP-MS. *Metallomics* **2012,** *4* (12), 1321-1332.

11. Smith, M. A.; Harris, P. L.; Sayre, L. M.; Perry, G., Iron accumulation in Alzheimer disease is a source of redox-generated free radicals. *Proceedings of the National Academy of Sciences of the United States of America* **1997,** *94* (18), 9866-9868.

12. Clements, A.; Allsop, D.; Walsh, D. M.; Williams, C. H., Aggregation and metal-binding properties of mutant forms of the amyloid A beta peptide of Alzheimer's disease. *Journal of Neurochemistry* **1996,** *66* (2), 740-747.

13. Miao, X.; Sun, W.; Fu, Y.; Miao, L.; Cai, L., Zinc homeostasis in the metabolic syndrome and diabetes. *Frontiers of Medicine* **2013,** *7* (1), 31-52.

14. Bekheirnia, M. R.; Shamshirsaz, A. A.; Kamgar, M.; Bouzari, N.; Erfanzadeh, G.; Pourzahedgilani, N.; Tabatabaie, S. M.; Abdollah Shamshirsaz, A.; Kimiagar, M.; Ezzati, F.; Larijani, B., Serum zinc and its relation to bone mineral density in beta-thalassemic adolescents. *Biological Trace Element Research* **2004,** *97* (3), 215-224.

15. Swardfager, W.; Herrmann, N.; McIntyre, R. S.; Mazereeuw, G.; Goldberger, K.; Cha, D. S.; Schwartz, Y.; Lanctôt, K. L., Potential roles of zinc in the pathophysiology and treatment of major depressive disorder. *Neuroscience and Biobehavioral Reviews* **2013,** *37* (5), 911-929.

16. Mirhosseini, N. Z.; Shahar, S.; Ghayour-Mobarhan, M.; Banihashem, A.; Kamaruddin, N. A.; Hatef, M. R.; Esmaili, H. A., Bone-related complications of transfusion-dependent beta thalassemia among children and adolescents. *Journal of Bone and Mineral Metabolism* **2013,** *31* (4), 468-476.

17. Ba, L. A.; Doering, M.; Burkholz, T.; Jacob, C., Metal trafficking: from maintaining the metal homeostasis to future drug design. *Metallomics: Integrated Biometal Science* **2009,** *1* (4), 292-311.

18. Zastrow, M. L.; Pecoraro, V. L., Designing hydrolytic zinc metalloenzymes. *Biochemistry* **2014,** *53* (6), 957-978.

19. Myers, L. C.; Terranova, M. P.; Ferentz, A. E.; Wagner, G.; Verdine, G. L., Repair of DNA methylphosphotriesters through a metalloactivated cysteine nucleophile. *Science (New York, N.Y.)* **1993,** *261* (5125), 1164-1167.

20. Smith, G. D.; Swenson, D. C.; Dodson, E. J.; Dodson, G. G.; Reynolds, C. D., Structural stability in the 4-zinc human insulin hexamer. *Proceedings of the National Academy of Sciences of the United States of America* **1984,** *81* (22), 7093-7097.

21. Sekler, I.; Sensi, S. L.; Hershfinkel, M.; Silverman, W. F., Mechanism and regulation of cellular zinc transport. *Molecular Medicine (Cambridge, Mass.)* **2007,** *13* (7-8), 337-343.

22. Guerinot, M. L., The ZIP family of metal transporters. *Biochimica Et Biophysica Acta* **2000,** *1465* (1-2), 190-198.

23. Liuzzi, J. P.; Cousins, R. J., Mammalian zinc transporters. *Annual Review of Nutrition* **2004,** *24*, 151-172.

24. Weser, U.; Bischoff, E., Incorporation of 65Zn in rat liver nuclei. *European journal of biochemistry / FEBS* **1970,** *12* (3), 571-575.

25. Krezel, A.; Hao, Q.; Maret, W., The zinc/thiolate redox biochemistry of metallothionein and the control of zinc ion fluctuations in cell signaling. *Archives of Biochemistry and Biophysics* **2007,** *463* (2), 188-200.

26. Spahl, D. U.; Berendji-Grün, D.; Suschek, C. V.; Kolb-Bachofen, V.; Kröncke, K.-D., Regulation of zinc homeostasis by inducible NO synthase-derived NO: nuclear metallothionein translocation and intranuclear Zn2+ release. *Proceedings of the National Academy of Sciences of the United States of America* **2003,** *100* (24), 13952-13957.

27. Nagano, T.; Itoh, N.; Ebisutani, C.; Takatani, T.; Miyoshi, T.; Nakanishi, T.; Tanaka, K., The transport mechanism of metallothionein is different from that of classical NLS-bearing protein. *Journal of Cellular Physiology* **2000,** *185* (3), 440-446.

28. Takahashi, Y.; Ogra, Y.; Suzuki, K. T., Nuclear trafficking of metallothionein requires oxidation of a cytosolic partner. *Journal of Cellular Physiology* **2005,** *202* (2), 563-569.

29. Liang, Z.; Ding, Q.; Wei, D.; Li, J.; Chen, S.; Ma, Y., Major controlling factors and predictions for cadmium transfer from the soil into spinach plants. *Ecotoxicology and Environmental Safety* **2013,** *93*, 180-185.

30. Xu, S.; Pi, H.; Chen, Y.; Zhang, N.; Guo, P.; Lu, Y.; He, M.; Xie, J.; Zhong, M.; Zhang, Y.; Yu, Z.; Zhou, Z., Cadmium induced Drp1-dependent mitochondrial fragmentation by disturbing calcium homeostasis in its hepatotoxicity. *Cell Death & Disease* **2013,** *4*.

31. Meharg, A. A.; Norton, G.; Deacon, C.; Williams, P.; Adomako, E. E.; Price, A.; Zhu, Y.; Li, G.; Zhao, F.-J.; McGrath, S.; Villada, A.; Sommella, A.; De Silva, P. M. C. S.; Brammer, H.; Dasgupta, T.; Islam, M. R., Variation in rice cadmium related to human exposure. *Environmental Science & Technology* **2013,** *47* (11), 5613-5618.

32. Hollis, L.; Hogstrand, C.; Wood, C. M., Tissue-specific cadmium accumulation, metallothionein induction, and tissue zinc and copper levels during chronic sublethal cadmium exposure in juvenile rainbow trout. *Archives of Environmental Contamination and Toxicology* **2001,** *41* (4), 468-474.

33. Kuboi, T.; Noguchi, A.; Yazaki, J., Family-dependent cadmium accumulation characteristics in higher plants. *Plant and Soil* **1986,** *92* (3), 405-415.

34. F. T. Bingham, A. L. P., Growth and Cadmium Accumulation of Plants Grown on a Soil Treated with a Cadmium-Enriched Sewage Sludge1. *Journal of Environmental Quality - J ENVIRON QUAL* **1975,** *4* (2).

35. Lehman, L. D.; Klaassen, C. D., Dosage-dependent disposition of cadmium administered orally to rats. *Toxicology and Applied Pharmacology* **1986,** *84* (1), 159-167.

36. Järup, L.; Akesson, A., Current status of cadmium as an environmental health problem. *Toxicology and Applied Pharmacology* **2009,** *238* (3), 201-208.

37. Klaassen, C. D.; Liu, J., Induction of metallothionein as an adaptive mechanism affecting the magnitude and progression of toxicological injury. *Environmental Health Perspectives* **1998,** *106 Suppl 1*, 297-300.

38. Huff, J.; Lunn, R. M.; Waalkes, M. P.; Tomatis, L.; Infante, P. F., Cadmium-induced cancers in animals and in humans. *International Journal of Occupational and Environmental Health* **2007,** *13* (2), 202-212.

39. Cai, Y.; Aoshima, K.; Katoh, T.; Teranishi, H.; Kasuya, M., Renal tubular dysfunction in male inhabitants of a cadmium-polluted area in Toyama, Japan--an eleven-year follow-up study. *Journal of Epidemiology / Japan Epidemiological Association* **2001,** *11* (4), 180-189.

40. Savolainen, H., Cadmium-associated renal disease. *Renal Failure* **1995,** *17* (5), 483-487.

41. Sauvageau, J.-A.; Jumarie, C., Different mechanisms for metal-induced adaptation to cadmium in the human lung cell lines A549 and H441. *Cell Biology and Toxicology* **2013,** *29* (3), 159-173.

42. Wang, Y.; Wu, Y.; Luo, K.; Liu, Y.; Zhou, M.; Yan, S.; Shi, H.; Cai, Y., The protective effects of selenium on cadmium-induced oxidative stress and apoptosis via mitochondria pathway in mice kidney. *Food and Chemical Toxicology: An International Journal Published for the British Industrial Biological Research Association* **2013,** *58*, 61-67.

43. Wang, L.; Li, J.; Li, J.; Liu, Z., Effects of lead and/or cadmium on the oxidative damage of rat kidney cortex mitochondria. *Biological Trace Element Research* **2010,** *137* (1), 69-78.

44. Pathak, N.; Khandelwal, S., Oxidative stress and apoptotic changes in murine splenocytes exposed to cadmium. *Toxicology* **2006,** *220* (1), 26-36.

45. Pathak, N.; Khandelwal, S., Influence of cadmium on murine thymocytes: potentiation of apoptosis and oxidative stress. *Toxicology Letters* **2006,** *165* (2), 121-132.

46. Wang, L.; Cao, J.; Chen, D.; Liu, X.; Lu, H.; Liu, Z., Role of oxidative stress, apoptosis, and intracellular homeostasis in primary cultures of rat proximal tubular cells exposed to cadmium. *Biological Trace Element Research* **2009,** *127* (1), 53-68.

47. López, E.; Arce, C.; Oset-Gasque, M. J.; Cañadas, S.; González, M. P., Cadmium induces reactive oxygen species generation and lipid peroxidation in cortical neurons in culture. *Free Radical Biology & Medicine* **2006,** *40* (6), 940-951.

48. Liu, J.; Qu, W.; Kadiiska, M. B., Role of oxidative stress in cadmium toxicity and carcinogenesis. *Toxicology and Applied Pharmacology* **2009,** *238* (3), 209-214.

49. Margoshes, M.; Vallee, B. L., A CADMIUM PROTEIN FROM EQUINE KIDNEY CORTEX. *Journal of the American Chemical Society* **1957,** *79* (17), 4813-4814.

50. Kagi, J. H.; Vallee, B. L., Metallothionein: a cadmium and zinc-containign protein from equine renal cortex. II. Physico-chemical properties. *The Journal of Biological Chemistry* **1961,** *236*, 2435-2442.

51. Nordberg, G. F.; Piscator, M.; Lind, B., Distribution of cadmium among protein fractions of mouse liver. *Acta Pharmacologica Et Toxicologica* **1971,** *29* (5), 456-470.

52. Kägi, J. H.; Himmelhoch, S. R.; Whanger, P. D.; Bethune, J. L.; Vallee, B. L., Equine hepatic and renal metallothioneins. Purification, molecular weight, amino acid composition, and metal content. *The Journal of Biological Chemistry* **1974,** *249* (11), 3537-3542.

53. Elinder, C. G.; Lundgren, G.; Nordberg, M.; Palm, B.; Piscator, M., Metallothionein in rabbit kidneys preserved for transplantation. *Environmental Health Perspectives* **1984,** *54*, 275-280.

54. Liu, J.; Klaassen, C. D., Absorption and distribution of cadmium in metallothionein-I transgenic mice. *Fundamental and Applied Toxicology: Official Journal of the Society of Toxicology* **1996,** *29* (2), 294-300.

55. Klaassen, C. D.; Choudhuri, S.; McKim, J. M.; Lehman-McKeeman, L. D.; Kershaw, W. C., In vitro and in vivo studies on the degradation of metallothionein. *Environmental Health Perspectives* **1994,** *102 Suppl 3*, 141-146.

56. Feldman, S. L.; Failla, M. L.; Cousins, R. J., Degradation of rat liver metallothioneins in vitro. *Biochimica Et Biophysica Acta* **1978,** *544* (3), 638-646.

57. Kershaw, W. C.; Klaassen, C. D., Degradation and metal composition of hepatic isometallothioneins in rats. *Toxicology and Applied Pharmacology* **1992,** *112* (1), 24-31.

58. Lau, A. T. Y.; Zhang, J.; Chiu, J.-F., Acquired tolerance in cadmium-adapted lung epithelial cells: roles of the c-Jun N-terminal kinase signaling pathway and basal level of metallothionein. *Toxicology and Applied Pharmacology* **2006,** *215* (1), 1-8.

59. Schmid, M.; Zimmermann, S.; Krug, H. F.; Sures, B., Influence of platinum, palladium and rhodium as compared with cadmium, nickel and chromium on cell viability and oxidative stress in human bronchial epithelial cells. *Environment International* **2007,** *33* (3), 385-390.

60. Waisberg, M.; Joseph, P.; Hale, B.; Beyersmann, D., Molecular and cellular mechanisms of cadmium carcinogenesis. *Toxicology* **2003,** *192* (2-3), 95-117.

61. Elinder, C. G.; Nordberg, M.; Palm, B.; Björk, L.; Jönsson, L., Cadmium, zinc, and copper in rabbit kidney metallothionein--relation to kidney toxicity. *Environmental Research* **1987,** *42* (2), 553-562.

62. Bellomo, E. A.; Meur, G.; Rutter, G. A., Glucose regulates free cytosolic Zn^{2+} concentration, Slc39 (ZiP), and metallothionein gene expression in primary pancreatic islet β-cells. *The Journal of Biological Chemistry* **2011,** *286* (29), 25778-25789.

63. Lehman-McKeeman, L. D.; Klaassen, C. D., Induction of metallothionein-I and metallothionein-II in rats by cadmium and zinc. *Toxicology and Applied Pharmacology* **1987,** *88* (2), 195-202.

64. Taubeneck, M. W.; Daston, G. P.; Rogers, J. M.; Keen, C. L., Altered maternal zinc metabolism following exposure to diverse developmental toxicants. *Reproductive Toxicology (Elmsford, N.Y.)* **1994,** *8* (1), 25-40.

65. Kershaw, W. C.; Iga, T.; Klaassen, C. D., Ethanol decreases cadmium hepatotoxicity in rats: possible role of hepatic metallothionein induction. *Toxicology and Applied Pharmacology* **1990,** *106* (3), 448-455.

66. Bauman, J. W.; Liu, Y. P.; Andrews, G. K.; Klaassen, C. D., Examination of potential mechanism(s) of metallothionein induction by diethyl maleate. *Toxicology and Applied Pharmacology* **1992,** *117* (2), 226-232.

67. Bauman, J. W.; McKim, J. M.; Liu, J.; Klaassen, C. D., Induction of metallothionein by diethyl maleate. *Toxicology and Applied Pharmacology* **1992,** *114* (2), 188-196.

68. Westin, G.; Schaffner, W., A zinc-responsive factor interacts with a metal-regulated enhancer element (MRE) of the mouse metallothionein-I gene. *The EMBO journal* **1988,** *7* (12), 3763-3770.

69. Heuchel, R.; Radtke, F.; Georgiev, O.; Stark, G.; Aguet, M.; Schaffner, W., The transcription factor MTF-1 is essential for basal and heavy metal-induced metallothionein gene expression. *The EMBO journal* **1994,** *13* (12), 2870-2875.

70. Palmiter, R. D., Regulation of metallothionein genes by heavy metals appears to be mediated by a zinc-sensitive inhibitor that interacts with a

constitutively active transcription factor, MTF-1. *Proceedings of the National Academy of Sciences of the United States of America* **1994,** *91* (4), 1219-1223.

71. Durnam, D. M.; Palmiter, R. D., Analysis of the detoxification of heavy metal ions by mouse metallothionein. *Experientia. Supplementum* **1987,** *52*, 457-463.

72. Klaassen, C. D.; Liu, J.; Choudhuri, S., Metallothionein: an intracellular protein to protect against cadmium toxicity. *Annual Review of Pharmacology and Toxicology* **1999,** *39*, 267-294.

73. Wong, K. L.; Cachia, R.; Klaassen, C. D., Comparison of the toxicity and tissue distribution of cadmium in newborn and adult rats after repeated administration. *Toxicology and Applied Pharmacology* **1980,** *56* (3), 317-325.

74. Goering, P. L.; Klaassen, C. D., Resistance to cadmium-induced hepatotoxicity in immature rats. *Toxicology and Applied Pharmacology* **1984,** *74* (3), 321-329.

75. Sauge-Merle, S.; Lecomte-Pradines, C.; Carrier, P.; Cuiné, S.; Dubow, M., Heavy metal accumulation by recombinant mammalian metallothionein within Escherichia coli protects against elevated metal exposure. *Chemosphere* **2012,** *88* (8), 918-924.

76. Honda, A.; Komuro, H.; Hasegawa, T.; Seko, Y.; Shimada, A.; Nagase, H.; Hozumi, I.; Inuzuka, T.; Hara, H.; Fujiwara, Y.; Satoh, M., Resistance of metallothionein-III null mice to cadmium-induced acute hepatotoxicity. *The Journal of Toxicological Sciences* **2010,** *35* (2), 209-215.

77. Park, J. D.; Liu, Y.; Klaassen, C. D., Protective effect of metallothionein against the toxicity of cadmium and other metals(1). *Toxicology* **2001,** *163* (2-3), 93-100.

78. Blumenthal, S. S.; Lewand, D. L.; Buday, M. A.; Kleinman, J. G.; Krezoski, S. K.; Petering, D. H., Cadmium inhibits glucose uptake in primary cultures of mouse cortical tubule cells. *The American Journal of Physiology* **1990,** *258* (6 Pt 2), F1625-1633.

79. Namdarghanbari, M.; Wobig, W.; Krezoski, S.; Tabatabai, N. M.; Petering, D. H., Mammalian metallothionein in toxicology, cancer, and cancer chemotherapy. *Journal of biological inorganic chemistry: JBIC: a publication of the Society of Biological Inorganic Chemistry* **2011,** *16* (7), 1087-1101.

80. Kothinti, R. K.; Blodgett, A. B.; Petering, D. H.; Tabatabai, N. M., Cadmium down-regulation of kidney Sp1 binding to mouse SGLT1 and SGLT2 gene promoters: possible reaction of cadmium with the zinc finger domain of Sp1. *Toxicology and Applied Pharmacology* **2010,** *244* (3), 254-262.

81. Blumenthal, S. S.; Ren, L.; Lewand, D. L.; Krezoski, S. K.; Petering, D. H., Cadmium decreases SGLT1 messenger RNA in mouse kidney cells. *Toxicology and Applied Pharmacology* **1998,** *149* (1), 49-54.

82. Tabatabai, N. M.; Blumenthal, S. S.; Lewand, D. L.; Petering, D. H., Differential regulation of mouse kidney sodium-dependent transporters mRNA by cadmium. *Toxicology and Applied Pharmacology* **2001,** *177* (3), 163-173.

83. Tabatabai, N. M.; Blumenthal, S. S.; Lewand, D. L.; Petering, D. H., Mouse kidney expresses mRNA of four highly related sodium-glucose cotransporters: regulation by cadmium. *Kidney International* **2003,** *64* (4), 1320-1330.

84. Tabatabai, N. M.; Blumenthal, S. S.; Petering, D. H., Adverse effect of cadmium on binding of transcription factor Sp1 to the GC-rich regions of the mouse sodium-glucose cotransporter 1, SGLT1, promoter. *Toxicology* **2005,** *207* (3), 369-382.

85. Huang, M.; Krepkiy, D.; Hu, W.; Petering, D. H., Zn-, Cd-, and Pb-transcription factor IIIA: properties, DNA binding, and comparison with TFIIIA-finger 3 metal complexes. *Journal of Inorganic Biochemistry* **2004,** *98* (5), 775-785.

86. Krepkiy, D.; Försterling, F. H.; Petering, D. H., Interaction of Cd2+ with Zn finger 3 of transcription factor IIIA: structures and binding to cognate DNA. *Chemical Research in Toxicology* **2004,** *17* (7), 863-870.

87. Wang, L.; Lin, S. Q.; He, Y. L.; Liu, G.; Wang, Z. Y., Protective effects of quercetin on cadmium-induced cytotoxicity in primary cultures of rat proximal tubular cells. *Biomedical and environmental sciences: BES* **2013,** *26* (4), 258-267.

88. Fujiwara, Y.; Lee, J.-Y.; Tokumoto, M.; Satoh, M., Cadmium renal toxicity via apoptotic pathways. *Biological & Pharmaceutical Bulletin* **2012,** *35* (11), 1892-1897.

89. Chang, K.-C.; Hsu, C.-C.; Liu, S.-H.; Su, C.-C.; Yen, C.-C.; Lee, M.-J.; Chen, K.-L.; Ho, T.-J.; Hung, D.-Z.; Wu, C.-C.; Lu, T.-H.; Su, Y.-C.; Chen, Y.-W.; Huang, C.-F., Cadmium Induces Apoptosis in Pancreatic β-Cells through a Mitochondria-Dependent Pathway: The Role of Oxidative Stress-Mediated c-Jun N-Terminal Kinase Activation. *PLoS ONE* **2013,** *8* (2).

90. Braga, M. M.; Dick, T.; de Oliveira, D. L.; Guerra, A. S.; Leite, M. C.; Ardais, A. P.; Souza, D. O.; Rocha, J. B. T., Cd modifies hepatic Zn deposition and modulates δ-ALA-D activity and MT levels by distinct mechanisms. *Journal of applied toxicology: JAT* **2012,** *32* (1), 20-25.

91. Martelli, A.; Rousselet, E.; Dycke, C.; Bouron, A.; Moulis, J. M., Cadmium toxicity in animal cells by interference with essential metals. *Biochimie* **2006,** *88* (11), 1807-1814.

92. Chouchene, L.; Banni, M.; Kerkeni, A.; Saïd, K.; Messaoudi, I., Cadmium-induced ovarian pathophysiology is mediated by change in gene expression pattern of zinc transporters in zebrafish (Danio rerio). *Chemico-Biological Interactions* **2011,** *193* (2), 172-179.

93. Zhu, J. Y.; Chan, K. M., Mechanism of cadmium-induced cytotoxicity on the ZFL zebrafish liver cell line. *Metallomics: Integrated Biometal Science* **2012,** *4* (10), 1064-1076.

94. Hartwig, A., Cadmium and cancer. *Metal Ions in Life Sciences* **2013,** *11*, 491-507.

95. Winge, D. R.; Premakumar, R.; Rajagopalan, K. V., Metal-induced formation of metallothionein in rat liver. *Archives of Biochemistry and Biophysics* **1975,** *170* (1), 242-252.

96. Leber, A. P.; Miya, T. S., A mechanism for cadmium- and zinc-induced tolerance to cadmium toxicity: involvement of metallothionein. *Toxicology and Applied Pharmacology* **1976,** *37* (3), 403-414.

97. Goering, P. L.; Klaassen, C. D., Tolerance to cadmium-induced hepatotoxicity following cadmium pretreatment. *Toxicology and Applied Pharmacology* **1984,** *74* (3), 308-313.

98. Stuart, G. W.; Searle, P. F.; Palmiter, R. D., Identification of multiple metal regulatory elements in mouse metallothionein-I promoter by assaying synthetic sequences. *Nature* **1985,** *317* (6040), 828-831.

99. Que, E. L.; Domaille, D. W.; Chang, C. J., Metals in neurobiology: probing their chemistry and biology with molecular imaging. *Chemical Reviews* **2008,** *108* (5), 1517-1549.

100. Domaille, D. W.; Que, E. L.; Chang, C. J., Synthetic fluorescent sensors for studying the cell biology of metals. *Nature Chemical Biology* **2008,** *4* (3), 168-175.

101. Jiang, P.; Guo, Z., Fluorescent detection of zinc in biological systems: recent development on the design of chemosensors and biosensors. *Coordination Chemistry Reviews* **2004,** *248* (1–2), 205-229.

102. Kikuchi, K.; Komatsu, K.; Nagano, T., Zinc sensing for cellular application. *Current Opinion in Chemical Biology* **2004,** *8* (2), 182-191.

103. Dai, Z.; Canary, J. W., Tailoring tripodal ligands for zinc sensing. *New Journal of Chemistry* **2007,** *31* (10), 1708-1718.

104. Chang, C. J.; Lippard, S. J., Zinc Metalloneurochemistry: Physiology, Pathology, and Probes. In *Neurodegenerative Diseases and Metal Ions*, Sigel, A.; Sigel, H.; Sigel, R. K. O., Eds. John Wiley & Sons, Ltd: 2006; pp 321-370.

105. McRae, R.; Bagchi, P.; Sumalekshmy, S.; Fahrni, C. J., In situ imaging of metals in cells and tissues. *Chemical Reviews* **2009,** *109* (10), 4780-4827.

106. Mahanand, D.; Houck, J. C., Fluorometric Determination of Zinc in Biologic Fluids. *Clinical Chemistry* **1968,** *14* (1), 6-11.

107. Watanabe, S.; Frantz, W.; Trottier, D., Fluorescence of magnesium-, calcium-, and zinc-8-quinolinol complexes. *Analytical Biochemistry* **1963,** *5*, 345-359.

108. Toroptsev, I. V.; Eshchenko, V. A., [Histochemical detection of zinc using fluorescent 8-(arensulfonilamino)-quinolines]. *Tsitologiia* **1970,** *12* (11), 1481-1484.

109. Toroptsev, I. V.; Eshchenko, V. A., [Zinc distribution in the islands of Langerhans in healthy and diabetic animals during tolbutamide administration]. *Biulleten' Eksperimental'noĭ Biologii I Meditsiny* **1971,** *72* (8), 118-120.

110. Eshchenko, V. A., [State of the islands of Langerhans in various animal species after administration of 8-(arensulfonylamino)-quinolines]. *Problemy Ėndokrinologii* **1978,** *24* (3), 103-107.

111. Toroptsev, I. V.; Eshchenko, V. A., [Toxic action of chelating agents on the animal hippocampus]. *Farmakologiia I Toksikologiia* **1982,** *45* (6), 82-84.

112. Frederickson, C. J.; Kasarskis, E. J.; Ringo, D.; Frederickson, R. E., A quinoline fluorescence method for visualizing and assaying the histochemically reactive zinc (bouton zinc) in the brain. *Journal of Neuroscience Methods* **1987,** *20* (2), 91-103.

113. Frederickson, C. J., Neurobiology of zinc and zinc-containing neurons. *International Review of Neurobiology* **1989,** *31*, 145-238.

114. Fahrni, C. J.; O'Halloran, T. V., Aqueous Coordination Chemistry of Quinoline-Based Fluorescence Probes for the Biological Chemistry of Zinc. *Journal of the American Chemical Society* **1999,** *121* (49), 11448-11458.

115. Koh, J. Y.; Suh, S. W.; Gwag, B. J.; He, Y. Y.; Hsu, C. Y.; Choi, D. W., The role of zinc in selective neuronal death after transient global cerebral ischemia. *Science (New York, N.Y.)* **1996,** *272* (5264), 1013-1016.

116. Meeusen, J. W.; Tomasiewicz, H.; Nowakowski, A.; Petering, D. H., TSQ (6-methoxy-8-p-toluenesulfonamido-quinoline), a common fluorescent sensor for cellular zinc, images zinc proteins. *Inorganic Chemistry* **2011,** *50* (16), 7563-7573.

117. Tønder, N.; Johansen, F. F.; Frederickson, C. J.; Zimmer, J.; Diemer, N. H., Possible role of zinc in the selective degeneration of dentate hilar neurons after cerebral ischemia in the adult rat. *Neuroscience Letters* **1990,** *109* (3), 247-252.

118. Kimura, E.; Koike, T., Recent development of zinc-fluorophores. *Chemical Society Reviews* **1998,** *27* (3), 179-184.

119. Hendrickson, K. M.; Geue, J. P.; Wyness, O.; Lincoln, S. F.; Ward, A. D., Coordination and fluorescence of the intracellular Zn2+ probe [2-methyl-8-(4-toluenesulfonamido)-6-quinolyloxy]acetic acid (Zinquin A) in ternary Zn2+ complexes. *Journal of the American Chemical Society* **2003,** *125* (13), 3889-3895.

120. Reyes, J. G.; Santander, M.; Martinez, P. L.; Arce, R.; Benos, D. J., A fluorescence method to determine picomole amounts of Zn(II) in biological systems. *Biological Research* **1994,** *27* (1), 49-56.

121. Zalewski, P.; Truong-Tran, A.; Lincoln, S.; Ward, D.; Shankar, A.; Coyle, P.; Jayaram, L.; Copley, A.; Grosser, D.; Murgia, C.; Lang, C.; Ruffin, R., Use of a zinc fluorophore to measure labile pools of zinc in body fluids and cell-conditioned media. *BioTechniques* **2006,** *40* (4), 509-520.

122. Zalewski, P. D.; Forbes, I. J.; Betts, W. H., Correlation of apoptosis with change in intracellular labile Zn(II) using zinquin [(2-methyl-8-p-toluenesulphonamido-6-quinolyloxy)acetic acid], a new specific fluorescent probe for Zn(II). *The Biochemical Journal* **1993,** *296 (Pt 2)*, 403-408.

123. Colvin, R. A.; Laskowski, M.; Fontaine, C. P., Zinquin identifies subcellular compartmentalization of zinc in cortical neurons. Relation to the trafficking of zinc and the mitochondrial compartment. *Brain Research* **2006,** *1085* (1), 1-10.

124. Snitsarev, V.; Budde, T.; Stricker, T. P.; Cox, J. M.; Krupa, D. J.; Geng, L.; Kay, A. R., Fluorescent detection of Zn(2+)-rich vesicles with Zinquin: mechanism of action in lipid environments. *Biophysical Journal* **2001,** *80* (3), 1538-1546.

125. Zalewski, P. D.; Forbes, I. J.; Seamark, R. F.; Borlinghaus, R.; Betts, W. H.; Lincoln, S. F.; Ward, A. D., Flux of intracellular labile zinc during apoptosis (gene-directed cell death) revealed by a specific chemical probe, Zinquin. *Chemistry & Biology* **1994,** *1* (3), 153-161.

126. Costello, L. C.; Levy, B. A.; Desouki, M. M.; Zou, J.; Bagasra, O.; Johnson, L. A.; Hanna, N.; Franklin, R. B., Decreased zinc and downregulation of ZIP3 zinc uptake transporter in the development of pancreatic adenocarcinoma. *Cancer Biology & Therapy* **2011,** *12* (4), 297-303.

127. Zhang, J. J.; Wu, M.; Schoene, N. W.; Cheng, W.-H.; Wang, T. T. Y.; Alshatwi, A. A.; Alsaif, M.; Lei, K. Y., Effect of resveratrol and zinc on intracellular zinc status in normal human prostate epithelial cells. *American Journal of Physiology. Cell Physiology* **2009,** *297* (3), C632-644.

128. Meeusen, J. W.; Nowakowski, A.; Petering, D. H., Reaction of metal-binding ligands with the zinc proteome: zinc sensors and N,N,N',N'-tetrakis(2-pyridylmethyl)ethylenediamine. *Inorganic Chemistry* **2012,** *51* (6), 3625-3632.

129. Nowakowski, A. B.; Petering, D. H., Reactions of the fluorescent sensor, Zinquin, with the zinc-proteome: adduct formation and ligand substitution. *Inorganic Chemistry* **2011,** *50* (20), 10124-10133.

130. Nasir, M. S.; Fahrni, C. J.; Suhy, D. A.; Kolodsick, K. J.; Singer, C. P.; O'Halloran, T. V., The chemical cell biology of zinc: structure and intracellular fluorescence of a zinc-quinolinesulfonamide complex. *Journal of biological inorganic chemistry: JBIC: a publication of the Society of Biological Inorganic Chemistry* **1999,** *4* (6), 775-783.

131. Nowakowski, A.; Petering, D., Sensor specific imaging of proteomic Zn2+ with zinquin and TSQ after cellular exposure to N-ethylmaleimide. *Metallomics: Integrated Biometal Science* **2012,** *4* (5), 448-456.

132. Qian, W. J.; Aspinwall, C. A.; Battiste, M. A.; Kennedy, R. T., Detection of secretion from single pancreatic beta-cells using extracellular fluorogenic reactions and confocal fluorescence microscopy. *Analytical Chemistry* **2000,** *72* (4), 711-717.

133. Eichelsdoerfer, J. L.; Evans, J. A.; Slaugenhaupt, S. A.; Cuajungco, M. P., Zinc dyshomeostasis is linked with the loss of mucolipidosis IV-associated TRPML1 ion channel. *The Journal of Biological Chemistry* **2010,** *285* (45), 34304-34308.

134. Ellman, G. L., Tissue sulfhydryl groups. *Archives of Biochemistry and Biophysics* **1959,** *82* (1), 70-77.

135. Krezel, A.; Maret, W., Dual nanomolar and picomolar Zn(II) binding properties of metallothionein. *Journal of the American Chemical Society* **2007,** *129* (35), 10911-10921.

136. Namdarghanbari, M. A.; Meeusen, J.; Bachowski, G.; Giebel, N.; Johnson, J.; Petering, D. H., Reaction of the zinc sensor FluoZin-3 with Zn(7)-metallothionein: Inquiry into the existence of a proposed weak binding site. *Journal of Inorganic Biochemistry* **2010,** *104* (3), 224-231.

137. Petering, D. H., Concerning the role of zinc in the antitumor activity of 3-ethoxy-2-oxobutyraldehyde bis(thiosemicarbazonato) zinc(II) and related chelates. *Biochemical Pharmacology* **1974,** *23* (3), 567-576.

138. Chemical Society, S. n. L. G.; Martell, A. E., *Stability constants of metal-ion complexes. Supplement no. 1. Supplement no. 1*. Burlington House: London, 1971.

139. Shaw, C. F.; Laib, J. E.; Savas, M. M.; Petering, D. H., Biphasic kinetics of aurothionein formation from gold sodium thiomalate: a novel metallochromic technique to probe zinc(2+) and cadmium(2+) displacement from metallothionein. *Inorganic Chemistry* **1990,** *29* (3), 403-408.

140. Gee, K. R.; Zhou, Z.-L.; Qian, W.-J.; Kennedy, R., Detection and imaging of zinc secretion from pancreatic beta-cells using a new fluorescent zinc indicator. *Journal of the American Chemical Society* **2002,** *124* (5), 776-778.

141. Kägi, J. H.; Vasák, M.; Lerch, K.; Gilg, D. E.; Hunziker, P.; Bernhard, W. R.; Good, M., Structure of mammalian metallothionein. *Environmental Health Perspectives* **1984,** *54*, 93-103.

142. July, *Metallothioneins: Synthesis, Structure and Properties of Metallothioneins: Phytochelatins, and Metal-Thiolate Complexes*. Wiley-VCH Verlag GmbH: New York, 1992; p 352.

143. Armitage, I. M.; Otvos, J. D.; Briggs, R. W.; Boulanger, Y., Structure elucidation of the metal-binding sites in metallothionein by 113Cd NMR. *Federation Proceedings* **1982,** *41* (13), 2974-2980.

144. Braun, W.; Vasák, M.; Robbins, A. H.; Stout, C. D.; Wagner, G.; Kägi, J. H.; Wüthrich, K., Comparison of the NMR solution structure and the x-ray crystal structure of rat metallothionein-2. *Proceedings of the National Academy of Sciences of the United States of America* **1992,** *89* (21), 10124-10128.

145. Casini, A.; Karotki, A.; Gabbiani, C.; Rugi, F.; Vašák, M.; Messori, L.; Dyson, P. J., Reactivity of an antimetastatic organometallic ruthenium compound with metallothionein-2: relevance to the mechanism of action. *Metallomics: Integrated Biometal Science* **2009,** *1* (5), 434-441.

146. Zangger, K.; Oz, G.; Otvos, J. D.; Armitage, I. M., Three-dimensional solution structure of mouse [Cd7]-metallothionein-1 by homonuclear and heteronuclear NMR spectroscopy. *Protein Science: A Publication of the Protein Society* **1999,** *8* (12), 2630-2638.

147. Petering, D. H.; Zhu, J.; Krezoski, S.; Meeusen, J.; Kiekenbush, C.; Krull, S.; Specher, T.; Dughish, M., Apo-metallothionein emerging as a major player in the cellular activities of metallothionein. *Experimental Biology and Medicine (Maywood, N.J.)* **2006,** *231* (9), 1528-1534.

148. Summers, K. L.; Sutherland, D. E. K.; Stillman, M. J., Single-domain metallothioneins: evidence of the onset of clustered metal binding domains in Zn-rhMT 1a. *Biochemistry* **2013,** *52* (14), 2461-2471.

149. Otvos, J. D.; Petering, D. H.; Shaw, C. F., Structure—Reactivity Relationships of Metallothionein, a Unique Metal-Binding Protein. *Comments on Inorganic Chemistry* **1989,** *9* (1), 1-35.

150. Hasler, D. W.; Jensen, L. T.; Zerbe, O.; Winge, D. R.; Vasák, M., Effect of the two conserved prolines of human growth inhibitory factor (metallothionein-3) on its biological activity and structure fluctuation: comparison with a mutant protein. *Biochemistry* **2000,** *39* (47), 14567-14575.

151. Banci, L.; Bertini, I., Metallomics and the cell: some definitions and general comments. *Metal Ions in Life Sciences* **2013,** *12*, 1-13.

152. Lichten, L. A.; Cousins, R. J., Mammalian zinc transporters: nutritional and physiologic regulation. *Annual Review of Nutrition* **2009,** *29*, 153-176.

153. Krezel, A.; Maret, W., Zinc-buffering capacity of a eukaryotic cell at physiological pZn. *Journal of biological inorganic chemistry: JBIC: a publication of the Society of Biological Inorganic Chemistry* **2006,** *11* (8), 1049-1062.

154. Eide, D. J., Zinc transporters and the cellular trafficking of zinc. *Biochimica Et Biophysica Acta* **2006,** *1763* (7), 711-722.

155. Namdarghanbari, M. A.; Petering, D. H., Cellular Zn^{2+} Trafficking: Proteomic Zn^{2+} Binding Sites Detected through Adduct Formation with Zincon.

156. David, H. P.; Rajendra, K.; Jeffrey, M.; Ujala, R., Cellular Inorganic Chemistry Concepts and Examples. In *Cellular and Molecular Biology of Metals*, CRC Press: 2010; pp 1-33.

157. Friberg, L., Cadmium and the kidney. *Environmental Health Perspectives* **1984,** *54*, 1-11.

158. Rana, U.; Kothinti, R.; Meeusen, J.; Tabatabai, N. M.; Krezoski, S.; Petering, D. H., Zinc binding ligands and cellular zinc trafficking: apo-metallothionein, glutathione, TPEN, proteomic zinc, and Zn-Sp1. *Journal of Inorganic Biochemistry* **2008,** *102* (3), 489-499.

159. Nettesheim, D. G.; Engeseth, H. R.; Otvos, J. D., Products of metal exchange reactions of metallothionein. *Biochemistry* **1985,** *24* (24), 6744-6751.

160. Ejnik, J.; Muñoz, A.; Gan, T.; Shaw, C. F.; Petering, D. H., Interprotein metal ion exchange between cadmium-carbonic anhydrase and apo- or zinc-metallothionein. *Journal of biological inorganic chemistry: JBIC: a publication of the Society of Biological Inorganic Chemistry* **1999,** *4* (6), 784-790.

161. Roesijadi, G.; Bogumil, R.; Vasák, M.; Kägi, J. H., Modulation of DNA binding of a tramtrack zinc finger peptide by the metallothionein-thionein conjugate pair. *The Journal of Biological Chemistry* **1998,** *273* (28), 17425-17432.

162. Petering, D. H.; Krezoski, S.; Tabatabai, N., Metallothionein Toxicology: Metal ion trafficking and cellular protection. *Met. Ions Life Sci.* **2009,** *5*, 353-397.

163. Masuoka, J.; Hegenauer, J.; Van Dyke, B. R.; Saltman, P., Intrinsic stoichiometric equilibrium constants for the binding of zinc(II) and copper(II) to the high affinity site of serum albumin. *The Journal of Biological Chemistry* **1993,** *268* (29), 21533-21537.

164. Berger, A.; Loewenstein, A.; Meiboom, S., Nuclear Magnetic Resonance Study of the Protolysis and Ionization of N-Methylacetamide1. *Journal of the American Chemical Society* **1959,** *81* (1), 62-67.

165. Schmid, F. X.; Baldwin, R. L., Acid catalysis of the formation of the slow-folding species of RNase A: evidence that the reaction is proline isomerization. *Proceedings of the National Academy of Sciences of the United States of America* **1978,** *75* (10), 4764-4768.

166. Wedemeyer, W. J.; Welker, E.; Scheraga, H. A., Proline cis-trans isomerization and protein folding. *Biochemistry* **2002,** *41* (50), 14637-14644.

167. Kägi, J. H. R.; Kojima, Y., In *Metallothionein II: proceedings of the Second International Meeting on Metallothionein and Other Low Molecular Weight Metal-binding Proteins : Zürich, August 21-24, 1985*, Birkhäuser Verlag: 1987; pp 25-61.

168. Reimer, U.; el Mokdad, N.; Schutkowski, M.; Fischer, G., Intramolecular assistance of cis/trans isomerization of the histidine-proline moiety. *Biochemistry* **1997,** *36* (45), 13802-13808.

169. Pattanaik, A.; Shaw Iii, C. F.; Petering, D. H.; Garvey, J.; Kraker, A. J., Basal metallothionein in tumors: Widespread presence of apoprotein. *Journal of Inorganic Biochemistry* **1994,** *54* (2), 91-105.

170. Namdarghanbari, M. A.; Betling, J.; Krezoski, S.; Petering, D. H., Toxic metal proteomics: Reaction of the mammalian zinc proteome with Cd^{2+}. *Journal of Inorganic Biochemistry* **2014,** *136* (6), 115-121.

Curriculum Vitae

Mohammad Ali Namdarghanbari

EDUCATION

Ph.D.	Biochemistry	2014	University of Wisconsin-Milwaukee
Dissertation:			Cellular Zinc Trafficking: The Zinc Proteome and Its Reactions with Cadmium
M.S.	Physical Chemistry	2001	Shiraz University
			Thesis: "Kinetic Parameters for Hydrogen Abstraction in the Reactions of "$CH_3 + SH_2$" and "C_2H_5S + •SH" From Ab Initio Calculations"
B.S.	Applied Chemistry	1998	University of Isfahan

PROFESSIONAL EXPERIENCE

Research and Teaching Assistant — September 2006 to December 2014

Research Project: Metal binding properties of Metallothionein and the Proteome and Toxic Metal Proteomics.

Courses Taught: Chem. 101, 102, 103, 221 Labs. & discussions and tutoring for all Chemistry Levels

UNIVERSITY OF WISCONSIN-MILWAUKEE
Milwaukee, Wisconsin

Research and Teaching Assistant — September 2005 to August 2006

Research Project: Theoretical Study of Actinide Complexation in Zeolites.

Suggested a multistep mechanism of oxygen exchange reaction in uranyl hydroxide and computed thermodynamic parameters for this mechanism using Density Functional Theory (DFT) method in gas and condensed-matter states. (Published in JACS 2008)

Courses taught: Chemistry of Main Group Elements and Introduction to Physical Chemistry Labs.

UNIVERSITY OF MANITOBA
Winnipeg, Manitoba

Chemical Lab Supervisor January 2004 to August 2005

Preparation of analysis methods for new products using USP, BP or internal methods.

Conducting analysis for new products licensed under foreign companies.

Deciding to accept or deny raw materials, in-process and finished products.

Determining the quantity of effective drug substances needed to issue batch sheets for using in the production section.

Supervising analysis of raw materials and finished products.

Reviewing analysis sheets for raw materials, in-process and finished products.

EXIR PHARMACEUTICAL COMPNAY
Boroujerd, Iran

Wastewater Researcher and Lab Analyst October 2001 to December 2003

Conducting cation-exchange experiments and analysis

Determining thermodynamic quantities of ion exchange reactions in zeolites in order to find optimized temperature and the best zeolite for industrial wastewater treatment.

INDUSTRIAL WASTEWATER TREATMENT Co.
Tehran, Iran

Research and Teaching Assistant September 1998 to July 2001

Research Projects: Determination of kinetic parameters of Hydrogen Abstraction Reactions in sulfur compounds by Ab Initio calculations.

Writing a program in FORTRAN to calculate kinetic parameters and tunneling effect on the kinetics of in Trimolecular, Bimolecular, and unimolecular Hydrogen Abstraction Reactions

Courses taught: Physical Chemistry I& II, and General Chemistry II Labs.

SHIRAZ UNIVERSITY
Shiraz, Iran

PEER REVIEWED JOURNAL PAPERS

- S. Hossein Mousavipour, Mohammad A. Namdar-Ghanbari, and Lila Sadeghian “A Theoretical Study on the Kinetics of Hydrogen Abstraction

Reactions of Methyl or Hydroxyl Radicals with Hydrogen Sulfide", J. Phys. Chem. A. 107 (2003), 3752-3758.

- Namdarghanbari MA., Meeusen J., Bachowski G., Giebel N., Johnson J., Petering DH. "Reaction of the zinc sensor FluoZin-3 with Zn 7-metallothionein: Inquiry into the existence of a proposed weak binding site", J Inorg. Biochem. 104 (2010), 224–231.
- Namdarghanbari M., Wobig W., Krezoski S., Tabatabai NM., Petering DH. "Mammalian metallothionein in toxicology, cancer, and cancer chemotherapy", J Biol. Inorg. Chem. 16 (2011), 1087-101.
- Namdarghanbari MA, Bertling J., Krezoski S., and Petering DH. "Toxic Metal Proteomics: Reaction of the Zinc Proteome with Cd^{2+}", J Inorg. Biochem. 136 (2014) 115-121.

CONFERENCE PAPERS

March 2001

S. H. Mousavipour and M. A. Namdar-Ghanbari, Hydrogen Abstraction from Hydrogen Sulfide by Methyl Radicals, 4th Physical Chemistry Conference, Kish, Iran.

August 2007

G. Schreckenbach, M. A. Namdarghanbari, G. A. Shamov, N. B. Svenda "Uranyl Hydroxide", poster presentation at the "16th Canadian Symposium on Theoretical Chemistry (CSTC2007)", St. John's, Newfoundland, Canada.

May 2009

Meeusen, J.; Namdarghanbari, M. A.; Giebel, N.; Petering, D.H. Dual native and non-native Zn(II) binding properties of metallothionein. 2nd Canadian Conference of Biological Inorganic Chemistry, Canada.

3939 N. Murray Ave. APT 205, Milwaukee WI 53211 E-mail: namdarg4@uwm.edu